Published for SISSA by Springer

Received: November 13, 2018
Revised: March 14, 2019
Accepted: March 26, 2019
Published: April 12, 2019

Search for Higgs boson pair production in the $b\bar{b}WW^*$ decay mode at $\sqrt{s} = 13$ TeV with the ATLAS detector

The ATLAS collaboration

E-mail: atlas.publications@cern.ch

Abstract: A search for Higgs boson pair production in the $b\bar{b}WW^*$ decay mode is performed in the $b\bar{b}\ell\nu qq$ final state using 36.1 fb^{-1} of proton-proton collision data at a centre-of-mass energy of 13 TeV recorded with the ATLAS detector at the Large Hadron Collider. No evidence of events beyond the background expectation is found. Upper limits on the non-resonant $pp \to HH$ production cross section of 10 pb and on the resonant production cross section as a function of the HH invariant mass are obtained. Resonant production limits are set for scalar and spin-2 graviton hypotheses in the mass range 500 to 3000 GeV.

Keywords: Hadron-Hadron scattering (experiments)

ArXiv ePrint: 1811.04671

https://doi.org/10.1007/JHEP04(2019)092

JHEP04(2019)092

Contents

JHEP04(2019)092

1 Introduction

The Higgs boson (H) is an essential part of the Standard Model (SM) and it has a crucial role in the electroweak symmetry breaking (EWSB) mechanism [1–6]. In this mechanism, an SU(2) doublet scalar field is subject to a potential energy term whose shape allows the doublet field to acquire a vacuum expectation value that breaks the SU(2) symmetry and produces the Higgs boson and its potential energy term. This potential is the last piece of the SM Lagrangian which is yet to be directly tested.

The shape of the Higgs boson potential in the SM can be expressed as a function of the Fermi coupling constant G_F and the Higgs boson mass m_H. A direct phenomenological prediction of the SM due to the potential is the interaction of the Higgs boson with itself at tree level (self-interaction), which can be probed by studying di-Higgs boson production in proton-proton collisions, as illustrated in figure 1(a). The self-interaction diagram together with the quark-loop contributions, primarily via the top-Higgs Yukawa coupling,

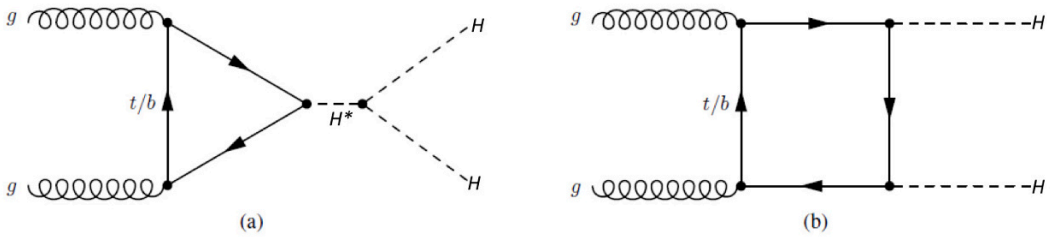

Figure 1. Leading-order Feynman diagrams for non-resonant production of Higgs boson pairs in the Standard Model through (a) the Higgs boson self-coupling and (b) the Higgs-fermion Yukawa interaction. The H^* refers to the off-shell Higgs boson mediator.

figure 1(b), are the leading-order Feynman diagrams for Higgs boson pair production. The SM cross section for $pp \to HH$ is extremely small, e.g. 33.4 fb at 13 TeV [7].

Physics beyond the SM can manifest in the increased production with respect to the SM predictions of the non-resonant HH final state or in the resonant production of particles that decay into a pair of SM Higgs bosons. The analysis presented here is potentially sensitive to cases where the decaying particle is a scalar, as in the MSSM [8] and 2HDM models [9], or a spin-2 graviton, as in Randall-Sundrum models [10]. The signals under study are non-resonant HH production with event kinematics predicted by the SM and resonant HH production with event kinematics consistent with the decays of heavy spin-0 or spin-2 resonances.

Previous searches for $pp \to HH$ production were performed by the ATLAS and CMS collaborations in Run 1 of the LHC at $\sqrt{s} = 8$ TeV. Decay modes with $4b$ [11, 12], $b\bar{b}\tau^+\tau^-$ [13, 14], $\gamma\gamma b\bar{b}$ [15, 16] and $\gamma\gamma WW^*$ [13] in the final state were studied. Furthermore, ATLAS also published a combination of all of the explored channels [13].

Results at $\sqrt{s} = 13$ TeV were published by the ATLAS Collaboration in the $4b$ [17], $b\bar{b}\tau^+\tau^-$ [18, 19], $b\bar{b}\gamma\gamma$ [20] and $WW\gamma\gamma$ [21] decay mode and by CMS in the $4b$ [22] , $b\bar{b}\tau^+\tau^-$ [23], $b\bar{b}\gamma\gamma$ [24] and in the $b\bar{b}WW^*$ channel using the dileptonic WW^* decay mode [25]. Given the low expected yield for SM HH non-resonant production, it is of great importance to understand the sensitivity for the observation of the Higgs boson pair production in all possible decay channels, including $b\bar{b}WW^*$, which will improve projections for future high-luminosity and high-energy colliders.

This paper reports results of a search for Higgs boson pair production where one Higgs boson decays via $H \to b\bar{b}$, and the other decays via $H \to WW^*$. The $H \to WW^*$ branching fraction is the second largest after $H \to b\bar{b}$, so the $b\bar{b}WW^*$ final state can be sensitive to HH production if the signal can be well separated from the dominant $t\bar{t}$ background. The WW^* system decays into $\ell\nu qq$, where ℓ is either an electron or a muon, and the small contamination from leptonic τ decays is not explicitly vetoed in the analysis. Figure 2 shows a schematic diagram of resonant production of the Higgs boson pair with the subsequent decays $H \to WW^*$ and $H \to b\bar{b}$.

Two complementary techniques are used to reconstruct the Higgs boson candidate that decays into two b quarks. Both techniques use the anti-k_t jet algorithm [26] but

JHEP04(2019)092

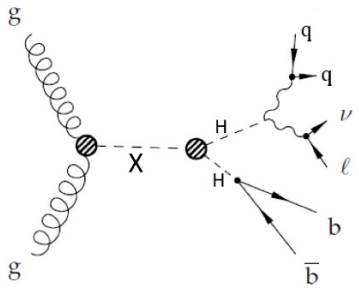

Figure 2. Schematic diagram of resonant Higgs boson pair production with the subsequent Higgs and W-boson decays.

with different radius parameters. The first technique employs jets with radius parameter $R = 0.4$ and it is used when each b quark from the $H \to b\bar{b}$ decay can be reconstructed as a distinct b jet. The second technique is used when this is not possible, due to the large boost of the b-quark pair. In this case the Higgs boson candidate is identified as a single anti-k_t jet with radius parameter $R = 1.0$. The analysis using the first technique is referred to as the "resolved" analysis and that using the second technique is referred to as the "boosted" analysis. In both analyses, the jets from the hadronically decaying W boson are reconstructed as anti-k_t jets with radius parameter $R = 0.4$. The resonant HH search is performed using both the resolved and the boosted analysis methods. The resolved analysis is performed between 500 and 3000 GeV, while the boosted analysis between 800 and 3000 GeV. The resolved analysis is divided into three selections, one targeting low mass values, a second designed for high mass values and a specific analysis for the 500 GeV mass value. Because the three resolved, and the boosted analyses do not select orthogonal samples, they are not combined statistically. However, results from all these different techniques are presented to illustrate their sensitivity reach. For the non-resonant search a dedicated selection of the resolved analysis is used.

The dominant background in the $b\bar{b}WW^*$ final state is $t\bar{t}$ production, with smaller contributions from W bosons produced in association with jets (W+jets) and multijet events in which a jet is misidentified as a lepton. The analysis defines one signal region for each signal hypothesis and, in order to avoid biases in the analysis selection, the analysis procedures and the event selection are optimised without reference to data in the signal regions.

2 Data and simulation samples

The ATLAS detector [27] is a general-purpose particle detector at the Large Hadron Collider optimised to discover and measure a broad range of physics processes. It consists of an inner tracking detector surrounded by a thin superconducting solenoid, electromagnetic and hadronic calorimeters, and a muon spectrometer incorporating three large superconducting toroid magnets.[1]

[1]ATLAS uses a right-handed coordinate system with its origin at the nominal interaction point (IP) in the centre of the detector and the z-axis along the beam pipe. The x-axis points from the IP to the centre

JHEP04(2019)092

The dataset used in this analysis corresponds to an integrated luminosity of 36.1 fb^{-1} (3.2 fb^{-1} from 2015 and 32.9 fb^{-1} from 2016) recorded by single-electron or single-muon triggers. The single-lepton trigger efficiency ranges from 75% to 90% (75% to 80%) for electrons (muons) depending on the signal mass, for selected lepton candidates above p_{T} thresholds defined in section 4.1. Samples of simulated signal and background events were used to design the event selection and estimate the signal acceptance and the background yields from various SM processes.

When searching for a new resonance (denoted by X in the following), specific simulation models must be employed. Therefore, the spin-0 states were treated as narrow heavy neutral Higgs bosons, while the spin-2 states were modelled as Randall-Sundrum (RS) gravitons [28, 29]. The parameters used in the RS graviton simulation were: $c = k/\bar{M}_{\mathrm{Pl}}$ equal to 1.0 or 2.0, where k is the curvature of the warped extra dimension and $\bar{M}_{\mathrm{Pl}} = 2.4 \times 10^{18}$ GeV is the effective four-dimensional Planck scale. The graviton signal samples were generated at leading order (LO) with MADGRAPH5_aMC@NLO [30] using the NNPDF2.3 [31] LO parton distribution function (PDF) set, and PYTHIA 8.186 [32] to model the parton showers and hadronisation process with a set of tuned underlying-event parameters called the A14 tune [33]. Only the $c = 2.0$ samples were fully simulated, while the $c = 1.0$ samples were obtained by reweighting them using the Monte Carlo (MC) generator-level m_{HH} distribution.

Scalar signal samples were generated at next-to-leading order (NLO) with MADGRAPH5_aMC@NLO interfaced to HERWIG++ [34] using the CT10 PDF set [35] and the UE-EE-5-CTEQ6L1 tune. The simulation produced the Higgs boson pair through gluon-gluon fusion using an effective field theory approach to take into account the finite value of the top-quark mass m_t [36]. Events were first generated with an effective Lagrangian in the infinite top-quark mass approximation, and then reweighted with form factors that take into account the finite mass of the top quark.

The non-resonant signal samples were simulated with MADGRAPH5_aMC@NLO + HERWIG++ using the CT10 PDF set; and the same approach for the inclusion of finite m_t effects was used [37]. In addition, scale factors dependent on the HH invariant mass m_{HH} at generator level were applied to match the MC m_{HH} distribution with an NLO calculation that computes exact finite m_t contributions [38]. All signal samples were generated with 100% of Higgs boson pairs decaying into $b\bar{b}WW^*$, and the samples were then normalised assuming $\mathcal{B}(H \to WW^*) = 0.22$ and $\mathcal{B}(H \to b\bar{b}) = 0.57$ [7].

SHERPA v2.2 [39] with the NNPDF 3.0 [40] PDF set was used as the baseline generator for the $(W \to \ell\nu)/(Z \to \ell\ell)$+jets background. The W/Z+jets samples were normalised using the FEWZ [41] inclusive cross section with NNLO accuracy. The diboson processes (WW, WZ and ZZ) were generated at NLO with SHERPA v2.1.1 [39] with the CT10 [35] PDF set and normalised using the SHERPA cross-section prediction.

The $t\bar{t}$ background samples were generated with POWHEG-BOX v2 [42] using the CT10 PDF set. POWHEG-BOX v2 was interfaced to PYTHIA 6.428 [43] for parton showers, using

of the LHC ring, and the y-axis points upwards. Cylindrical coordinates (r, ϕ) are used in the transverse plane, ϕ being the azimuthal angle around the z-axis. The pseudorapidity is defined in terms of the polar angle θ as $\eta = -\ln\tan(\theta/2)$. The angular distance is measured in units of $\Delta R \equiv \sqrt{(\Delta\eta)^2 + (\Delta\phi)^2}$.

JHEP04(2019)092

the PERUGIA2012 [44] tune with the CTEQ6L1 [45] set of PDFs for the underlying-event description. EVTGEN v1.2.0 [46] was used to simulate the bottom- and charm-hadron decays. The mass of the top quark was set to $m_t = 172.5$ GeV. At least one top quark in the $t\bar{t}$ event was required to decay into a final state with a lepton. For the $t\bar{t}$ sample the parameter HDAMP, used to regulate the high-p_{T} gluon emission in POWHEG, was set to m_t, giving good modelling of the high-p_{T} region [47]. The interference between the $t\bar{t}$ background and the signal is extremely small due to the small width of the Higgs boson ($\Gamma_H \sim 4$ MeV) and it has been neglected in this analysis. The $t\bar{t}$ cross section is calculated to next-to-next-to-leading order in QCD including resummation of soft gluon contributions at next-to-next-to-leading-logarithm (NNLL) accuracy using TOP++ 2.0 [48].

Single-top-quark events in the W-*top*, s, and t channels were generated using POWHEG-BOX v1 [49, 50]. The overall normalisation of single-top-quark production in each channel was rescaled according to its approximate NNLO cross section [51–53].

The effect of multiple pp interactions in the same and neighbouring bunch crossings (pile-up) was included by overlaying minimum-bias collisions, simulated with PYTHIA 8.186, on each generated signal and background event. The interval between proton bunches was 25 ns in all of the data analysed. The number of overlaid collisions was such that the distribution of the number of interactions per pp bunch crossing in the simulation matches that observed in the data: on average 14 interactions per bunch crossing in 2015 and 23.5 interactions per bunch crossing in 2016. The generated samples were processed through a GEANT4-based detector simulation [54, 55] with the standard ATLAS reconstruction software used for collision data.

3 Object reconstruction

In the present work an "object" is defined to be a reconstructed jet, electron, or muon. Electrons are required to pass the "TightLH" selection as described in refs. [56, 57], have $p_{\mathrm{T}} > 27$ GeV and be within $|\eta| < 2.47$, excluding the transition region between the barrel and endcaps in the LAr calorimeter ($1.37 < |\eta| < 1.52$). In addition, the electron is required to be isolated. In order to calculate the isolation variable, the p_{T} of the tracks in a cone of ΔR around the lepton track is summed ($\sum p_{\mathrm{T}}$), where $\Delta R = \min(10\ \mathrm{GeV}/p_{\mathrm{T}}^{e}, 0.2)$ and p_{T}^{e} is the electron transverse momentum. The ratio $\sum p_{\mathrm{T}}/p_{\mathrm{T}}^{e}$ (isolation variable) is required to be less than 0.06.

Muons are reconstructed as described in ref. [58] and required to pass the "Medium" identification criterion and have $|\eta| < 2.5$. The muon isolation variables are similar to the electron isolation variables with the only difference being that the maximum cone size is $\Delta R = 0.3$ rather than 0.2.

Jets are reconstructed using the anti-k_t algorithm [26] with a radius parameter of 0.4, and are required to have $p_{\mathrm{T}} > 20$ GeV and $|\eta| < 2.5$. Suppression of jets likely to have originated from pile-up interactions is achieved using a boosted decision tree in an algorithm that has an efficiency of 90% for jets with $p_{\mathrm{T}} < 50$ GeV and $|\eta| < 2.5$ [59]. The jet-flavour tagging algorithm [60] is used to select signal events and to suppress multijet, W+jets, Z+jets and diboson backgrounds. The jets containing b hadrons are called b jets in this

JHEP04(2019)092

work. The jet-flavour tagging algorithm parameters were chosen such that the b-tagging efficiency is 85% for jets with p_{T} of at least 20 GeV as determined in simulated inclusive $t\bar{t}$ events [60] . At this efficiency, for jets with a p_{T} distribution similar to that originating from jets in $t\bar{t}$ events, the charm-quark component is suppressed by a factor of 3.1 while the light-quark component is suppressed by a factor of 34. Jets that are not tagged as b jets are collectively referred to as "light-quark jets".

Large-R jets are reconstructed using the anti-k_t algorithm with a radius parameter of 1.0 and are trimmed to reduce pile-up contributions to the jet, as described in ref. [61]. The jet mass (m_{J}) resolution is improved at high momentum using tracking in addition to calorimeter information [62]. This leads to a smaller mass resolution and better estimate of the median mass value than obtained using only calorimeter energy clusters. The energy and mass scales of the trimmed jets are then calibrated using p_{T}- and η-dependent calibration factors derived from simulation [63]. Large-R jets are required to have $p_{\mathrm{T}} > 250\,\mathrm{GeV}$, $m_{\mathrm{J}} > 30\,\mathrm{GeV}$ and $|\eta| < 2.0$. The identification of large-R jets consistent with boosted Higgs boson decays uses jets built from tracks reconstructed from the ATLAS Inner Detector (referred to as track-jets) to identify the b jets within the large-R jets. The track-jets are built with the anti-k_t algorithm with $R = 0.2$ [64]. They are required to have $p_{\mathrm{T}} > 10\,\mathrm{GeV}$, $|\eta| < 2.5$, and are matched to the large-R jets with a ghost-association algorithm [65]. The small radius parameter of the track-jets enables two nearby b hadrons to be identified when their ΔR separation is less than 0.4, which is beneficial when reconstructing high-p_{T} Higgs boson candidates. The b-tagging requirements of the boosted analyses use working points that lead to an efficiency of 77% for b jets with $p_{\mathrm{T}} > 20\,\mathrm{GeV}$ when evaluated in a sample of simulated $t\bar{t}$ events. At this efficiency, for jets with a p_{T} distribution similar to that originating from jets in $t\bar{t}$ events, the charm-quark component is suppressed by a factor of 12 (7.1) for the R = 0.4 jets (track-jets), while the light-quark component is suppressed by a factor of 380 for the jets with R = 0.4 and 120 for the track-jets.

The calorimeter-based missing transverse momentum with magnitude $E_{\mathrm{T}}^{\mathrm{miss}}$ is calculated as the negative vectorial sum of the transverse momenta of all calibrated selected objects, such as electrons and jets, and is corrected to take into account the transverse momentum of muons. Tracks with $p_{\mathrm{T}}^{\mathrm{track}} > 500$ MeV, compatible with the primary vertex but not matched to any reconstructed object, are included in the reconstruction to take into account the soft-radiation component that does not get clustered into any hard object [66].

To avoid double-counting, overlapping objects are removed from the analysis according to the following procedure. Muons sharing their track with an electron are removed if they are calorimeter-tagged.[2] Otherwise, the electron is removed. Jets overlapping with electrons within an angular distance $\Delta R = 0.2$ are removed. Jets overlapping with muons within $\Delta R = 0.2$ and having less than three tracks or carrying less than 50% of the muon p_{T} are removed. Electrons overlapping with remaining jets within $\Delta R = \min(0.4, 0.04 + 10\ \mathrm{GeV}/p_{\mathrm{T}}^{e})$ are removed. Muons overlapping with remaining jets within $\Delta R = \min(0.4, 0.04 + 10\ \mathrm{GeV}/p_{\mathrm{T}}^{\mu})$ are removed.

[2]Muons are identified by matching an Inner Detector reconstructed track with a track in the Muon Spectrometer or by matching an energy deposit, compatible with a minimum ionising particle, in the outer layers of the Tile Calorimeter (calorimeter-tagged muons).

JHEP04(2019)092

4 Resolved analysis

4.1 Resolved analysis: event selection

At lowest order in QCD the final-state particles consist of one charged lepton, one neutrino, and jets of colourless hadrons from four quarks, two being b quarks. Therefore, the corresponding detector signature is one charged lepton (e/μ), large $E_{\mathrm{T}}^{\mathrm{miss}}$, and four or more jets. Two of these jets are b-tagged jets from the Higgs boson decay, and two jets are not b-tagged jets from the hadronic W boson decay.

The data used in the analysis were recorded by several single-electron or single-muon triggers in 2015 and 2016. In 2015, the electron (muon) trigger required a $p_{\mathrm{T}} > 24$ (20) GeV electron (muon) candidate. Because of a higher instantaneous luminosity, in 2016 the electron trigger required a $p_{\mathrm{T}} > 26\,\mathrm{GeV}$ electron candidate, while muons were triggered using a p_{T} threshold of 24 GeV at the beginning of data taking, and 26 GeV for the rest of the year. In both 2015 and 2016, a threshold of $p_{\mathrm{T}} > 27\,\mathrm{GeV}$ was applied offline on the selected lepton candidate.

The analysis selects events that contain at least one reconstructed electron or muon matching a trigger-lepton candidate. In order to ensure that the leptons originate from the interaction point, requirements on the transverse (d_0) and longitudinal (z_0) impact parameters of the leptons relative to the primary vertex are imposed. In particular, defining σ_{d_0} as the uncertainty in the measured d_0 and θ as the angle of the track relative to the beam axis, the requirements $|d_0|/\sigma_{d_0} < 2$ and $|z_0 \sin\theta| < 0.5$ mm are applied. The requirement on $|d_0|/\sigma_{d_0}$ is relaxed to define control regions in order to estimate the multijet background. The highest p_T lepton is then retained as the analysis lepton.

Events are required to have exactly two b-tagged jets, which form the Higgs boson candidate. Since events are accepted if they contain two or more light-quark jets, in events with more than two light-quark jets, the three leading jets are considered, and the pair with the lowest ΔR between them is selected as the W boson candidate. From MC simulation it was found that, when the light quarks from the W boson are matched to reconstructed jets by requiring that the ΔR between the jet and the quark is less than 0.3, this procedure yields the correct jet assignment in 70% of the cases.

The event kinematics of the $H \to WW^* \to \ell\nu qq$ topology can be fully reconstructed. Among all four-momenta of the final-state particles, only the component of the neutrino momentum along the beam axis, referred to as longitudinal momentum (p_z) in the following, is unknown while its transverse momentum is assumed to be the $E_{\mathrm{T}}^{\mathrm{miss}}$. The longitudinal momentum of the neutrino is computed by solving a quadratic equation in p_z, employing the four-momenta of the lepton and the hadronic W boson, the $E_{\mathrm{T}}^{\mathrm{miss}}$, and the $m_H = 125\,\mathrm{GeV}$ constraint on the WW^* system. No W-boson mass constraint is applied to either the hadronic or the leptonic W boson decay, allowing either W boson to be off-shell. Whenever two real solutions are obtained, the ν candidate with the smallest ΔR relative to the lepton direction is retained. Studies performed by matching the ν candidate with the MC generator-level neutrino show that this procedure finds the correct solution for the neutrino p_z in 60% (75%) of cases for a resonant signal of mass 700 (3000) GeV. If two complex solutions are found, only the real part of the solutions is retained. With the neutrino

JHEP04(2019)092

Definition of the $HH \to b\bar{b}WW^*$ kinematic variables	
p_{T} of the $b\bar{b}$ system	$p_{\mathrm{T}}^{b\bar{b}}$
p_{T} of the WW^* system	$p_{\mathrm{T}}^{WW^*}$
ΔR of the WW^* system	ΔR_{WW^*}
WW^* system mass	m_{WW^*}
$b\bar{b}$ system mass	$m_{b\bar{b}}$
Di-Higgs boson system invariant mass	m_{HH}

Table 1. Selection variables used to identify the $HH \to b\bar{b}WW^*$ decay chain in the resolved analysis. The m_{WW^*} variable is exactly equal to m_H if a real solution for the neutrino p_z is found. It is larger otherwise.

longitudinal momentum computed, the di-Higgs invariant mass can be fully reconstructed and employed to discriminate against backgrounds.

Kinematic selections are used to suppress the $t\bar{t}$ background relative to the signal. The $t\bar{t}$ events are typically characterised by two b jets and two W bosons such that the ΔR separation between the b jets is large, and similarly the ΔR separation between the W bosons is also large. In contrast, in particular when the invariant mass of the heavy resonance is large, the signal is characterised by two b jets and two W bosons which are closer in ΔR in signal events with respect to the $t\bar{t}$ background events. Moreover, for the signal the two b jets have an invariant mass equal to m_H, while this is not the case for the $t\bar{t}$ background, where a much broader distribution is expected. The symbols of the kinematic variables that discriminate between signal and background are listed in table 1.

The selection requirements on the kinematic variables defining the signal region were chosen to maximise the expected sensitivity to various signals. The optimisation was performed for a spin-0 signal considering resonance masses (m_X) from 500 GeV to 3000 GeV in steps of 100 GeV. The same selection was used for the spin-2 signal models while SM Higgs pair production was used to optimise the non-resonant analysis. Below 500 GeV the top-quark background increases significantly, and hence rapidly reduces sensitivity.

The selection criteria define four sets of requirements, referred as *non-res*, *m500*, *low-mass* and *high-mass* in the following. They are shown in table 2. The *non-res* and *m500* selections are exclusively used for non-resonant signal and resonant signal with mass 500 GeV respectively. The *low-mass* selection is used for signal masses from 600 to 1300 GeV, while the *high-mass* selection is used for signals with masses between 1400 and 3000 GeV. In addition, requirements are placed on the reconstructed di-Higgs invariant mass m_{HH} as a function of the signal resonance mass m_X, as shown in table 3. The resolution of the reconstructed m_{HH} ranges from 6% at 500 GeV to 10% at 3000 GeV.

4.2 Resolved analysis: background determination

In this analysis the presence of a signal is indicated by an excess of events over the SM prediction for the background yield in the signal regions, so it is of great importance to properly estimate the amount of background in those regions. The dominant background

JHEP04(2019)092

Variable	*non-res*	*m500*	*low-mass*	*high-mass*
$E_{\mathrm{T}}^{\mathrm{miss}}$ [GeV]	> 25	> 25	> 25	> 25
m_{WW^*} [GeV]	< 130	< 130	< 130	none
$p_{\mathrm{T}}^{b\bar{b}}$ [GeV]	> 300	> 210	> 210	> 350
$p_{\mathrm{T}}^{WW^*}$ [GeV]	> 250	> 150	> 250	> 250
ΔR_{WW^*}	none	none	none	< 1.5
$m_{b\bar{b}}$ [GeV]	105–135	105–135	105–135	105–135

Table 2. Criteria for non-resonant, *m500*, *low-mass* and *high-mass* selections in the resolved analysis.

m_X [GeV]	500	600	700	750	800
m_{HH} window [GeV]	480–530	560–640	625–775	660–840	695–905
m_X [GeV]	900	1000	1100	1200	1300
m_{HH} window [GeV]	760–967	840–1160	925–1275	1010–1390	1095–1505
m_X [GeV]	1400	1500	1600	1800	2000
m_{HH} window [GeV]	1250–1550	1340–1660	1430–1770	1750–2020	1910–2170
m_X [GeV]	2250	2500	2750	3000	
m_{HH} window [GeV]	2040–2460	2330–2740	2570–2950	2760–3210	

Table 3. Window requirements on m_{HH} as a function of the resonance mass m_X in the resolved analysis.

is the $t\bar{t}$ process. Dedicated control regions are used to normalise and validate the estimate of this background. The $t\bar{t}$ normalisation is performed using three data control regions, one for the *non-res*, a second for the *m500* and *low-mass*, and a third for the *high-mass* selection. These control regions are obtained by selecting events outside the $m_{b\bar{b}}$ window [100, 140] GeV and applying only the $E_{\mathrm{T}}^{\mathrm{miss}}$, m_{WW^*} (where applicable) and $p_{\mathrm{T}}^{b\bar{b}}$ requirements shown in table 2 for the respective selections.

In all regions, the event yields of W/Z+jets, single-top-quark and diboson events are modelled using simulated events and normalised to the expected SM cross sections.

The multijet component of the background originates from events where either a jet is incorrectly identified as a lepton, or a non-prompt lepton is produced in heavy-flavour decays, or from photon conversions. It is characterised by low $E_{\mathrm{T}}^{\mathrm{miss}}$ and high $|d_0|/\sigma_{d_0}$ values of the lepton. The multijet background makes a significant contamination in the top control regions. Therefore, this background is estimated in top-background control region and signal region using a data-driven two-dimensional sideband method, labelled the ABCD method, that uses three additional regions denoted in the following by B, C and D. The region of interest, signal or control region, is indicated by A.

JHEP04(2019)092

Process	*non-res*	*m500* and *low-mass*	*high-mass*
$t\bar{t}$	110 ± 6	532 ± 13	8570 ± 50
Multijet	33 ± 4	250 ± 30	1540 ± 250
W+jets	29 ± 1	125 ± 3	2259 ± 8
Single top	20 ± 2	76 ± 4	1780 ± 20
Dibosons	2.2 ± 0.4	8.3 ± 0.8	171 ± 4
Z+jets	6.7 ± 0.2	27.1 ± 0.8	404 ± 2
Background sum	201 ± 8	1015 ± 34	14720 ± 260
Data	206	1069	14862

Table 4. Data and estimated background yields in the *non-res*, *m500* and *low-mass*, and *high-mass* top-background control regions of the resolved analysis. The uncertainty shown for the multijet background is due to the number of data events in the C region (as defined in the text). For all other backgrounds the uncertainties are due to the finite MC sample sizes.

The B, C and D regions are defined in the following way:

- region B: $E_{\mathrm{T}}^{\mathrm{miss}} < 25$ GeV and $|d_0|/\sigma_{d_0} < 2.0$,
- region C: $E_{\mathrm{T}}^{\mathrm{miss}} > 25$ GeV and $|d_0|/\sigma_{d_0} > 2.0$, and
- region D: $E_{\mathrm{T}}^{\mathrm{miss}} < 25$ GeV and $|d_0|/\sigma_{d_0} > 2.0$,

while N_A,N_B,N_C and N_D indicate the number of events in the A,B,C and D regions, respectively. In the absence of correlations between the $E_{\mathrm{T}}^{\mathrm{miss}}$ and $|d_0|/\sigma_{d_0}$ variables, the relation $N_{\mathrm{A}} = N_{\mathrm{C}}N_{\mathrm{B}}/N_{\mathrm{D}}$ holds, while in practice a correlation among variables results in a correction factor F to be applied to the computed ratio $N_{\mathrm{A}}^{\mathrm{corrected}} = FN_{\mathrm{C}}N_{\mathrm{B}}/N_{\mathrm{D}}$. The correction factor F is estimated from data at an early stage of the analysis selection once a veto on the signal candidates is applied by inverting the requirement on the $m_{b\bar{b}}$ variable. It is computed using the relation $F = N_{\mathrm{A}}N_{\mathrm{D}}/(N_{\mathrm{C}}N_{\mathrm{B}})$. Systematic uncertainties in F are described in section 4.3. In order to reduce statistical uncertainties in the computation, the shape of the $m_{b\bar{b}}$ distribution is derived at an earlier stage of the selection sequence, after applying the $m_{WW^*} < 130$ GeV and $p_{\mathrm{T}}^{b\bar{b}} > 210$ GeV requirements for the *non-res*, *m500* and *low-mass* analyses and the $p_{\mathrm{T}}^{b\bar{b}} > 350$ GeV and $p_{\mathrm{T}}^{WW^*} > 250$ GeV requirements for the *high-mass* analysis. It was verified that subsequent requirements do not affect the $m_{b\bar{b}}$ shape, which can therefore be used at the end of the selection sequence.

Table 4 summarises the numbers of observed and estimated events in the three top-quark control regions. The event yields in the control regions are used as input to the statistical analysis. Major contamination in the $t\bar{t}$ control regions comes from multijet and W+jets backgrounds; as a result the $t\bar{t}$ purity ranges from 52% to 58%.

The modelling of the background was checked at all selection stages and, in general, shows good agreement with data. Figure 3 shows the m_{T} distribution of the leptonic W

JHEP04(2019)092

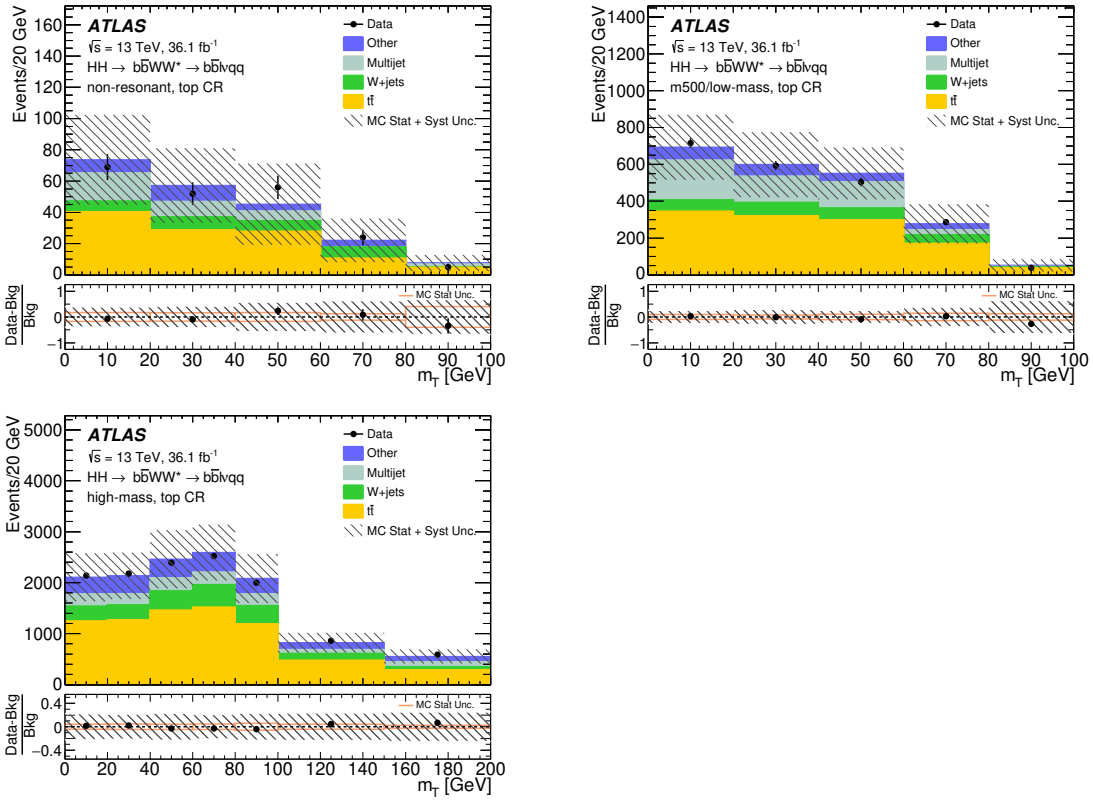

Figure 3. The m_{T} distribution in the three top-background control regions for the *non-res*, *low-mass*, and the *high-mass* selections of the resolved analyses. The signal contamination is negligible, and hence not shown. The lower panel shows the fractional difference between the data and the total expected background with the corresponding statistical and total uncertainty.

boson candidate in the three top control regions. The m_{T} variable is defined as:

$$m_{\mathrm{T}} = \sqrt{2p_{\mathrm{T}}^{\ell}E_{\mathrm{T}}^{\mathrm{miss}} \cdot (1 - \cos\Delta\phi)}\,,$$

where $\Delta\phi$ is the azimuthal angle between p_{T}^{ℓ} and $E_{\mathrm{T}}^{\mathrm{miss}}$. The multijet background populates the low values of the m_{T} distribution, so any mis-modelling of the multijet background would be clearly visible in the m_{T} distribution.

Figures 4 and 5 show the $m_{b\bar{b}}$ distributions at the selection stage where all requirements, including the m_{HH} cut, are applied except the one on $m_{b\bar{b}}$ itself. The expected background is in agreement with the data over the entire distribution, and close to the signal region in particular. All simulated backgrounds are normalised according to their theoretical cross-sections, except $t\bar{t}$, which is normalised in the top CRs.

4.3 Resolved analysis: systematic uncertainties

The main systematic uncertainties in the background estimate arise from the potential mis-modelling of background components. For $t\bar{t}$ background, MC simulation is used to derive the acceptances in all analysis regions, while the normalisation is taken from the top

JHEP04(2019)092

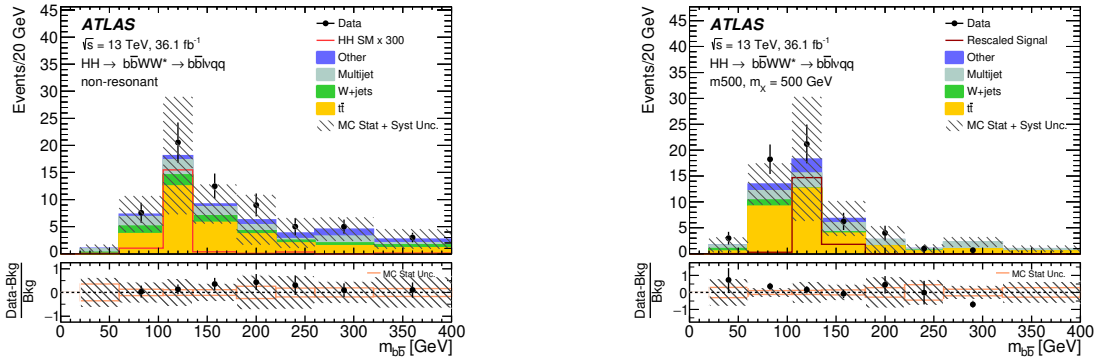

Figure 4. The $m_{b\bar{b}}$ distribution in the resolved analysis for the *non-res* and *m500* selections at the end of the selection sequence, before applying the $m_{b\bar{b}}$ requirement. The signals shown are from SM non-resonant HH production scaled up by a factor of 300 (left) and from a scalar resonance with mass 500 GeV scaled to the expected upper-limit cross section reported in section 6 (right). The lower panel shows the fractional difference between data and the total expected background with the corresponding statistical and total uncertainty.

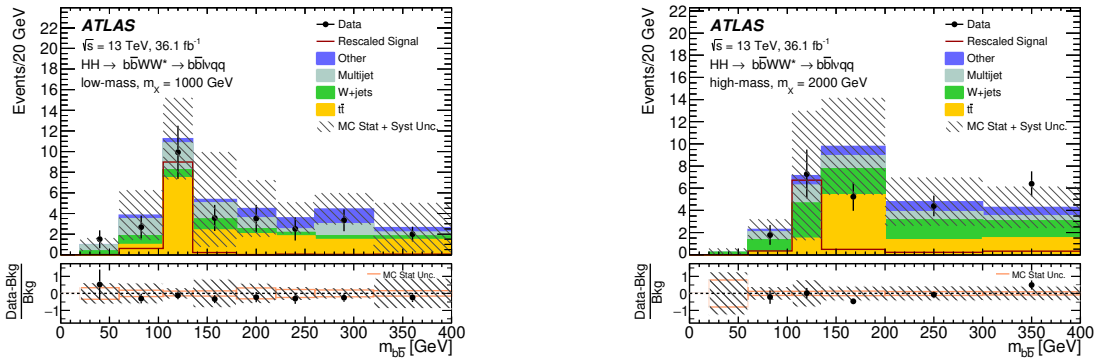

Figure 5. The $m_{b\bar{b}}$ distribution in the resolved analysis for the *low-mass* and *high-mass* selections at the end of the selection sequence, before applying the $m_{b\bar{b}}$ requirement. The signals shown are from scalar resonances with mass 1000 GeV (left) and 2000 GeV (right) scaled to the expected upper-limit cross section reported in section 6. The lower panel shows the fractional difference between data and the total expected background with the corresponding statistical and total uncertainty.

control region and applied in the signal regions. Therefore, the acceptance ratio between signal and control regions is affected by theoretical uncertainties in the simulated $t\bar{t}$ sample. These uncertainties are estimated by considering five sources: the matrix element generator used for the $t\bar{t}$ simulation and the matching scheme used to match the NLO matrix element with the parton shower, the parton shower modelling, the initial-state (Initial State Radiation, ISR) and final-state (Final State Radiation, FSR) gluon emission modelling, the dependence on the choice of the PDF set and the dependence on the renormalisation and factorisation scales. Matrix element generator and matching systematic uncertainties are computed by comparing samples generated by aMC@NLO [30] and Powheg, both interfaced with Herwig++ for showering and fragmentation. Parton shower systematic

JHEP04(2019)092

Source	*non-res* (%)	*m500* and *low-mass* (%)	*high-mass* (%)
Matrix element	7	0.5	4
Parton shower	4	16	10
ISR/FSR	15	5	8
PDF	5	3	6
Scale	3	2	4
Total	18	17	15

Table 5. Percentage uncertainties from $t\bar{t}$ modelling on the $t\bar{t}$ background contributions in all signal regions of the resolved analysis.

Source	*non-res* (%)		*m500 and low-mass* (%)		*high-mass* (%)	
	SR	CR	SR	CR	SR	CR
Modelling/Parton Shower	40	40	40	40	20	20
PDF	30	7	40	10	30	20
Scale	20	30	20	30	30	30

Table 6. Theoretical percentage uncertainties on the predicted W/Z+jets event yield in the top control regions and the signal regions for all selections.

uncertainties are computed by comparing samples generated using Powheg+Pythia6 and Powheg+Herwig++. Initial-state and final-state radiation systematic uncertainties are computed by varying the generator parameters from their nominal values to increase or decrease the amount of radiation. The PDF uncertainties are computed using the eigenvectors of the CT10 PDF set. Uncertainties due to missing higher-order corrections, labelled scale uncertainties, are computed by independently scaling the renormalisation and factorisation scales in aMC@NLO+Herwig++ by a factor of two, while keeping the renormalisation/factorisation scaling ratio between 1/2 and 2. These systematic uncertainties are summarised in table 5.

Uncertainties in the modelling of W+jets background are computed in each signal region (SR) and top control region (CR). Three sources of uncertainty are considered: scale variation, PDF set variation and generator modelling uncertainties. Scale uncertainties are computed by scaling the nominal renormalisation and factorisation scales by a factor of two. PDF uncertainties are computed using the NNPDF [40] error set, while generator modelling uncertainties are obtained by comparing the nominal Sherpa-generated sample with a sample generated with Alpgen [67] and showered with Pythia6 [43]. The values obtained in each region are summarised in table 6.

For the data-driven multijet background, three sources of uncertainty are identified. The non-closure correction term F is computed using data at an early stage of the selection sequence, where contamination by the signal can be considered negligible. Its difference from the value obtained using a simulated multijet event sample is 40% and is assigned as an

JHEP04(2019)092

uncertainty in the multijet estimation. The F value can be affected by the analysis selection requirements. A systematic uncertainty (extrapolation uncertainty) is added by comparing the maximum variation among the F values evaluated after each selection requirement. Finally, the uncertainty due to the dependence of the F value on lepton flavour (flavour uncertainty) is computed as the maximum difference between the nominal F value and the F value calculated for electrons and muons separately. The extrapolation (flavour) uncertainty is found to be 16% (9%) for the *non-res* selection, 32% (9%) for the *m500* and *low-mass* resonant selections, and 45% (6%) for the *high-mass* resonant selection.

Single-top-quark production is one of the smaller backgrounds in this analysis. Theoretical cross-section uncertainties vary from 5% for associated Wt production to 4% for s- and t-channel single-top production. The largest of these is conservatively assigned to all single-top production modes. Further modelling systematic uncertainties are calculated by employing the difference between the nominal sample using the Diagram Removal scheme described in ref. [68] and a sample using the Diagram Subtraction scheme for the dominant single-top production mode, Wt. The uncertainties are 50%, for the *non-res*, *m500* and *low-mass* analyses, and 80% for the *high-mass* analysis.

Systematic uncertainties in the signal acceptance are computed by varying the renormalisation and factorisation scales with a variation of up to a factor of two, and using the same procedure as for the $t\bar{t}$ background. PDF uncertainties are computed using PDF4LHC15_30 [69] PDF sets, which include the envelope of three PDF sets, namely CT14, MMHT14, NNPDF3.0. The resulting uncertainties are less than 1.1% for the scale and less than 1.3% for the PDFs. Parton shower uncertainties are computed by comparing the Herwig++ showering with that of Pythia8, and this results in less than 2% uncertainty.

The detector-related systematic uncertainties affect both the background estimate and the signal yield. In this analysis the largest of these uncertainties are related to the jet energy scale (JES), jet energy resolution (JER), b-tagging efficiencies and mis-tagging rates. The JES uncertainties for the small-R jets are derived from $\sqrt{s} = 13$ TeV data and simulations [70], while the JER uncertainties are extrapolated from 8 TeV data using MC simulations [71]. The uncertainty due to b-tagging is evaluated following the procedure described in ref. [60]. The uncertainties associated with lepton reconstruction and energy measurements have a negligible impact on the final results. All lepton and jet measurement uncertainties are propagated to the calculation of $E_{\mathrm{T}}^{\mathrm{miss}}$, and additional uncertainties are included in the scale and resolution of the soft term. The overall impact of the $E_{\mathrm{T}}^{\mathrm{miss}}$ soft-term uncertainties is also small. Finally, the uncertainty in the combined integrated luminosity is 3.2% [72].

5 Boosted analysis

5.1 Boosted analysis: event selection

As in the resolved analysis, data used in the boosted analysis were recorded by single-lepton triggers, and only events that contain at least one reconstructed electron or muon matching the trigger lepton candidate are analysed. Requirements on p_{T}, $|d_0|/\sigma_{d_0}$ and $|z_0 \sin\theta|$ of the lepton tracks are also the same as in the resolved analysis.

JHEP04(2019)092

Events are required to have at least one large-R jet with an angular distance $\Delta R > 1.0$ from the reconstructed lepton. The highest-p_{T} large-R jet is identified as the $H \to b\bar{b}$ candidate. The large-R jet mass is required to be between 30 GeV and 300 GeV. In order to reconstruct the $H \to WW^*$ system, events with at least two small-R jets with an angular distance $\Delta R > 1.4$ from the $H \to b\bar{b}$ candidate are selected. The hadronically and leptonically decaying W bosons are then reconstructed following the same algorithm as in the resolved analysis. In order to reduce the $t\bar{t}$ background, events are rejected if they contain any small-R jet passing the b-tagging requirement on the small-R jet as described in section 3.

Signal regions (SR) are defined with at least two associated track jets within the large-R jet and requiring that the two highest-p_{T} track jets pass the b-tagging requirement on track jets as described in section 3. The large-R jet mass must be between 90 GeV and 140 GeV. An additional requirement of $E_{\mathrm{T}}^{\mathrm{miss}} > 50\,\mathrm{GeV}$ is imposed to reject multijet backgrounds. For narrow-width scalar signals, the selection efficiency ranges between 3% and 0.6% for masses from 1000 GeV to 3000 GeV. Similarly, for graviton signals with c=1.0 (c=2.0), the selection efficiency ranges between 3% (3%) and 0.4% (0.8%) for masses from 1000 GeV to 3000 GeV. In order to assess the modelling of the dominant $t\bar{t}$ background, a validation region (VR) is defined outside the large-R jet signal region mass window and labelled top VR. Any event with a large-R jet mass $m_{\text{Large-}R\text{ jet}} < 90$ GeV or $m_{\text{Large-}R\text{ jet}} > 140$ GeV falls in the top VR. By construction, the top VR is orthogonal to the SR.

5.2 Boosted analysis: background determination

In the boosted analysis the presence of a signal is indicated by an excess of events above the SM prediction of the background m_{HH} distribution at the end of the event selection. Similarly to the resolved analysis, the $t\bar{t}$ process is the dominant background. Therefore, a dedicated validation region is used to check its modelling as defined in section 5.1. The event yields from $t\bar{t}$, W/Z+jets, single-top-quark and diboson processes in the signal region and the top VR are modelled using simulation and normalised to the expected SM cross section described in section 2.

The multijet component of the background is estimated using the data-driven method as in the resolved analysis. In the boosted analysis a higher requirement on $E_{\mathrm{T}}^{\mathrm{miss}}$ ($E_{\mathrm{T}}^{\mathrm{miss}} > 50$ GeV) is applied, while the cut on $|d_0|/\sigma_{d_0}$ is the same. For the boosted analysis, the correlation between $|d_0|/\sigma_{d_0}$ and $E_{\mathrm{T}}^{\mathrm{miss}}$ is estimated in multiple MC background samples and also in data, and it is found to be negligible. Hence, the multijet yield in region A can be estimated using the relation $N_{\mathrm{A}} = N_{\mathrm{C}} N_{\mathrm{B}}/N_{\mathrm{D}}$. The multijet estimation is performed separately for the muon and the electron channel. The $N_{\mathrm{B}}/N_{\mathrm{D}}$ ratio is calculated inclusively in the large-R jet mass distribution. The m_{HH} distribution of the multijet background is estimated by subtracting the prompt-lepton MC backgrounds from the data in the 1-tag region, where the 1-tag region is defined as the region where all selections are applied except that the large-R jet is required to have only one track jet tagged as a b jet.

The modelling of the background is checked in the top VR. Table 7 reports the numbers of observed and predicted background events in the top VR, showing good agreement between the two. In order to check the validity of the multijet background determination, the m_{T} distribution is shown in figure 6. This variable is particularly sensitive to the

JHEP04(2019)092

Process	Events
$t\bar{t}$	1000 ± 21
W+jets	570 ± 10
Multijet	380 ± 20
Single top	160 ± 7
Dibosons	40 ± 3
Z+jets	56 ± 2
Background sum	2206 ± 31
Data	2179

Table 7. Predicted and observed event yields in the top VR for the boosted analysis. The uncertainty shown for the multijet background is due to the number of data events in the C region. For all other backgrounds the uncertainties are due to the finite MC sample sizes.

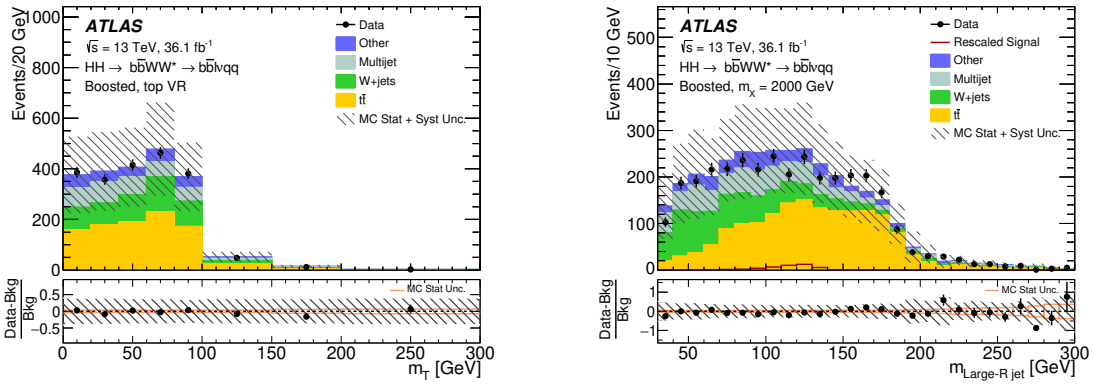

Figure 6. The m_{T} distribution (left) in the top VR, and inclusive $m_{\text{Large-}R\text{ jet}}$ distribution (right) after applying all selections. The signal distribution is negligible in the left plot, while in the right plot it has been scaled to the expected upper-limit cross section reported in section 6. The lower panel shows the fractional difference between data and the total expected background with the corresponding statistical and total uncertainty.

multijet background contamination. Additionally, the $m_{\text{Large-}R\text{ jet}}$ variable used to define the signal region and the top VR is shown in the same figure. The data and predicted background agree well, which builds confidence in the estimated efficiency of the $m_{\text{Large-}R\text{ jet}}$ requirement for signal and background.

5.3 Boosted analysis: systematic uncertainties

The evaluation of detector modelling uncertainties in the boosted analysis follows the same approach as in the resolved analysis. The significant additions to those described in section 4.3 are the uncertainties related to the large-R jets. The large-R jet energy resolution and scale, and jet mass resolution and scale uncertainties are derived *in situ* from 8 TeV pp collision data, taking into account MC simulation extrapolations for the

JHEP04(2019)092

Source	Uncertainty (%)
Matrix element	7.1
Parton shower	7.8
ISR/FSR	8.4
PDF	1.9
Scale	5.0
Total	14.5

Table 8. Uncertainties from different sources in the predicted yield of the $t\bar{t}$ background in the signal region of the boosted analysis.

different detector and beam conditions present in 8 and 13 TeV data-taking periods [73]. The uncertainty in the b-tagging efficiency for track jets is evaluated with the same method used for resolved calorimeter jets. The impact of these uncertainties on the final fit are shown in table 13.

All SM backgrounds, except multijet, are modelled using MC simulation. Therefore, predicted yields in both the signal and the top validation regions are affected by theoretical uncertainties. These uncertainties are computed following the same procedure as in the resolved analysis for $t\bar{t}$, W/Z+jets, single-top-quark and diboson backgrounds. For the $t\bar{t}$ background in the signal region, the uncertainties are summarised in table 8. The uncertainties on single top quark production range from 20% for ISR/FSR to 70%, stemming from the difference between the diagram removal and diagram subtraction schemes. Uncertainties in the modelling of W/Z+jets background range from 10% stemming from PDF uncertainties to 45% stemming from scale uncertainties. Diboson processes have a negligible impact on the total background.

For the normalisation of the multijet background predicted in region A (See section 5.2), several sources of uncertainty are considered. The uncertainties in the normalisation of $t\bar{t}$ and W/Z+jets in regions B, C and D contribute a systematic uncertainty of 25% and 30% respectively. The relative difference between the large-R jet mass acceptance in the 1-tag region C and in the 2-tag region C accounts for 15%. The propagation of the statistical uncertainty in the multijet yield in region C and the uncertainty in the $N_{\mathrm{B}}/N_{\mathrm{D}}$ ratio contribute about 23%. The propagation of detector modelling systematic uncertainties, including the modelling uncertainty of the $|d_0|/\sigma_{d_0}$ requirement and of the MC backgrounds with prompt leptons subtracted from data in regions B, D and C, contribute about 45%. As an additional check on the prediction of the multijet yield with the ABCD method, a conditional background-only likelihood fit of the large-R jet mass distribution is performed in the VR. The difference between the multijet yield estimated with this method and the ABCD prediction is assigned as an uncertainty. This error accounts for 23% of the total uncertainty in the multijet estimation. All different sources of uncertainty are treated as independent and added in quadrature for the final uncertainty of 80% in the multijet normalisation.

JHEP04(2019)092

For the simulated backgrounds, the systematic uncertainty in the m_{HH} distribution shape is determined by comparing the nominal MC sample with the corresponding alternative (variation) MC samples described in section 4.3. The shape systematic uncertainty is determined by fitting a first-order polynomial to the ratio of the variation m_{HH} distribution to the nominal m_{HH} distribution, while keeping the same normalisation. For the data-driven multijet background, the uncertainty in the m_{HH} distribution shape is determined by comparing the shapes in the 2-tag and 1-tag C regions.

Theoretical systematic uncertainties in the signal acceptance are computed following the same algorithm as the resolved analysis. The resulting uncertainties are less than 0.5% for uncertainties due to missing higher-order corrections (labelled scale), less than 0.5% for those due to PDFs, and approximately 2% (5%) in the lower (higher) mass range for those due to the parton shower.

6 Results

Resolved and boosted analyses have non-trivial event overlap. In fact, a set of energy deposits in the calorimeter can be reconstructed both as two jets of $\Delta R = 0.4$ and one Large-R jet with $\Delta R = 1.0$. Due to this difficulty the two analyses are not statistically combined. The results from each analysis for the entire explored mass range are presented here. For the non-resonant signal search, only the resolved analysis is used. For the resonance search, the sensitivity of the analyses vary as a function of the resonance mass. This dependence is different for the narrow scalar search and the RS graviton search.

In the following, section 6.1 describes the resolved analysis and provides results of the non-resonant signal search and of the resonant signal search for the *m500*, the *low-mass* and the *high-mass* selections. Section 6.2 provides results for the resonant signal search in the boosted selection for both the narrow scalar and the RS graviton signal models. Section 6.3 summarises the final results, both for the non-resonant case and for the resonant case. In the resonant case, for each mass point, the result of the analysis having the best sensitivity is presented.

6.1 Resolved analysis

The resolved analysis is described in detail in section 4. The event selection is described in section 4.1 and summarised in table 2. For each selected event, the invariant mass of the HH system (m_{HH}) is reconstructed and its distribution is shown in figure 7 for the *non-res* and the *m500* analyses, and in figure 8 for the *low-mass* and the *high-mass* analyses. Data are generally in good agreement with the expected background predictions within the total uncertainty. The signal m_{HH} distribution is shown in the figure for the non-resonant, the scalar resonance, and the two graviton hypotheses with $c = 1.0$ and $c = 2.0$. Because the scalar-resonance samples are simulated in the narrow-width approximation, the reconstructed resonance width is exclusively due to the detector resolution. The same holds for graviton samples with $c = 1.0$, while $c = 2.0$ graviton samples have a significant intrinsic width that leads to a loss of sensitivity.

JHEP04(2019)092

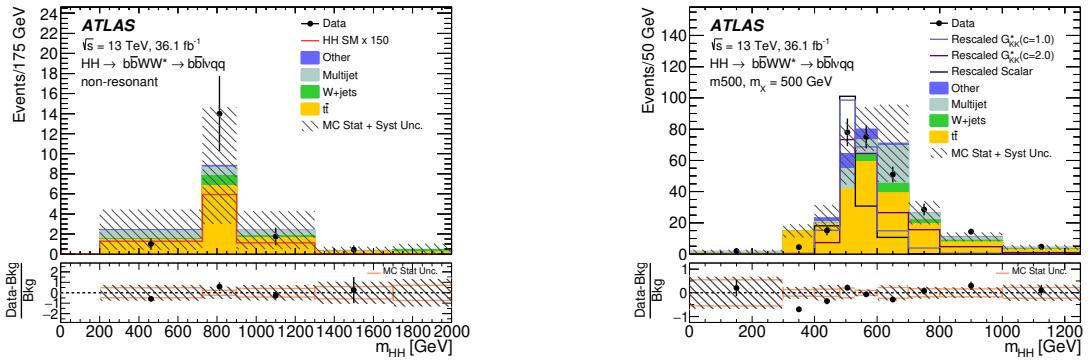

Figure 7. m_{HH} distributions for non-resonant and *m500* selections in the resolved analysis. For each selection the corresponding signal hypothesis, non-resonant, scalar resonance, and graviton with $c = 1.0$ and $c = 2.0$, is shown. For scalar and graviton signals, resonances with mass 500 GeV are shown. The lower panel shows the fractional difference between data and the total expected background with the corresponding statistical and total uncertainty. The non-resonant signal is multiplied by a factor of 150 with respect to the expected SM cross section. The scalar signal is multiplied by a factor of 5, the graviton $c = 1.0$ by a factor of 5 and the graviton $c = 2.0$ by a factor of 1 with respect to the expected upper-limit cross section reported in section 6.

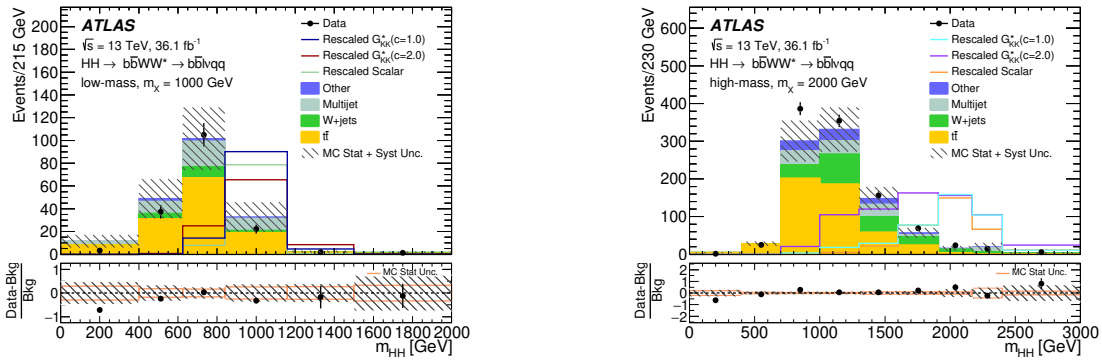

Figure 8. m_{HH} distributions in the resolved analysis selections. For each selection the corresponding signal hypothesis, scalar resonance, and graviton with $c = 1.0$ and $c = 2.0$, and mass 1000 (2000) GeV for the *low-mass* (*high-mass*) analysis, are shown. The lower panel shows the fractional difference between data and the total expected background with the corresponding statistical and total uncertainty. In the plot on the left the scalar signal is multiplied by a factor of 8, the graviton $c = 1.0$ by a factor of 10 and the graviton $c = 2.0$ by a factor of 2 with respect to the expected upper-limit cross section reported in section 6; for the plot on the right the multiplying factors are 20 for the scalar signal, 10 for the graviton $c = 1.0$ signal and 5 for the graviton $c = 2.0$ signal.

JHEP04(2019)092

The m_{HH} distribution is sampled with resonance-mass-dependent m_{HH} requirements as reported in table 3. The numbers of events in the signal and control regions (the $t\bar{t}$ control region and the C region of the multijet estimation procedure) are simultaneously fit using a maximum-likelihood approach. The fit includes six contributions: signal, W+jets, Z+jets, $t\bar{t}$, single-top-quark production, diboson and multijet. The $t\bar{t}$ and multijet normalisations are free to float, the C region of the ABCD method being directly used in the fit, while the diboson, W+jets and Z+jets backgrounds are constrained to the expected SM cross sections within their uncertainties.

The fit is performed after combining the electron and muon channels. Statistical uncertainties due to the limited sample sizes of the simulated background processes are taken into account in the fit by means of nuisance parameters, which are parameterised by Poisson priors. Systematic uncertainties are taken into account as nuisance parameters with Gaussian constraints. For each source of systematic uncertainty, the correlations across bins and between different kinematic regions, as well as those between signal and background, are taken into account. Table 9 shows the post-fit number of predicted backgrounds, observed data, and the signal events normalised to the expected upper limit cross sections. Expected event yields vary across mass because of varying selections. For instance, the requirement on $p_{\mathrm{T}}^{b\bar{b}}$ is higher in *non-res* selection than in *low-mass* selection. Similarly, even within *low-mass* or *high-mass* selection, the requirement on m_{HH} vary across mass.

No significant excess over the expectation is observed and the results are used to evaluate an upper limit at the 95% confidence level (CL) on the production cross section times the branching fraction for the signal hypotheses under consideration. The exclusion limits are calculated with a modified frequentist method [74], also known as $\mathrm{CL_s}$, and the profile-likelihood test statistic [75]. None of the considered systematic uncertainties is significantly constrained or pulled in the likelihood fit. In the non-resonant signal hypothesis the observed (expected) upper limit on the $\sigma(pp \to HH) \times \mathcal{B}(HH \to b\bar{b}WW^*)$ at 95% CL is:

$$\sigma(pp \to HH) \cdot \mathcal{B}(HH \to b\bar{b}WW^*) < 2.5 \left(2.5^{+1.0}_{-0.7}\right) \text{ pb}.$$

The branching fraction $\mathcal{B}(HH \to b\bar{b}WW^*) = 2 \times \mathcal{B}(H \to b\bar{b}) \times \mathcal{B}(H \to WW^*) = 0.248$ is used to obtain the following observed (expected) limit on the HH production cross section at 95% CL:

$$\sigma(pp \to HH) < 10 \left(10^{+4}_{-3}\right) \text{ pb},$$

which corresponds to 300 $\left(300^{+100}_{-80}\right)$ times the SM predicted cross section. Including only the statistical uncertainty, the expected upper limit for the non-resonant production is 190 times the SM prediction. This result, when compared with other HH decay channels, is not competitive. This is mainly due to the similarity of the reconstructed m_{HH} spectrum between the non-resonant SM signal and the $t\bar{t}$ background that makes the separation between the two processes difficult.

Figure 9 shows the expected and observed limit curves for the production cross section of a scalar S and graviton G^*_{KK} particle. The graviton case is studied for the two values of the model parameter c described previously. Different selections are used in different resonance mass ranges without attempting to statistically combine them. The switch from

JHEP04(2019)092

Resonant analysis					
m_X [GeV]	S	G^*_{KK} ($c = 1.0$)	G^*_{KK} ($c = 2.0$)	Total Bkg.	Data
500	18 ± 5	20 ± 5	18 ± 5	19 ± 6	26
600	13 ± 2	15 ± 2	13 ± 2	17 ± 6	16
700	16 ± 2	17 ± 2	16 ± 2	25 ± 8	22
750	20 ± 2	22 ± 2	20 ± 2	22 ± 9	27
800	18.4 ± 1.5	19.7 ± 1.6	18.2 ± 1.5	20 ± 8	28
900	16.3 ± 1.6	17.0 ± 1.7	16.1 ± 1.6	20 ± 7	23
1000	12.0 ± 1.3	12.3 ± 1.4	11.9 ± 1.3	14 ± 5	11
1100	9.6 ± 1.2	9.8 ± 1.2	9.5 ± 1.1	8 ± 3	8
1200	8.1 ± 0.9	8.2 ± 0.9	8.1 ± 0.9	6 ± 3	5
1300	5.1 ± 0.7	5.1 ± 0.7	6.2 ± 0.8	3.5 ± 1.8	1
1400	4.3 ± 0.3	4.1 ± 0.3	4.0 ± 0.3	1.1 ± 0.2	0
1500	3.5 ± 0.3	3.5 ± 0.3	3.5 ± 0.3	1.1 ± 0.2	0
1600	3.1 ± 0.3	3.1 ± 0.3	3.2 ± 0.3	0.4 ± 0.3	1
1800	14.1 ± 1.8	14 ± 2	14 ± 2	17 ± 5	21
2000	8.7 ± 1.0	8.9 ± 1.0	8.8 ± 1.0	8 ± 3	9
2250	7.9 ± 1.1	8.2 ± 1.2	8.2 ± 1.2	6 ± 2	7
2500	5.5 ± 0.8	5.6 ± 0.8	5.6 ± 0.8	3.3 ± 1.4	3
2750	5.7 ± 1.0	6.1 ± 1.1	6.0 ± 1.1	3.1 ± 1.3	3
3000	4.3 ± 0.7	4.6 ± 0.7	4.5 ± 0.7	2.1 ± 1.0	1

Non-resonant analysis		
Rescaled SM signal	Total Bkg.	Data
17 ± 2	21 ± 8	22

Table 9. Data event yields, and post-fit signal and background event yields in the final signal region for the non-resonant analysis and the resonant analysis in the 500–3000 GeV mass range. The errors shown are the MC statistical and systematic uncertainties described in section 4.3. The yields are shown for three signal models: a scalar (S) and two Randall-Sundrum gravitons with $c = 1.0$ and $c = 2.0$ (G^*_{KK}). Signal event yields are normalised to the expected upper-limit cross section.

one selection to another is performed based on the best expected limit for that resonance mass. The outcome of this procedure is that the *m500* selection is used to set limits on resonances of mass of 500 GeV, the *low-mass* selection is used up to masses of 1600 GeV, while the *high-mass* selection is used in the mass range 1600–3000 GeV.

Overall, the resolved analysis is most sensitive for a mass value of 1300 GeV with an expected upper limit of 0.35 pb on $\sigma(pp \to HH)$. At this mass the observed exclusion limit is 0.2 pb. In both the non-resonant and resonant cases, the impact of the systematic

JHEP04(2019)092

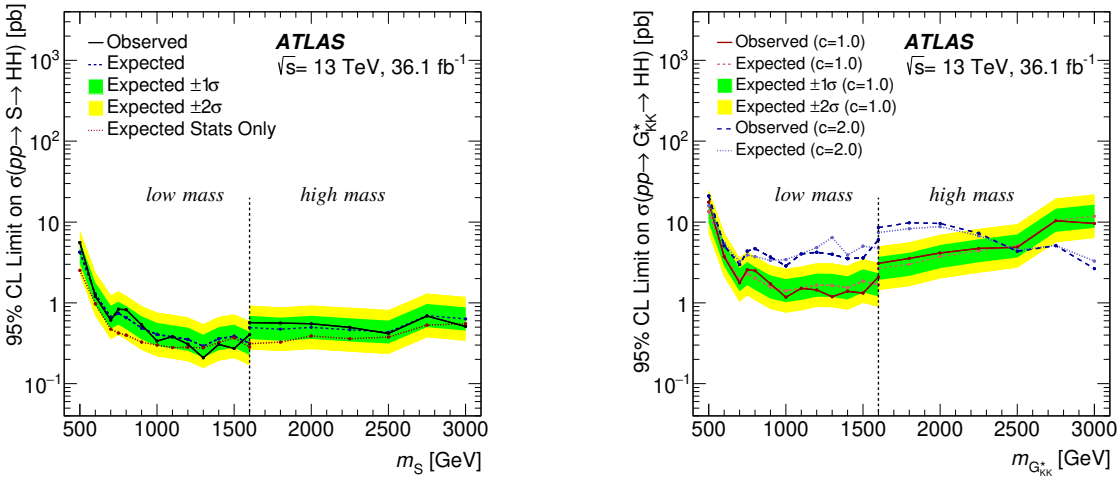

Figure 9. Expected and observed upper limit at 95% CL on the cross section of resonant pair production for the resolved analysis in the heavy scalar boson S model (left) and the spin-2 graviton model in two c parameter hypotheses (right). The left plot also shows the expected limit without including the systematic errors in order to show their impact. The impact of systematic errors is similar for the graviton models.

uncertainties is observed to be large. In order to quantify the impact of the systematic uncertainties, a fit is performed where the estimated signal yield, normalised to an arbitrary cross-section value, is multiplied by a scaling factor α_{sig}, which is treated as the parameter of interest in the fit. The fit is performed using pseudo-data and the contribution to the uncertainty in α_{sig} from several sources is determined. The contribution of the statistical uncertainty to the total uncertainty in α_{sig}, shown in table 10, is decomposed into signal region statistics, top CR statistics and multijet CR statistics. The contribution of the systematic uncertainties to the total uncertainty is decomposed into the dominant components and shown in table 11. The dominant systematic uncertainties vary across the mass range, but some of the most relevant ones are due to $t\bar{t}$ modelling, b-tagging systematic uncertainties, and those related to jet measurements.

JHEP04(2019)092

Statistical source	Resolved analysis			
	Non-Res (%)	500 GeV (%)	1000 GeV (%)	2000 GeV (%)
Signal region	+60/–40	+60/–60	+70/–60	+80/–70
Top control region	+40/–30	+28/–30	+20/–12	+13/–13
Multijet control region	+40/–30	+24/–26	+30/–30	+30/–30
Total statistical	+80/–60	+70/–70	+80/–70	+90/–80

Table 10. Statistical contribution (in percentage) to the total error in the scaling factor α_{sig} for the non-resonant signal and three scalar-signal mass hypotheses, 500 GeV, 1000 GeV and 2000 GeV, in the resolved analysis. The values are extracted by calculating the difference in quadrature between the total statistical error and the error obtained after setting constant the normalisation factor of the background that dominates the region of interest.

Systematic source	Resolved analysis			
	Non-Res (%)	500 GeV (%)	1000 GeV (%)	2000 GeV (%)
$t\bar{t}$ modelling ISR/FSR	+30/–20	+10/–5	+7 / –4	+2/–2
Multijet uncertainty	+10/–10	+20/–10	+20 / –20	+30/–30
$t\bar{t}$ Matrix Element	+10/–10	—	—	—
W+jets modelling PDF	+4/–7	+10/–10	+2 / –6	+7/–5
W+jets modelling scale	+9/–10	+9/–4	+9 / –2	+20/–10
W+jets modelling gen.	+10/–8	+10/–10	+9 / –1	+9/–9
$t\bar{t}$ modelling PS	+3/–2	+30/–20	+20 / –20	+2/–2
b tagging	+30/–20	+11/–5	+7 / –6	+30/–30
JES/JER	+13/–20	+20/–20	+50 / –50	+10/–6
$E_{\text{T}}^{\text{miss}}$ soft term res.	+20/–20	+8/–1	+9 / –7	+7/–7
Pile-up reweighting	+3/–10	+5/–3	+9 / –10	+6/–6
Total systematic	+60/–80	+70/–70	+60/–70	+40/–60

Table 11. Systematic contributions (in percentage) to the total error in the scaling factor α_{sig} for the non-resonant signal and three scalar-signal mass hypotheses, 500 GeV, 1000 GeV and 2000 GeV, in the resolved analysis. The first column quotes the source of the systematic uncertainty. The "–" symbol indicates that the specified source is negligible. The contribution is obtained by calculating the difference in quadrature between the total error in α_{sig} and that obtained by setting constant the nuisance parameter(s) relative to the contribution(s) under study.

JHEP04(2019)092

m_X [GeV]	S	G^*_{KK} ($c = 1.0$)	G^*_{KK} ($c = 2.0$)	Total Bkg.	Data
2000	28 ± 0.5	36.4 ± 0.8	43.0 ± 0.7	1255 ± 27	1107

Table 12. Data event yields, and post-fit signal and background event yields in the final signal region for the boosted analysis and the scalar S and graviton ($c = 1.0$ and $c = 2.0$) G^*_{KK} particle hypotheses. The errors shown are the MC statistical and systematic uncertainties described in section 5.3. For illustration a signal mass point of 2000 GeV is reported in the table. The signal samples are normalised to the expected upper limit cross sections.

6.2 Boosted analysis

The boosted analysis applies the selection criteria described in section 5.1. After applying the large-R jet mass requirement $90 < m_{\text{Large-}R\text{ jet}} < 140$ GeV, the m_{HH} distribution is reconstructed and its shape is fit to data using MC signal and background templates. The distribution is fit using 17 bins, with almost uniform width except at low and high m_{HH}, where the bin width is modified in order to have a MC statistical uncertainty smaller than 20%. All backgrounds, except multijet, are simulated using MC generators and normalised using the cross section of the simulated process. The multijet background is estimated using the ABCD method, and its normalisation obtained from this method is kept fixed in the fit. The bias due to possible signal contamination in the ABCD regions was studied and found to have negligible effect on the result. The integral of the m_{HH} distribution for the boosted analysis is shown in table 12.

Systematic uncertainties affecting the m_{HH} shape are parameterised as linear functions of m_{HH}, and the function parameters are treated as nuisance parameters in the fit. Statistical uncertainties due to the limited sample sizes of the simulated background processes are taken into account in the fit by means of further nuisance parameters, which are parameterised by Poisson priors.

The systematic uncertainties included in the fit are described in section 5.3. The contribution of the systematic uncertainties to the total uncertainty is decomposed into the dominant components and summarised in table 13. The most relevant systematic uncertainties are due to the limited size of the MC samples, the $t\bar{t}$ modelling and the b-tagging systematic uncertainties.

Figure 10 shows the m_{HH} distribution for data and the background components for the boosted analysis. Data are generally in good agreement with the background expectations within the quoted systematic errors. The signal m_{HH} distribution is shown in the figure for the scalar resonance, and the two graviton hypotheses with $c = 1.0$ and $c = 2.0$. Figure 11 shows the observed and the expected upper limit on the production cross section of the scalar S and the two graviton ($c = 1.0$ and $c = 2.0$) G^*_{KK} particles.

JHEP04(2019)092

Uncertainty source	Boosted analysis			
	1500 GeV [%]	2000 GeV [%]	2500 GeV [%]	3000 GeV [%]
Data statistics	+50/–52	+59/–61	+64/–66	+70/–72
Total systematic	+87/–85	+81/–79	+76/–75	+71/–69
MC statistics	+42/–48	+42/–50	+39/–48	+39/–49
$t\bar{t}$ modelling	+29/–31	+36/–38	+40/–45	+32/–39
Multijet uncertainty	+11/–14	+19/–23	+16/–20	+11/–16
W+jets modelling	+27/–30	+8/–12	+11/–10	+11/–10
Single-top modelling	+22/–26	+5/–6	+4/–5	+5/–5
b tagging	+31/–19	+36/–22	+36/–17	+34/–14
JES/JER	+14/–14	+6/–6	+14/–11	+7/–9
Large-R jet	+29/–10	+27/–8	+27/–7	+29/–8

Table 13. Statistical and systematic contributions (in percentage) to the total error in the scaling factor α_{sig} in the boosted analysis for four mass hypotheses: 1500 GeV, 2000 GeV, 2500 GeV and 3000 GeV. The first column quotes the source of the uncertainty. The contribution is obtained by calculating the difference in quadrature between the total error in α_{sig} and that obtained by setting constant the nuisance parameter(s) relative to the contribution(s) under study.

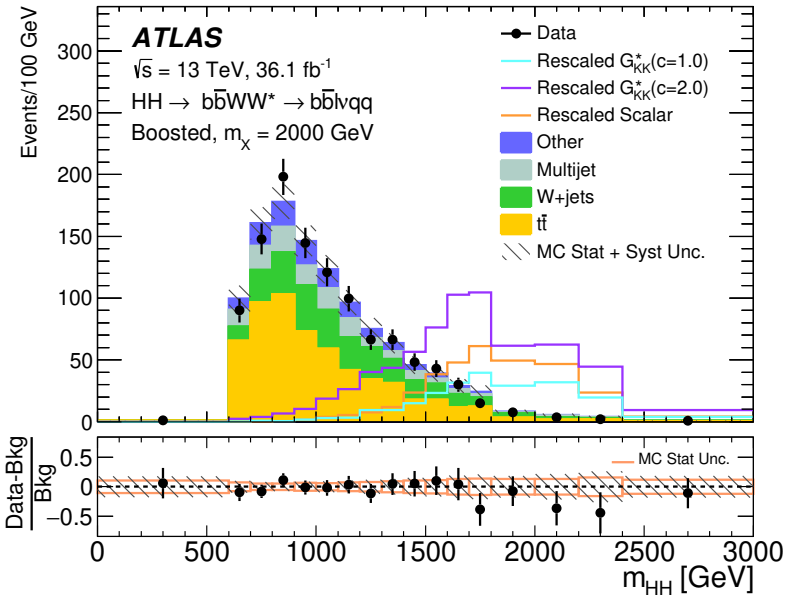

Figure 10. m_{HH} distributions after the global likelihood fit for the boosted analysis. The lower panel shows the fractional difference between data and the total expected background with the corresponding statistical and total uncertainty. The signals shown correspond to resonances of mass 2000 GeV. The scalar signal is multiplied by a factor of 4, and both graviton signal samples by a factor of 20 with respect to the expected upper-limit cross section reported in section 6.

JHEP04(2019)092

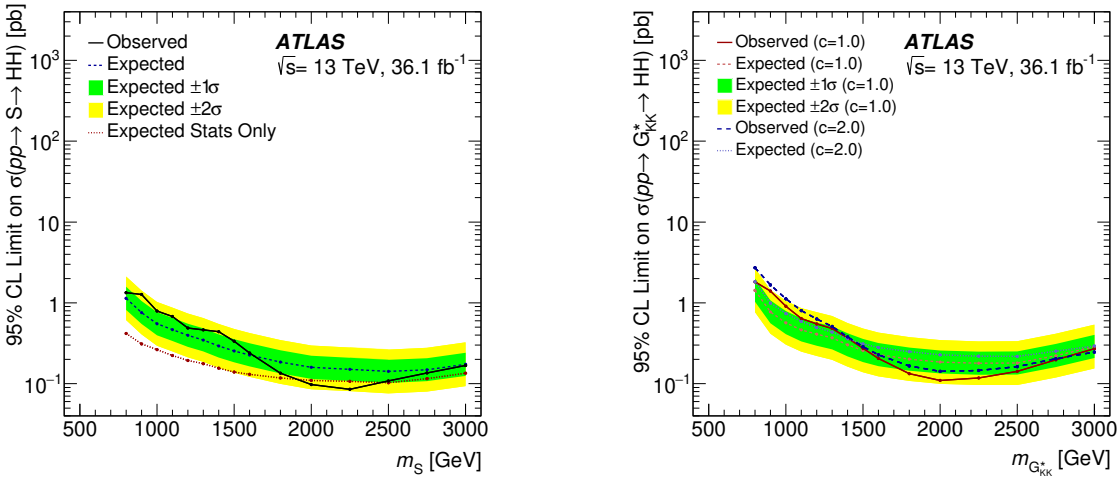

Figure 11. Expected and observed upper limits at 95% CL on the cross section of resonant pair production for the heavy scalar boson S model (left) and for spin-2 graviton model in two c parameter hypotheses (right) in the boosted analysis. The left plot also shows the expected limits without including the systematic errors in order to show their impact. The impact of systematic errors is similar for the graviton models.

6.3 Summary

Results of the two analyses are summarised in figure 12 (left) for the scalar interpretation, and figure 12 (right) for the RS graviton interpretation. The sensitivity of the boosted analysis is higher than the resolved analysis (the expected limit being lower) for masses larger than 1300 GeV in the scalar interpretation, and for masses larger than 800 GeV in the RS graviton interpretation. For masses lower than these values, the limits of the resolved analysis are presented in the figure, otherwise the boosted-analysis limits are shown. In addition, the expected limits of both analyses are shown near the mass values where the switch between the two limit curves occurs.

Finally, the observed upper limits on the production cross sections range from 5.6 pb for $m_X = 500$ GeV to 0.51 pb for $m_X = 3000$ GeV for the scalar signal model. For graviton signals in the same mass interval, they range from 21 pb (18 pb) to 0.28 pb (0.31 pb) for a RS graviton model with $c = 2.0$ (1.0). No boosted analysis was performed for the non-resonant SM signal model.

For the non-resonant signal hypothesis the observed (expected) upper limit on the $\sigma(pp \to HH) \times \mathcal{B}(HH \to b\bar{b}WW^*)$ at 95% CL is:

$$\sigma(pp \to HH) \cdot \mathcal{B}(HH \to b\bar{b}WW^*) < 2.5 \left(2.5^{+1.0}_{-0.7}\right) \text{ pb},$$

which corresponds to 300 $\left(300^{+100}_{-80}\right)$ times the SM predicted cross section.

JHEP04(2019)092

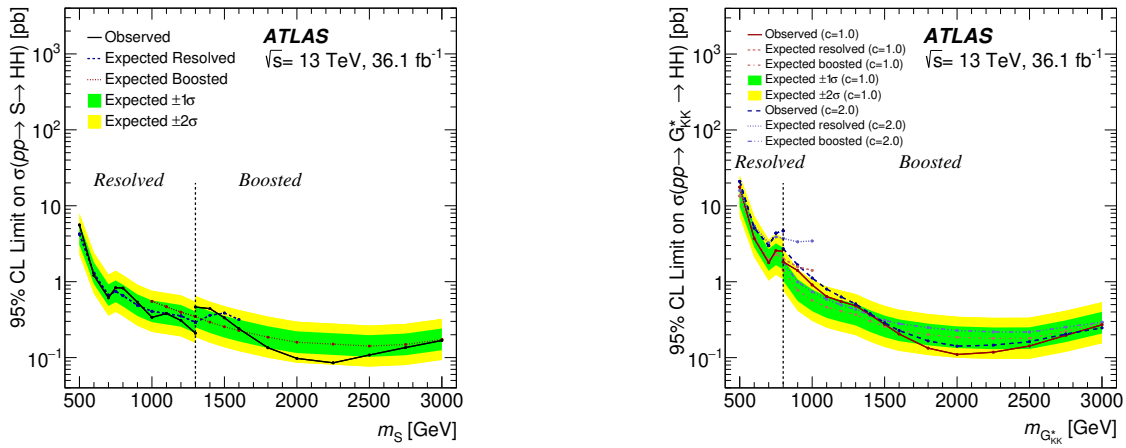

Figure 12. Expected and observed upper limits at 95% CL on the cross-section of the resonant scalar signal model (left) and the resonant graviton signal model for the $c = 1.0$ and $c = 2.0$ hypotheses (right). The observed limits of the scalar and graviton signal models are switched at a mass of 1300 GeV and 800 GeV respectively. The expected limits of both analyses are shown in a region around the switching points. The switching point is chosen at the mass value where the boosted analysis becomes more sensitive than the resolved analysis.

7 Conclusion

A search for resonant and non-resonant Higgs boson pair production in the $b\bar{b}WW^*$ decay mode is performed in the $b\bar{b}\ell\nu qq$ final state using pp collision data corresponding to an integrated luminosity of 36.1 fb^{-1}, collected at $\sqrt{s} = 13$ TeV by the ATLAS detector at the Large Hadron Collider. No evidence of an excess of events over the background expectation is found. Limits are set on resonant production as a function of the resonance mass for a scalar resonance and for spin-2 gravitons in the mass range 500 to 3000 GeV. An upper limit is set on the cross section of non-resonant pair production $\sigma(pp \to HH) \cdot \mathcal{B}(HH \to b\bar{b}WW^*) < 2.5$ pb at 95% CL corresponding to 300 times the predicted SM cross section. Given the result of this work, in order to bring relevant sensitivity improvement to the HH non-resonant SM searches in this channel at the LHC and at future colliders, more advanced analysis techniques, development of new methods for the normalisation of the $t\bar{t}$ background, and a more refined estimation of the multijet background, need to be deployed.

Acknowledgments

We thank CERN for the very successful operation of the LHC, as well as the support staff from our institutions without whom ATLAS could not be operated efficiently.

We acknowledge the support of ANPCyT, Argentina; YerPhI, Armenia; ARC, Australia; BMWFW and FWF, Austria; ANAS, Azerbaijan; SSTC, Belarus; CNPq and FAPESP, Brazil; NSERC, NRC and CFI, Canada; CERN; CONICYT, Chile; CAS, MOST and NSFC, China; COLCIENCIAS, Colombia; MSMT CR, MPO CR and VSC CR, Czech Republic; DNRF and DNSRC, Denmark; IN2P3-CNRS, CEA-DRF/IRFU, France;

JHEP04(2019)092

SRNSFG, Georgia; BMBF, HGF, and MPG, Germany; GSRT, Greece; RGC, Hong Kong SAR, China; ISF and Benoziyo Center, Israel; INFN, Italy; MEXT and JSPS, Japan; CNRST, Morocco; NWO, Netherlands; RCN, Norway; MNiSW and NCN, Poland; FCT, Portugal; MNE/IFA, Romania; MES of Russia and NRC KI, Russian Federation; JINR; MESTD, Serbia; MSSR, Slovakia; ARRS and MIZŠ, Slovenia; DST/NRF, South Africa; MINECO, Spain; SRC and Wallenberg Foundation, Sweden; SERI, SNSF and Cantons of Bern and Geneva, Switzerland; MOST, Taiwan; TAEK, Turkey; STFC, United Kingdom; DOE and NSF, United States of America. In addition, individual groups and members have received support from BCKDF, CANARIE, CRC and Compute Canada, Canada; COST, ERC, ERDF, Horizon 2020, and Marie Skłodowska-Curie Actions, European Union; Investissements d' Avenir Labex and Idex, ANR, France; DFG and AvH Foundation, Germany; Herakleitos, Thales and Aristeia programmes co-financed by EU-ESF and the Greek NSRF, Greece; BSF-NSF and GIF, Israel; CERCA Programme Generalitat de Catalunya, Spain; The Royal Society and Leverhulme Trust, United Kingdom.

The crucial computing support from all WLCG partners is acknowledged gratefully, in particular from CERN, the ATLAS Tier-1 facilities at TRIUMF (Canada), NDGF (Denmark, Norway, Sweden), CC-IN2P3 (France), KIT/GridKA (Germany), INFN-CNAF (Italy), NL-T1 (Netherlands), PIC (Spain), ASGC (Taiwan), RAL (U.K.) and BNL (U.S.A.), the Tier-2 facilities worldwide and large non-WLCG resource providers. Major contributors of computing resources are listed in ref. [76].

References

[1] F. Englert and R. Brout, *Broken symmetry and the mass of gauge vector mesons*, *Phys. Rev. Lett.* **13** (1964) 321 [INSPIRE].

[2] P.W. Higgs, *Broken symmetries, massless particles and gauge fields*, *Phys. Lett.* **12** (1964) 132 [INSPIRE].

[3] P.W. Higgs, *Broken symmetries and the masses of gauge bosons*, *Phys. Rev. Lett.* **13** (1964) 508 [INSPIRE].

[4] G.S. Guralnik, C.R. Hagen and T.W.B. Kibble, *Global conservation laws and massless particles*, *Phys. Rev. Lett.* **13** (1964) 585 [INSPIRE].

[5] P.W. Higgs, *Spontaneous symmetry breakdown without massless bosons*, *Phys. Rev.* **145** (1966) 1156 [INSPIRE].

[6] T.W.B. Kibble, *Symmetry breaking in non-Abelian gauge theories*, *Phys. Rev.* **155** (1967) 1554 [INSPIRE].

[7] LHC Higgs Cross Section Working Group collaboration, *Handbook of LHC Higgs cross sections: 4. Deciphering the nature of the Higgs sector*, arXiv:1610.07922 [INSPIRE].

[8] H.E. Haber and G.L. Kane, *The search for supersymmetry: probing physics beyond the Standard Model*, *Phys. Rept.* **117** (1985) 75 [INSPIRE].

JHEP04(2019)092

[9] G.C. Branco, P.M. Ferreira, L. Lavoura, M.N. Rebelo, M. Sher and J.P. Silva, *Theory and phenomenology of two-Higgs-doublet models*, *Phys. Rept.* **516** (2012) 1 [arXiv:1106.0034] [INSPIRE].

[10] L. Randall and R. Sundrum, *A large mass hierarchy from a small extra dimension*, *Phys. Rev. Lett.* **83** (1999) 3370 [hep-ph/9905221] [INSPIRE].

[11] ATLAS collaboration, *Search for Higgs boson pair production in the $b\bar{b}b\bar{b}$ final state from pp collisions at $\sqrt{s} = 8$ TeV with the ATLAS detector*, *Eur. Phys. J.* **C 75** (2015) 412 [arXiv:1506.00285] [INSPIRE].

[12] CMS collaboration, *Search for resonant pair production of Higgs bosons decaying to two bottom quark-antiquark pairs in proton-proton collisions at 8 TeV*, *Phys. Lett.* **B 749** (2015) 560 [arXiv:1503.04114] [INSPIRE].

[13] ATLAS collaboration, *Searches for Higgs boson pair production in the $hh \to bb\tau\tau$, $\gamma\gamma WW^*$, $\gamma\gamma bb$, bbbb channels with the ATLAS detector*, *Phys. Rev.* **D 92** (2015) 092004 [arXiv:1509.04670] [INSPIRE].

[14] CMS collaboration, *Searches for a heavy scalar boson H decaying to a pair of 125 GeV Higgs bosons hh or for a heavy pseudoscalar boson A decaying to Zh, in the final states with $h \to \tau\tau$*, *Phys. Lett.* **B 755** (2016) 217 [arXiv:1510.01181] [INSPIRE].

[15] CMS collaboration, *Search for two Higgs bosons in final states containing two photons and two bottom quarks in proton-proton collisions at 8 TeV*, *Phys. Rev.* **D 94** (2016) 052012 [arXiv:1603.06896] [INSPIRE].

[16] ATLAS collaboration, *Search for Higgs boson pair production in the $\gamma\gamma b\bar{b}$ final state using pp collision data at $\sqrt{s} = 8$ TeV from the ATLAS detector*, *Phys. Rev. Lett.* **114** (2015) 081802 [arXiv:1406.5053] [INSPIRE].

[17] ATLAS collaboration, *Search for pair production of Higgs bosons in the $b\bar{b}b\bar{b}$ final state using proton-proton collisions at $\sqrt{s} = 13$ TeV with the ATLAS detector*, *JHEP* **01** (2019) 030 [arXiv:1804.06174] [INSPIRE].

[18] ATLAS collaboration, *Search for resonant and non-resonant Higgs boson pair production in the $b\bar{b}\tau^+\tau^-$ decay channel in pp collisions at $\sqrt{s} = 13$ TeV with the ATLAS detector*, *Phys. Rev. Lett.* **121** (2018) 191801 [*Erratum ibid.* **122** (2019) 089901] [arXiv:1808.00336] [INSPIRE].

[19] CMS collaboration, *Search for heavy resonances decaying into two Higgs bosons or into a Higgs boson and a W or Z boson in proton-proton collisions at 13 TeV*, *JHEP* **01** (2019) 051 [arXiv:1808.01365] [INSPIRE].

[20] ATLAS collaboration, *Search for Higgs boson pair production in the $\gamma\gamma b\bar{b}$ final state with 13 TeV pp collision data collected by the ATLAS experiment*, *JHEP* **11** (2018) 040 [arXiv:1807.04873] [INSPIRE].

[21] ATLAS collaboration, *Search for Higgs boson pair production in the $\gamma\gamma WW^*$ channel using pp collision data recorded at $\sqrt{s} = 13$ TeV with the ATLAS detector*, *Eur. Phys. J.* **C 78** (2018) 1007 [arXiv:1807.08567] [INSPIRE].

[22] CMS collaboration, *Search for resonant pair production of Higgs bosons decaying to bottom quark-antiquark pairs in proton-proton collisions at 13 TeV*, *JHEP* **08** (2018) 152 [arXiv:1806.03548] [INSPIRE].

[23] CMS collaboration, *Search for Higgs boson pair production in events with two bottom quarks and two tau leptons in proton-proton collisions at $\sqrt{s} = 13$ TeV*, *Phys. Lett.* **B 778** (2018) 101 [arXiv:1707.02909] [INSPIRE].

JHEP04(2019)092

[24] CMS collaboration, *Search for Higgs boson pair production in the $\gamma\gamma b\bar{b}$ final state in pp collisions at $\sqrt{s} = 13$ TeV*, *Phys. Lett.* **B 788** (2019) 7 [arXiv:1806.00408] [INSPIRE].

[25] CMS collaboration, *Search for resonant and nonresonant Higgs boson pair production in the $b\bar{b}\ell\nu\ell\nu$ final state in proton-proton collisions at $\sqrt{s} = 13$ TeV*, *JHEP* **01** (2018) 054 [arXiv:1708.04188] [INSPIRE].

[26] M. Cacciari, G.P. Salam and G. Soyez, *The anti-k_t jet clustering algorithm*, *JHEP* **04** (2008) 063 [arXiv:0802.1189] [INSPIRE].

[27] ATLAS collaboration, *The ATLAS experiment at the CERN Large Hadron Collider*, 2008 *JINST* **3** S08003 [INSPIRE].

[28] K. Agashe, H. Davoudiasl, G. Perez and A. Soni, *Warped gravitons at the LHC and beyond*, *Phys. Rev.* **D 76** (2007) 036006 [hep-ph/0701186] [INSPIRE].

[29] A.L. Fitzpatrick, J. Kaplan, L. Randall and L.-T. Wang, *Searching for the Kaluza-Klein graviton in bulk RS models*, *JHEP* **09** (2007) 013 [hep-ph/0701150] [INSPIRE].

[30] J. Alwall et al., *The automated computation of tree-level and next-to-leading order differential cross sections and their matching to parton shower simulations*, *JHEP* **07** (2014) 079 [arXiv:1405.0301] [INSPIRE].

[31] R.D. Ball et al., *Parton distributions with LHC data*, *Nucl. Phys.* **B 867** (2013) 244 [arXiv:1207.1303] [INSPIRE].

[32] T. Sjöstrand, S. Mrenna and P.Z. Skands, *A brief introduction to PYTHIA* 8.1, *Comput. Phys. Commun.* **178** (2008) 852 [arXiv:0710.3820] [INSPIRE].

[33] ATLAS collaboration, *ATLAS run* 1 *PYTHIA*8 *tunes*, ATL-PHYS-PUB-2014-021, CERN, Geneva, Switzerland (2014).

[34] M. Bahr et al., *HERWIG++ physics and manual*, *Eur. Phys. J.* **C 58** (2008) 639 [arXiv:0803.0883] [INSPIRE].

[35] H.-L. Lai et al., *New parton distributions for collider physics*, *Phys. Rev.* **D 82** (2010) 074024 [arXiv:1007.2241] [INSPIRE].

[36] B. Hespel, D. Lopez-Val and E. Vryonidou, *Higgs pair production via gluon fusion in the two-Higgs-doublet model*, *JHEP* **09** (2014) 124 [arXiv:1407.0281] [INSPIRE].

[37] R. Frederix et al., *Higgs pair production at the LHC with NLO and parton-shower effects*, *Phys. Lett.* **B 732** (2014) 142 [arXiv:1401.7340] [INSPIRE].

[38] S. Borowka et al., *Higgs boson pair production in gluon fusion at next-to-leading order with full top-quark mass dependence*, *Phys. Rev. Lett.* **117** (2016) 012001 [*Erratum ibid.* **117** (2016) 079901] [arXiv:1604.06447] [INSPIRE].

[39] T. Gleisberg et al., *Event generation with SHERPA* 1.1, *JHEP* **02** (2009) 007 [arXiv:0811.4622] [INSPIRE].

[40] NNPDF collaboration, *Parton distributions for the LHC run II*, *JHEP* **04** (2015) 040 [arXiv:1410.8849] [INSPIRE].

[41] R. Gavin, Y. Li, F. Petriello and S. Quackenbush, *FEWZ* 2.0*: a code for hadronic Z production at next-to-next-to-leading order*, *Comput. Phys. Commun.* **182** (2011) 2388 [arXiv:1011.3540] [INSPIRE].

[42] S. Frixione, P. Nason and C. Oleari, *Matching NLO QCD computations with parton shower simulations: the POWHEG method*, *JHEP* **11** (2007) 070 [arXiv:0709.2092] [INSPIRE].

JHEP04(2019)092

[43] T. Sjöstrand, S. Mrenna and P.Z. Skands, *PYTHIA* 6.4 *physics and manual*, *JHEP* **05** (2006) 026 [hep-ph/0603175] [INSPIRE].

[44] P.Z. Skands, *Tuning Monte Carlo generators: the Perugia tunes*, *Phys. Rev.* **D 82** (2010) 074018 [arXiv:1005.3457] [INSPIRE].

[45] J. Pumplin, D.R. Stump, J. Huston, H.L. Lai, P.M. Nadolsky and W.K. Tung, *New generation of parton distributions with uncertainties from global QCD analysis*, *JHEP* **07** (2002) 012 [hep-ph/0201195] [INSPIRE].

[46] D.J. Lange, *The EvtGen particle decay simulation package*, *Nucl. Instrum. Meth.* **A 462** (2001) 152 [INSPIRE].

[47] ATLAS collaboration, *Comparison of Monte Carlo generator predictions for gap fraction and jet multiplicity observables in top-antitop events*, ATL-PHYS-PUB-2014-005, CERN, Geneva, Switzerland (2014).

[48] M. Czakon and A. Mitov, *Top++: a program for the calculation of the top-pair cross-section at hadron colliders*, *Comput. Phys. Commun.* **185** (2014) 2930 [arXiv:1112.5675] [INSPIRE].

[49] S. Alioli, P. Nason, C. Oleari and E. Re, *NLO single-top production matched with shower in POWHEG: s- and t-channel contributions*, *JHEP* **09** (2009) 111 [*Erratum ibid.* **02** (2010) 011] [arXiv:0907.4076] [INSPIRE].

[50] E. Re, *Single-top Wt-channel production matched with parton showers using the POWHEG method*, *Eur. Phys. J.* **C 71** (2011) 1547 [arXiv:1009.2450] [INSPIRE].

[51] N. Kidonakis, *Next-to-next-to-leading-order collinear and soft gluon corrections for t-channel single top quark production*, *Phys. Rev.* **D 83** (2011) 091503 [arXiv:1103.2792] [INSPIRE].

[52] N. Kidonakis, *Two-loop soft anomalous dimensions for single top quark associated production with a W^- or H^-*, *Phys. Rev.* **D 82** (2010) 054018 [arXiv:1005.4451] [INSPIRE].

[53] N. Kidonakis, *NNLL resummation for s-channel single top quark production*, *Phys. Rev.* **D 81** (2010) 054028 [arXiv:1001.5034] [INSPIRE].

[54] GEANT4 collaboration, *GEANT4: a simulation toolkit*, *Nucl. Instrum. Meth.* **A 506** (2003) 250 [INSPIRE].

[55] ATLAS collaboration, *The ATLAS simulation infrastructure*, *Eur. Phys. J.* **C 70** (2010) 823 [arXiv:1005.4568] [INSPIRE].

[56] ATLAS collaboration, *Electron efficiency measurements with the ATLAS detector using* 2012 *LHC proton-proton collision data*, *Eur. Phys. J.* **C 77** (2017) 195 [arXiv:1612.01456] [INSPIRE].

[57] ATLAS collaboration, *Electron efficiency measurements with the ATLAS detector using the* 2015 *LHC proton-proton collision data*, ATLAS-CONF-2016-024, CERN, Geneva, Switzerland (2016).

[58] ATLAS collaboration, *Muon reconstruction performance of the ATLAS detector in proton-proton collision data at* $\sqrt{s} = 13$ *TeV*, *Eur. Phys. J.* **C 76** (2016) 292 [arXiv:1603.05598] [INSPIRE].

[59] ATLAS collaboration, *Tagging and suppression of pileup jets with the ATLAS detector*, ATLAS-CONF-2014-018, CERN, Geneva, Switzerland (2014).

[60] ATLAS collaboration, *Measurements of b-jet tagging efficiency with the ATLAS detector using* $t\bar{t}$ *events at* $\sqrt{s} = 13$ *TeV*, *JHEP* **08** (2018) 089 [arXiv:1805.01845] [INSPIRE].

JHEP04(2019)092

[61] D. Krohn, J. Thaler and L.-T. Wang, *Jet trimming*, *JHEP* **02** (2010) 084 [arXiv:0912.1342] [INSPIRE].

[62] ATLAS collaboration, *Jet mass reconstruction with the ATLAS detector in early run 2 data*, ATLAS-CONF-2016-035, CERN, Geneva, Switzerland (2016).

[63] ATLAS collaboration, *Performance of jet substructure techniques for large-R jets in proton-proton collisions at* $\sqrt{s} = 7$ *TeV using the ATLAS detector*, *JHEP* **09** (2013) 076 [arXiv:1306.4945] [INSPIRE].

[64] ATLAS collaboration, *Boosted Higgs* $(\to b\bar{b})$ *boson identification with the ATLAS detector at* $\sqrt{s} = 13$ *TeV*, ATLAS-CONF-2016-039, CERN, Geneva, Switzerland (2016).

[65] M. Cacciari, G.P. Salam and G. Soyez, *The catchment area of jets*, *JHEP* **04** (2008) 005 [arXiv:0802.1188] [INSPIRE].

[66] ATLAS collaboration, *Expected performance of missing transverse momentum reconstruction for the ATLAS detector at* $\sqrt{s} = 13$ *TeV*, ATL-PHYS-PUB-2015-023, CERN, Geneva, Switzerland (2015).

[67] M.L. Mangano, M. Moretti, F. Piccinini, R. Pittau and A.D. Polosa, *ALPGEN, a generator for hard multiparton processes in hadronic collisions*, *JHEP* **07** (2003) 001 [hep-ph/0206293] [INSPIRE].

[68] S. Frixione, E. Laenen, P. Motylinski, B.R. Webber and C.D. White, *Single-top hadroproduction in association with a W boson*, *JHEP* **07** (2008) 029 [arXiv:0805.3067] [INSPIRE].

[69] J. Butterworth et al., *PDF4LHC recommendations for LHC run II*, *J. Phys.* **G 43** (2016) 023001 [arXiv:1510.03865] [INSPIRE].

[70] ATLAS collaboration, *Jet energy scale measurements and their systematic uncertainties in proton-proton collisions at* $\sqrt{s} = 13$ *TeV with the ATLAS detector*, *Phys. Rev.* **D 96** (2017) 072002 [arXiv:1703.09665] [INSPIRE].

[71] ATLAS collaboration, *Jet calibration and systematic uncertainties for jets reconstructed in the ATLAS detector at* $\sqrt{s} = 13$ *TeV*, ATL-PHYS-PUB-2015-015, CERN, Geneva, Switzerland (2015).

[72] ATLAS collaboration, *Luminosity determination in pp collisions at* $\sqrt{s} = 8$ *TeV using the ATLAS detector at the LHC*, *Eur. Phys. J.* **C 76** (2016) 653 [arXiv:1608.03953] [INSPIRE].

[73] ATLAS collaboration, *Identification of boosted, hadronically-decaying W and Z bosons in* $\sqrt{s} = 13$ *TeV Monte Carlo simulations for ATLAS*, ATL-PHYS-PUB-2015-033, CERN, Geneva, Switzerland (2015).

[74] A.L. Read, *Presentation of search results: the* CL_s *technique*, *J. Phys.* **G 28** (2002) 2693 [INSPIRE].

[75] G. Cowan, K. Cranmer, E. Gross and O. Vitells, *Asymptotic formulae for likelihood-based tests of new physics*, *Eur. Phys. J.* **C 71** (2011) 1554 [*Erratum ibid.* **C 73** (2013) 2501] [arXiv:1007.1727] [INSPIRE].

[76] ATLAS collaboration, *ATLAS computing acknowledgements*, ATL-GEN-PUB-2016-002, CERN, Geneva, Switzerland (2016).

JHEP04(2019)092

The ATLAS collaboration

M. Aaboud[34d], G. Aad[99], B. Abbott[124], O. Abdinov[13,*], B. Abeloos[128], D.K. Abhayasinghe[91], S.H. Abidi[164], O.S. AbouZeid[39], N.L. Abraham[153], H. Abramowicz[158], H. Abreu[157], Y. Abulaiti[6], B.S. Acharya[64a,64b,o], S. Adachi[160], L. Adam[97], L. Adamczyk[81a], J. Adelman[119], M. Adersberger[112], A. Adiguzel[12c,ag], T. Adye[141], A.A. Affolder[143], Y. Afik[157], C. Agheorghiesei[27c], J.A. Aguilar-Saavedra[136f,136a], F. Ahmadov[77,ae], G. Aielli[71a,71b], S. Akatsuka[83], T.P.A. Åkesson[94], E. Akilli[52], A.V. Akimov[108], G.L. Alberghi[23b,23a], J. Albert[173], P. Albicocco[49], M.J. Alconada Verzini[86], S. Alderweireldt[117], M. Aleksa[35], I.N. Aleksandrov[77], C. Alexa[27b], D. Alexandre[19], T. Alexopoulos[10], M. Alhroob[124], B. Ali[138], G. Alimonti[66a], J. Alison[36], S.P. Alkire[145], C. Allaire[128], B.M.M. Allbrooke[153], B.W. Allen[127], P.P. Allport[21], A. Aloisio[67a,67b], A. Alonso[39], F. Alonso[86], C. Alpigiani[145], A.A. Alshehri[55], M.I. Alstaty[99], B. Alvarez Gonzalez[35], D. Álvarez Piqueras[171], M.G. Alviggi[67a,67b], B.T. Amadio[18], Y. Amaral Coutinho[78b], A. Ambler[101], L. Ambroz[131], C. Amelung[26], D. Amidei[103], S.P. Amor Dos Santos[136a,136c], S. Amoroso[44], C.S. Amrouche[52], F. An[76], C. Anastopoulos[146], L.S. Ancu[52], N. Andari[142], T. Andeen[11], C.F. Anders[59b], J.K. Anders[20], K.J. Anderson[36], A. Andreazza[66a,66b], V. Andrei[59a], C.R. Anelli[173], S. Angelidakis[37], I. Angelozzi[118], A. Angerami[38], A.V. Anisenkov[120b,120a], A. Annovi[69a], C. Antel[59a], M.T. Anthony[146], M. Antonelli[49], D.J.A. Antrim[168], F. Anulli[70a], M. Aoki[79], J.A. Aparisi Pozo[171], L. Aperio Bella[35], G. Arabidze[104], J.P. Araque[136a], V. Araujo Ferraz[78b], R. Araujo Pereira[78b], A.T.H. Arce[47], R.E. Ardell[91], F.A. Arduh[86], J-F. Arguin[107], S. Argyropoulos[75], J.-H. Arling[44], A.J. Armbruster[35], L.J. Armitage[90], A Armstrong[168], O. Arnaez[164], H. Arnold[118], M. Arratia[31], O. Arslan[24], A. Artamonov[109,*], G. Artoni[131], S. Artz[97], S. Asai[160], N. Asbah[57], E.M. Asimakopoulou[169], L. Asquith[153], K. Assamagan[29], R. Astalos[28a], R.J. Atkin[32a], M. Atkinson[170], N.B. Atlay[148], K. Augsten[138], G. Avolio[35], R. Avramidou[58a], M.K. Ayoub[15a], A.M. Azoulay[165b], G. Azuelos[107,at], A.E. Baas[59a], M.J. Baca[21], H. Bachacou[142], K. Bachas[65a,65b], M. Backes[131], P. Bagnaia[70a,70b], M. Bahmani[82], H. Bahrasemani[149], A.J. Bailey[171], J.T. Baines[141], M. Bajic[39], C. Bakalis[10], O.K. Baker[180], P.J. Bakker[118], D. Bakshi Gupta[8], S. Balaji[154], E.M. Baldin[120b,120a], P. Balek[177], F. Balli[142], W.K. Balunas[133], J. Balz[97], E. Banas[82], A. Bandyopadhyay[24], S. Banerjee[178,k], A.A.E. Bannoura[179], L. Barak[158], W.M. Barbe[37], E.L. Barberio[102], D. Barberis[53b,53a], M. Barbero[99], T. Barillari[113], M-S. Barisits[35], J. Barkeloo[127], T. Barklow[150], R. Barnea[157], S.L. Barnes[58c], B.M. Barnett[141], R.M. Barnett[18], Z. Barnovska-Blenessy[58a], A. Baroncelli[72a], G. Barone[29], A.J. Barr[131], L. Barranco Navarro[171], F. Barreiro[96], J. Barreiro Guimarães da Costa[15a], R. Bartoldus[150], A.E. Barton[87], P. Bartos[28a], A. Basalaev[134], A. Bassalat[128], R.L. Bates[55], S.J. Batista[164], S. Batlamous[34e], J.R. Batley[31], M. Battaglia[143], M. Bauce[70a,70b], F. Bauer[142], K.T. Bauer[168], H.S. Bawa[150,m], J.B. Beacham[122], T. Beau[132], P.H. Beauchemin[167], P. Bechtle[24], H.C. Beck[51], H.P. Beck[20,r], K. Becker[50], M. Becker[97], C. Becot[44], A. Beddall[12d], A.J. Beddall[12a], V.A. Bednyakov[77], M. Bedognetti[118], C.P. Bee[152], T.A. Beermann[74], M. Begalli[78b], M. Begel[29], A. Behera[152], J.K. Behr[44], A.S. Bell[92], G. Bella[158], L. Bellagamba[23b], A. Bellerive[33], M. Bellomo[157], P. Bellos[9], K. Belotskiy[110], N.L. Belyaev[110], O. Benary[158,*], D. Benchekroun[34a], M. Bender[112], N. Benekos[10], Y. Benhammou[158], E. Benhar Noccioli[180], J. Benitez[75], D.P. Benjamin[6], M. Benoit[52], J.R. Bensinger[26], S. Bentvelsen[118], L. Beresford[131], M. Beretta[49], D. Berge[44], E. Bergeaas Kuutmann[169], N. Berger[5], L.J. Bergsten[26], J. Beringer[18], S. Berlendis[7], N.R. Bernard[100], G. Bernardi[132], C. Bernius[150], F.U. Bernlochner[24], T. Berry[91], P. Berta[97], C. Bertella[15a], G. Bertoli[43a,43b], I.A. Bertram[87], G.J. Besjes[39], O. Bessidskaia Bylund[179], M. Bessner[44], N. Besson[142], A. Bethani[98], S. Bethke[113], A. Betti[24], A.J. Bevan[90], J. Beyer[113], R. Bi[135], R.M. Bianchi[135], O. Biebel[112], D. Biedermann[19], R. Bielski[35], K. Bierwagen[97],

JHEP04(2019)092

N.V. Biesuz[69a,69b], M. Biglietti[72a], T.R.V. Billoud[107], M. Bindi[51], A. Bingul[12d], C. Bini[70a,70b], S. Biondi[23b,23a], M. Birman[177], T. Bisanz[51], J.P. Biswal[158], C. Bittrich[46], D.M. Bjergaard[47], J.E. Black[150], K.M. Black[25], T. Blazek[28a], I. Bloch[44], C. Blocker[26], A. Blue[55], U. Blumenschein[90], Dr. Blunier[144a], G.J. Bobbink[118], V.S. Bobrovnikov[120b,120a], S.S. Bocchetta[94], A. Bocci[47], D. Boerner[179], D. Bogavac[112], A.G. Bogdanchikov[120b,120a], C. Bohm[43a], V. Boisvert[91], P. Bokan[169], T. Bold[81a], A.S. Boldyrev[111], A.E. Bolz[59b], M. Bomben[132], M. Bona[90], J.S. Bonilla[127], M. Boonekamp[142], H.M. Borecka-Bielska[88], A. Borisov[140], G. Borissov[87], J. Bortfeldt[35], D. Bortoletto[131], V. Bortolotto[71a,71b], D. Boscherini[23b], M. Bosman[14], J.D. Bossio Sola[30], K. Bouaouda[34a], J. Boudreau[135], E.V. Bouhova-Thacker[87], D. Boumediene[37], C. Bourdarios[128], S.K. Boutle[55], A. Boveia[122], J. Boyd[35], D. Boye[32b], I.R. Boyko[77], A.J. Bozson[91], J. Bracinik[21], N. Brahimi[99], A. Brandt[8], G. Brandt[179], O. Brandt[59a], F. Braren[44], U. Bratzler[161], B. Brau[100], J.E. Brau[127], W.D. Breaden Madden[55], K. Brendlinger[44], L. Brenner[44], R. Brenner[169], S. Bressler[177], B. Brickwedde[97], D.L. Briglin[21], D. Britton[55], D. Britzger[113], I. Brock[24], R. Brock[104], G. Brooijmans[38], T. Brooks[91], W.K. Brooks[144b], E. Brost[119], J.H Broughton[21], P.A. Bruckman de Renstrom[82], D. Bruncko[28b], A. Bruni[23b], G. Bruni[23b], L.S. Bruni[118], S. Bruno[71a,71b], B.H. Brunt[31], M. Bruschi[23b], N. Bruscino[135], P. Bryant[36], L. Bryngemark[94], T. Buanes[17], Q. Buat[35], P. Buchholz[148], A.G. Buckley[55], I.A. Budagov[77], M.K. Bugge[130], F. Bührer[50], O. Bulekov[110], D. Bullock[8], T.J. Burch[119], S. Burdin[88], C.D. Burgard[118], A.M. Burger[5], B. Burghgrave[119], K. Burka[82], S. Burke[141], I. Burmeister[45], J.T.P. Burr[131], V. Büscher[97], E. Buschmann[51], P. Bussey[55], J.M. Butler[25], C.M. Buttar[55], J.M. Butterworth[92], P. Butti[35], W. Buttinger[35], A. Buzatu[155], A.R. Buzykaev[120b,120a], G. Cabras[23b,23a], S. Cabrera Urbán[171], D. Caforio[138], H. Cai[170], V.M.M. Cairo[2], O. Cakir[4a], N. Calace[52], P. Calafiura[18], A. Calandri[99], G. Calderini[132], P. Calfayan[63], G. Callea[55], L.P. Caloba[78b], S. Calvente Lopez[96], D. Calvet[37], S. Calvet[37], T.P. Calvet[152], M. Calvetti[69a,69b], R. Camacho Toro[132], S. Camarda[35], D. Camarero Munoz[96], P. Camarri[71a,71b], D. Cameron[130], R. Caminal Armadans[100], C. Camincher[35], S. Campana[35], M. Campanelli[92], A. Camplani[39], A. Campoverde[148], V. Canale[67a,67b], M. Cano Bret[58c], J. Cantero[125], T. Cao[158], Y. Cao[170], M.D.M. Capeans Garrido[35], I. Caprini[27b], M. Caprini[27b], M. Capua[40b,40a], R.M. Carbone[38], R. Cardarelli[71a], F.C. Cardillo[146], I. Carli[139], T. Carli[35], G. Carlino[67a], B.T. Carlson[135], L. Carminati[66a,66b], R.M.D. Carney[43a,43b], S. Caron[117], E. Carquin[144b], S. Carrá[66a,66b], J.W.S. Carter[164], D. Casadei[32b], M.P. Casado[14,g], A.F. Casha[164], D.W. Casper[168], R. Castelijn[118], F.L. Castillo[171], V. Castillo Gimenez[171], N.F. Castro[136a,136e], A. Catinaccio[35], J.R. Catmore[130], A. Cattai[35], J. Caudron[24], V. Cavaliere[29], E. Cavallaro[14], D. Cavalli[66a], M. Cavalli-Sforza[14], V. Cavasinni[69a,69b], E. Celebi[12b], F. Ceradini[72a,72b], L. Cerda Alberich[171], A.S. Cerqueira[78a], A. Cerri[153], L. Cerrito[71a,71b], F. Cerutti[18], A. Cervelli[23b,23a], S.A. Cetin[12b], A. Chafaq[34a], D Chakraborty[119], S.K. Chan[57], W.S. Chan[118], J.D. Chapman[31], B. Chargeishvili[156b], D.G. Charlton[21], C.C. Chau[33], C.A. Chavez Barajas[153], S. Che[122], A. Chegwidden[104], S. Chekanov[6], S.V. Chekulaev[165a], G.A. Chelkov[77,as], M.A. Chelstowska[35], C. Chen[58a], C.H. Chen[76], H. Chen[29], J. Chen[58a], J. Chen[38], S. Chen[133], S.J. Chen[15c], X. Chen[15b,ar], Y. Chen[80], Y-H. Chen[44], H.C. Cheng[61a], H.J. Cheng[15d], A. Cheplakov[77], E. Cheremushkina[140], R. Cherkaoui El Moursli[34e], E. Cheu[7], K. Cheung[62], T.J.A. Chevalérias[142], L. Chevalier[142], V. Chiarella[49], G. Chiarelli[69a], G. Chiodini[65a], A.S. Chisholm[35,21], A. Chitan[27b], I. Chiu[160], Y.H. Chiu[173], M.V. Chizhov[77], K. Choi[63], A.R. Chomont[128], S. Chouridou[159], Y.S. Chow[118], V. Christodoulou[92], M.C. Chu[61a], J. Chudoba[137], A.J. Chuinard[101], J.J. Chwastowski[82], L. Chytka[126], D. Cinca[45], V. Cindro[89], I.A. Cioară[24], A. Ciocio[18], F. Cirotto[67a,67b], Z.H. Citron[177], M. Citterio[66a], A. Clark[52], M.R. Clark[38], P.J. Clark[48], C. Clement[43a,43b], Y. Coadou[99], M. Cobal[64a,64c], A. Coccaro[53b,53a], J. Cochran[76], H. Cohen[158], A.E.C. Coimbra[177], L. Colasurdo[117], B. Cole[38], A.P. Colijn[118], J. Collot[56],

JHEP04(2019)092

P. Conde Muiño[136a,136b], E. Coniavitis[50], S.H. Connell[32b], I.A. Connelly[98], S. Constantinescu[27b], F. Conventi[67a,au], A.M. Cooper-Sarkar[131], F. Cormier[172], K.J.R. Cormier[164], L.D. Corpe[92], M. Corradi[70a,70b], E.E. Corrigan[94], F. Corriveau[101,ac], A. Cortes-Gonzalez[35], M.J. Costa[171], F. Costanza[5], D. Costanzo[146], G. Cottin[31], G. Cowan[91], B.E. Cox[98], J. Crane[98], K. Cranmer[121], S.J. Crawley[55], R.A. Creager[133], G. Cree[33], S. Crépé-Renaudin[56], F. Crescioli[132], M. Cristinziani[24], V. Croft[121], G. Crosetti[40b,40a], A. Cueto[96], T. Cuhadar Donszelmann[146], A.R. Cukierman[150], S. Czekierda[82], P. Czodrowski[35], M.J. Da Cunha Sargedas De Sousa[58b], C. Da Via[98], W. Dabrowski[81a], T. Dado[28a,x], S. Dahbi[34e], T. Dai[103], F. Dallaire[107], C. Dallapiccola[100], M. Dam[39], G. D'amen[23b,23a], J. Damp[97], J.R. Dandoy[133], M.F. Daneri[30], N.P. Dang[178,k], N.D Dann[98], M. Danninger[172], V. Dao[35], G. Darbo[53b], S. Darmora[8], O. Dartsi[5], A. Dattagupta[127], T. Daubney[44], S. D'Auria[66a,66b], W. Davey[24], C. David[44], T. Davidek[139], D.R. Davis[47], E. Dawe[102], I. Dawson[146], K. De[8], R. De Asmundis[67a], A. De Benedetti[124], M. De Beurs[118], S. De Castro[23b,23a], S. De Cecco[70a,70b], N. De Groot[117], P. de Jong[118], H. De la Torre[104], F. De Lorenzi[76], A. De Maria[69a,69b], D. De Pedis[70a], A. De Salvo[70a], U. De Sanctis[71a,71b], M. De Santis[71a,71b], A. De Santo[153], K. De Vasconcelos Corga[99], J.B. De Vivie De Regie[128], C. Debenedetti[143], D.V. Dedovich[77], N. Dehghanian[3], M. Del Gaudio[40b,40a], J. Del Peso[96], Y. Delabat Diaz[44], D. Delgove[128], F. Deliot[142], C.M. Delitzsch[7], M. Della Pietra[67a,67b], D. Della Volpe[52], A. Dell'Acqua[35], L. Dell'Asta[25], M. Delmastro[5], C. Delporte[128], P.A. Delsart[56], D.A. DeMarco[164], S. Demers[180], M. Demichev[77], S.P. Denisov[140], D. Denysiuk[118], L. D'Eramo[132], D. Derendarz[82], J.E. Derkaoui[34d], F. Derue[132], P. Dervan[88], K. Desch[24], C. Deterre[44], K. Dette[164], M.R. Devesa[30], P.O. Deviveiros[35], A. Dewhurst[141], S. Dhaliwal[26], F.A. Di Bello[52], A. Di Ciaccio[71a,71b], L. Di Ciaccio[5], W.K. Di Clemente[133], C. Di Donato[67a,67b], A. Di Girolamo[35], G. Di Gregorio[69a,69b], B. Di Micco[72a,72b], R. Di Nardo[100], K.F. Di Petrillo[57], R. Di Sipio[164], D. Di Valentino[33], C. Diaconu[99], M. Diamond[164], F.A. Dias[39], T. Dias Do Vale[136a], M.A. Diaz[144a], J. Dickinson[18], E.B. Diehl[103], J. Dietrich[19], S. Díez Cornell[44], A. Dimitrievska[18], J. Dingfelder[24], F. Dittus[35], F. Djama[99], T. Djobava[156b], J.I. Djuvsland[59a], M.A.B. Do Vale[78c], M. Dobre[27b], D. Dodsworth[26], C. Doglioni[94], J. Dolejsi[139], Z. Dolezal[139], M. Donadelli[78d], J. Donini[37], A. D'onofrio[90], M. D'Onofrio[88], J. Dopke[141], A. Doria[67a], M.T. Dova[86], A.T. Doyle[55], E. Drechsler[51], E. Dreyer[149], T. Dreyer[51], Y. Du[58b], F. Dubinin[108], M. Dubovsky[28a], A. Dubreuil[52], E. Duchovni[177], G. Duckeck[112], A. Ducourthial[132], O.A. Ducu[107,w], D. Duda[113], A. Dudarev[35], A.C. Dudder[97], E.M. Duffield[18], L. Duflot[128], M. Dührssen[35], C. Dülsen[179], M. Dumancic[177], A.E. Dumitriu[27b,e], A.K. Duncan[55], M. Dunford[59a], A. Duperrin[99], H. Duran Yildiz[4a], M. Düren[54], A. Durglishvili[156b], D. Duschinger[46], B. Dutta[44], D. Duvnjak[1], M. Dyndal[44], S. Dysch[98], B.S. Dziedzic[82], C. Eckardt[44], K.M. Ecker[113], R.C. Edgar[103], T. Eifert[35], G. Eigen[17], K. Einsweiler[18], T. Ekelof[169], M. El Kacimi[34c], R. El Kosseifi[99], V. Ellajosyula[99], M. Ellert[169], F. Ellinghaus[179], A.A. Elliot[90], N. Ellis[35], J. Elmsheuser[29], M. Elsing[35], D. Emeliyanov[141], A. Emerman[38], Y. Enari[160], J.S. Ennis[175], M.B. Epland[47], J. Erdmann[45], A. Ereditato[20], S. Errede[170], M. Escalier[128], C. Escobar[171], O. Estrada Pastor[171], A.I. Etienvre[142], E. Etzion[158], H. Evans[63], A. Ezhilov[134], M. Ezzi[34e], F. Fabbri[55], L. Fabbri[23b,23a], V. Fabiani[117], G. Facini[92], R.M. Faisca Rodrigues Pereira[136a], R.M. Fakhrutdinov[140], S. Falciano[70a], P.J. Falke[5], S. Falke[5], J. Faltova[139], Y. Fang[15a], M. Fanti[66a,66b], A. Farbin[8], A. Farilla[72a], E.M. Farina[68a,68b], T. Farooque[104], S. Farrell[18], S.M. Farrington[175], P. Farthouat[35], F. Fassi[34e], P. Fassnacht[35], D. Fassouliotis[9], M. Faucci Giannelli[48], A. Favareto[53b,53a], W.J. Fawcett[31], L. Fayard[128], O.L. Fedin[134,p], W. Fedorko[172], M. Feickert[41], S. Feigl[130], L. Feligioni[99], C. Feng[58b], E.J. Feng[35], M. Feng[47], M.J. Fenton[55], A.B. Fenyuk[140], L. Feremenga[8], J. Ferrando[44], A. Ferrari[169], P. Ferrari[118], R. Ferrari[68a], D.E. Ferreira de Lima[59b], A. Ferrer[171], D. Ferrere[52], C. Ferretti[103], F. Fiedler[97], A. Filipčič[89], F. Filthaut[117], K.D. Finelli[25], M.C.N. Fiolhais[136a,136c,a], L. Fiorini[171],

JHEP04(2019)092

C. Fischer[14], W.C. Fisher[104], N. Flaschel[44], I. Fleck[148], P. Fleischmann[103], R.R.M. Fletcher[133], T. Flick[179], B.M. Flierl[112], L.M. Flores[133], L.R. Flores Castillo[61a], F.M. Follega[73a,73b], N. Fomin[17], G.T. Forcolin[73a,73b], A. Formica[142], F.A. Förster[14], A.C. Forti[98], A.G. Foster[21], D. Fournier[128], H. Fox[87], S. Fracchia[146], P. Francavilla[69a,69b], M. Franchini[23b,23a], S. Franchino[59a], D. Francis[35], L. Franconi[143], M. Franklin[57], M. Frate[168], M. Fraternali[68a,68b], A.N. Fray[90], D. Freeborn[92], B. Freund[107], W.S. Freund[78b], E.M. Freundlich[45], D.C. Frizzell[124], D. Froidevaux[35], J.A. Frost[131], C. Fukunaga[161], E. Fullana Torregrosa[171], T. Fusayasu[114], J. Fuster[171], O. Gabizon[157], A. Gabrielli[23b,23a], A. Gabrielli[18], G.P. Gach[81a], S. Gadatsch[52], P. Gadow[113], G. Gagliardi[53b,53a], L.G. Gagnon[107], C. Galea[27b], B. Galhardo[136a,136c], E.J. Gallas[131], B.J. Gallop[141], P. Gallus[138], G. Galster[39], R. Gamboa Goni[90], K.K. Gan[122], S. Ganguly[177], J. Gao[58a], Y. Gao[88], Y.S. Gao[150,m], C. García[171], J.E. García Navarro[171], J.A. García Pascual[15a], M. Garcia-Sciveres[18], R.W. Gardner[36], N. Garelli[150], S. Gargiulo[50], V. Garonne[130], K. Gasnikova[44], A. Gaudiello[53b,53a], G. Gaudio[68a], I.L. Gavrilenko[108], A. Gavrilyuk[109], C. Gay[172], G. Gaycken[24], E.N. Gazis[10], C.N.P. Gee[141], J. Geisen[51], M. Geisen[97], M.P. Geisler[59a], C. Gemme[53b], M.H. Genest[56], C. Geng[103], S. Gentile[70a,70b], S. George[91], D. Gerbaudo[14], G. Gessner[45], S. Ghasemi[148], M. Ghasemi Bostanabad[173], M. Ghneimat[24], B. Giacobbe[23b], S. Giagu[70a,70b], N. Giangiacomi[23b,23a], P. Giannetti[69a], A. Giannini[67a,67b], S.M. Gibson[91], M. Gignac[143], D. Gillberg[33], G. Gilles[179], D.M. Gingrich[3,at], M.P. Giordani[64a,64c], F.M. Giorgi[23b], P.F. Giraud[142], P. Giromini[57], G. Giugliarelli[64a,64c], D. Giugni[66a], F. Giuli[131], M. Giulini[59b], S. Gkaitatzis[159], I. Gkialas[9,j], E.L. Gkougkousis[14], P. Gkountoumis[10], L.K. Gladilin[111], C. Glasman[96], J. Glatzer[14], P.C.F. Glaysher[44], A. Glazov[44], M. Goblirsch-Kolb[26], J. Godlewski[82], S. Goldfarb[102], T. Golling[52], D. Golubkov[140], A. Gomes[136a,136b,136d], R. Goncalves Gama[51], R. Gonçalo[136a], G. Gonella[50], L. Gonella[21], A. Gongadze[77], F. Gonnella[21], J.L. Gonski[57], S. González de la Hoz[171], S. Gonzalez-Sevilla[52], L. Goossens[35], P.A. Gorbounov[109], H.A. Gordon[29], B. Gorini[35], E. Gorini[65a,65b], A. Gorišek[89], A.T. Goshaw[47], C. Gössling[45], M.I. Gostkin[77], C.A. Gottardo[24], C.R. Goudet[128], D. Goujdami[34c], A.G. Goussiou[145], N. Govender[32b,c], C. Goy[5], E. Gozani[157], I. Grabowska-Bold[81a], P.O.J. Gradin[169], E.C. Graham[88], J. Gramling[168], E. Gramstad[130], S. Grancagnolo[19], V. Gratchev[134], P.M. Gravila[27f], F.G. Gravili[65a,65b], C. Gray[55], H.M. Gray[18], Z.D. Greenwood[93,aj], C. Grefe[24], K. Gregersen[94], I.M. Gregor[44], P. Grenier[150], K. Grevtsov[44], N.A. Grieser[124], J. Griffiths[8], A.A. Grillo[143], K. Grimm[150,b], S. Grinstein[14,y], Ph. Gris[37], J.-F. Grivaz[128], S. Groh[97], E. Gross[177], J. Grosse-Knetter[51], G.C. Grossi[93], Z.J. Grout[92], C. Grud[103], A. Grummer[116], L. Guan[103], W. Guan[178], J. Guenther[35], A. Guerguichon[128], F. Guescini[165a], D. Guest[168], R. Gugel[50], B. Gui[122], T. Guillemin[5], S. Guindon[35], U. Gul[55], C. Gumpert[35], J. Guo[58c], W. Guo[103], Y. Guo[58a,s], Z. Guo[99], R. Gupta[44], S. Gurbuz[12c], G. Gustavino[124], B.J. Gutelman[157], P. Gutierrez[124], C. Gutschow[92], C. Guyot[142], M.P. Guzik[81a], C. Gwenlan[131], C.B. Gwilliam[88], A. Haas[121], C. Haber[18], H.K. Hadavand[8], N. Haddad[34e], A. Hadef[58a], S. Hageböck[24], M. Hagihara[166], H. Hakobyan[181,*], M. Haleem[174], J. Haley[125], G. Halladjian[104], G.D. Hallewell[99], K. Hamacher[179], P. Hamal[126], K. Hamano[173], A. Hamilton[32a], G.N. Hamity[146], K. Han[58a,ai], L. Han[58a], S. Han[15d], K. Hanagaki[79,u], M. Hance[143], D.M. Handl[112], B. Haney[133], R. Hankache[132], P. Hanke[59a], E. Hansen[94], J.B. Hansen[39], J.D. Hansen[39], M.C. Hansen[24], P.H. Hansen[39], K. Hara[166], A.S. Hard[178], T. Harenberg[179], S. Harkusha[105], P.F. Harrison[175], N.M. Hartmann[112], Y. Hasegawa[147], A. Hasib[48], S. Hassani[142], S. Haug[20], R. Hauser[104], L. Hauswald[46], L.B. Havener[38], M. Havranek[138], C.M. Hawkes[21], R.J. Hawkings[35], D. Hayden[104], C. Hayes[152], C.P. Hays[131], J.M. Hays[90], H.S. Hayward[88], S.J. Haywood[141], M.P. Heath[48], V. Hedberg[94], L. Heelan[8], S. Heer[24], K.K. Heidegger[50], J. Heilman[33], S. Heim[44], T. Heim[18], B. Heinemann[44,ao], J.J. Heinrich[112], L. Heinrich[121], C. Heinz[54], J. Hejbal[137], L. Helary[35], A. Held[172], S. Hellesund[130], C.M. Helling[143],

JHEP04(2019)092

S. Hellman[43a,43b], C. Helsens[35], R.C.W. Henderson[87], Y. Heng[178], S. Henkelmann[172], A.M. Henriques Correia[35], G.H. Herbert[19], H. Herde[26], V. Herget[174], Y. Hernández Jiménez[32c], H. Herr[97], M.G. Herrmann[112], T. Herrmann[46], G. Herten[50], R. Hertenberger[112], L. Hervas[35], T.C. Herwig[133], G.G. Hesketh[92], N.P. Hessey[165a], A. Higashida[160], S. Higashino[79], E. Higón-Rodriguez[171], K. Hildebrand[36], E. Hill[173], J.C. Hill[31], K.K. Hill[29], K.H. Hiller[44], S.J. Hillier[21], M. Hils[46], I. Hinchliffe[18], F. Hinterkeuser[24], M. Hirose[129], D. Hirschbuehl[179], B. Hiti[89], O. Hladik[137], D.R. Hlaluku[32c], X. Hoad[48], J. Hobbs[152], N. Hod[165a], M.C. Hodgkinson[146], A. Hoecker[35], M.R. Hoeferkamp[116], F. Hoenig[112], D. Hohn[50], D. Hohov[128], T.R. Holmes[36], M. Holzbock[112], M. Homann[45], B.H. Hommels[31], S. Honda[166], T. Honda[79], T.M. Hong[135], A. Hönle[113], B.H. Hooberman[170], W.H. Hopkins[127], Y. Horii[115], P. Horn[46], A.J. Horton[149], L.A. Horyn[36], J-Y. Hostachy[56], A. Hostiuc[145], S. Hou[155], A. Hoummada[34a], J. Howarth[98], J. Hoya[86], M. Hrabovsky[126], I. Hristova[19], J. Hrivnac[128], A. Hrynevich[106], T. Hryn'ova[5], P.J. Hsu[62], S.-C. Hsu[145], Q. Hu[29], S. Hu[58c], Y. Huang[15a], Z. Hubacek[138], F. Hubaut[99], M. Huebner[24], F. Huegging[24], T.B. Huffman[131], M. Huhtinen[35], R.F.H. Hunter[33], P. Huo[152], A.M. Hupe[33], N. Huseynov[77,ae], J. Huston[104], J. Huth[57], R. Hyneman[103], G. Iacobucci[52], G. Iakovidis[29], I. Ibragimov[148], L. Iconomidou-Fayard[128], Z. Idrissi[34e], P. Iengo[35], R. Ignazzi[39], O. Igonkina[118,aa], R. Iguchi[160], T. Iizawa[52], Y. Ikegami[79], M. Ikeno[79], D. Iliadis[159], N. Ilic[150], F. Iltzsche[46], G. Introzzi[68a,68b], M. Iodice[72a], K. Iordanidou[38], V. Ippolito[70a,70b], M.F. Isacson[169], N. Ishijima[129], M. Ishino[160], M. Ishitsuka[162], W. Islam[125], C. Issever[131], S. Istin[157], F. Ito[166], J.M. Iturbe Ponce[61a], R. Iuppa[73a,73b], A. Ivina[177], H. Iwasaki[79], J.M. Izen[42], V. Izzo[67a], P. Jacka[137], P. Jackson[1], R.M. Jacobs[24], V. Jain[2], G. Jäkel[179], K.B. Jakobi[97], K. Jakobs[50], S. Jakobsen[74], T. Jakoubek[137], D.O. Jamin[125], R. Jansky[52], J. Janssen[24], M. Janus[51], P.A. Janus[81a], G. Jarlskog[94], N. Javadov[77,ae], T. Javůrek[35], M. Javurkova[50], F. Jeanneau[142], L. Jeanty[18], J. Jejelava[156a,af], A. Jelinskas[175], P. Jenni[50,d], J. Jeong[44], N. Jeong[44], S. Jézéquel[5], H. Ji[178], J. Jia[152], H. Jiang[76], Y. Jiang[58a], Z. Jiang[150,q], S. Jiggins[50], F.A. Jimenez Morales[37], J. Jimenez Pena[171], S. Jin[15c], A. Jinaru[27b], O. Jinnouchi[162], H. Jivan[32c], P. Johansson[146], K.A. Johns[7], C.A. Johnson[63], W.J. Johnson[145], K. Jon-And[43a,43b], R.W.L. Jones[87], S.D. Jones[153], S. Jones[7], T.J. Jones[88], J. Jongmanns[59a], P.M. Jorge[136a,136b], J. Jovicevic[165a], X. Ju[18], J.J. Junggeburth[113], A. Juste Rozas[14,y], A. Kaczmarska[82], M. Kado[128], H. Kagan[122], M. Kagan[150], T. Kaji[176], E. Kajomovitz[157], C.W. Kalderon[94], A. Kaluza[97], S. Kama[41], A. Kamenshchikov[140], L. Kanjir[89], Y. Kano[160], V.A. Kantserov[110], J. Kanzaki[79], L.S. Kaplan[178], D. Kar[32c], M.J. Kareem[165b], E. Karentzos[10], S.N. Karpov[77], Z.M. Karpova[77], V. Kartvelishvili[87], A.N. Karyukhin[140], L. Kashif[178], R.D. Kass[122], A. Kastanas[43a,43b], Y. Kataoka[160], C. Kato[58d,58c], J. Katzy[44], K. Kawade[80], K. Kawagoe[85], T. Kawamoto[160], G. Kawamura[51], E.F. Kay[88], V.F. Kazanin[120b,120a], R. Keeler[173], R. Kehoe[41], J.S. Keller[33], E. Kellermann[94], J.J. Kempster[21], J. Kendrick[21], O. Kepka[137], S. Kersten[179], B.P. Kerševan[89], S. Ketabchi Haghighat[164], R.A. Keyes[101], M. Khader[170], F. Khalil-Zada[13], A. Khanov[125], A.G. Kharlamov[120b,120a], T. Kharlamova[120b,120a], E.E. Khoda[172], A. Khodinov[163], T.J. Khoo[52], E. Khramov[77], J. Khubua[156b], S. Kido[80], M. Kiehn[52], C.R. Kilby[91], Y.K. Kim[36], N. Kimura[64a,64c], O.M. Kind[19], B.T. King[88], D. Kirchmeier[46], J. Kirk[141], A.E. Kiryunin[113], T. Kishimoto[160], D. Kisielewska[81a], V. Kitali[44], O. Kivernyk[5], E. Kladiva[28b,*], T. Klapdor-Kleingrothaus[50], M.H. Klein[103], M. Klein[88], U. Klein[88], K. Kleinknecht[97], P. Klimek[119], A. Klimentov[29], T. Klingl[24], T. Klioutchnikova[35], F.F. Klitzner[112], P. Kluit[118], S. Kluth[113], E. Kneringer[74], E.B.F.G. Knoops[99], A. Knue[50], A. Kobayashi[160], D. Kobayashi[85], T. Kobayashi[160], M. Kobel[46], M. Kocian[150], P. Kodys[139], P.T. Koenig[24], T. Koffas[33], E. Koffeman[118], N.M. Köhler[113], T. Koi[150], M. Kolb[59b], I. Koletsou[5], T. Kondo[79], N. Kondrashova[58c], K. Köneke[50], A.C. König[117], T. Kono[79], R. Konoplich[121,al], V. Konstantinides[92], N. Konstantinidis[92], B. Konya[94], R. Kopeliansky[63], S. Koperny[81a],

JHEP04(2019)092

K. Korcyl[82], K. Kordas[159], G. Koren[158], A. Korn[92], I. Korolkov[14], E.V. Korolkova[146], N. Korotkova[111], O. Kortner[113], S. Kortner[113], T. Kosek[139], V.V. Kostyukhin[24], A. Kotwal[47], A. Koulouris[10], A. Kourkoumeli-Charalampidi[68a,68b], C. Kourkoumelis[9], E. Kourlitis[146], V. Kouskoura[29], A.B. Kowalewska[82], R. Kowalewski[173], T.Z. Kowalski[81a], C. Kozakai[160], W. Kozanecki[142], A.S. Kozhin[140], V.A. Kramarenko[111], G. Kramberger[89], D. Krasnopevtsev[58a], M.W. Krasny[132], A. Krasznahorkay[35], D. Krauss[113], J.A. Kremer[81a], J. Kretzschmar[88], P. Krieger[164], K. Krizka[18], K. Kroeninger[45], H. Kroha[113], J. Kroll[137], J. Kroll[133], J. Krstic[16], U. Kruchonak[77], H. Krüger[24], N. Krumnack[76], M.C. Kruse[47], T. Kubota[102], S. Kuday[4b], J.T. Kuechler[179], S. Kuehn[35], A. Kugel[59a], T. Kuhl[44], V. Kukhtin[77], R. Kukla[99], Y. Kulchitsky[105,ah], S. Kuleshov[144b], Y.P. Kulinich[170], M. Kuna[56], T. Kunigo[83], A. Kupco[137], T. Kupfer[45], O. Kuprash[158], H. Kurashige[80], L.L. Kurchaninov[165a], Y.A. Kurochkin[105], A. Kurova[110], M.G. Kurth[15d], E.S. Kuwertz[35], M. Kuze[162], J. Kvita[126], T. Kwan[101], A. La Rosa[113], J.L. La Rosa Navarro[78d], L. La Rotonda[40b,40a], F. La Ruffa[40b,40a], C. Lacasta[171], F. Lacava[70a,70b], J. Lacey[44], D.P.J. Lack[98], H. Lacker[19], D. Lacour[132], E. Ladygin[77], R. Lafaye[5], B. Laforge[132], T. Lagouri[32c], S. Lai[51], S. Lammers[63], W. Lampl[7], E. Lançon[29], U. Landgraf[50], M.P.J. Landon[90], M.C. Lanfermann[52], V.S. Lang[44], J.C. Lange[51], R.J. Langenberg[35], A.J. Lankford[168], F. Lanni[29], K. Lantzsch[24], A. Lanza[68a], A. Lapertosa[53b,53a], S. Laplace[132], J.F. Laporte[142], T. Lari[66a], F. Lasagni Manghi[23b,23a], M. Lassnig[35], T.S. Lau[61a], A. Laudrain[128], M. Lavorgna[67a,67b], M. Lazzaroni[66a,66b], B. Le[102], O. Le Dortz[132], E. Le Guirriec[99], E.P. Le Quilleuc[142], M. LeBlanc[7], T. LeCompte[6], F. Ledroit-Guillon[56], C.A. Lee[29], G.R. Lee[144a], L. Lee[57], S.C. Lee[155], B. Lefebvre[101], M. Lefebvre[173], F. Legger[112], C. Leggett[18], K. Lehmann[149], N. Lehmann[179], G. Lehmann Miotto[35], W.A. Leight[44], A. Leisos[159,v], M.A.L. Leite[78d], R. Leitner[139], D. Lellouch[177], K.J.C. Leney[92], T. Lenz[24], B. Lenzi[35], R. Leone[7], S. Leone[69a], C. Leonidopoulos[48], G. Lerner[153], C. Leroy[107], R. Les[164], A.A.J. Lesage[142], C.G. Lester[31], M. Levchenko[134], J. Levêque[5], D. Levin[103], L.J. Levinson[177], D. Lewis[90], B. Li[15b], B. Li[103], C-Q. Li[58a,ak], H. Li[58a], H. Li[58b], L. Li[58c], M. Li[15a], Q. Li[15d], Q.Y. Li[58a], S. Li[58d,58c], X. Li[58c], Y. Li[148], Z. Liang[15a], B. Liberti[71a], A. Liblong[164], K. Lie[61c], S. Liem[118], A. Limosani[154], C.Y. Lin[31], K. Lin[104], T.H. Lin[97], R.A. Linck[63], J.H. Lindon[21], B.E. Lindquist[152], A.L. Lionti[52], E. Lipeles[133], A. Lipniacka[17], M. Lisovyi[59b], T.M. Liss[170,aq], A. Lister[172], A.M. Litke[143], J.D. Little[8], B. Liu[76], B.L Liu[6], H.B. Liu[29], H. Liu[103], J.B. Liu[58a], J.K.K. Liu[131], K. Liu[132], M. Liu[58a], P. Liu[18], Y. Liu[15a], Y.L. Liu[58a], Y.W. Liu[58a], M. Livan[68a,68b], A. Lleres[56], J. Llorente Merino[15a], S.L. Lloyd[90], C.Y. Lo[61b], F. Lo Sterzo[41], E.M. Lobodzinska[44], P. Loch[7], T. Lohse[19], K. Lohwasser[146], M. Lokajicek[137], J.D. Long[170], R.E. Long[87], L. Longo[65a,65b], K.A. Looper[122], J.A. Lopez[144b], I. Lopez Paz[98], A. Lopez Solis[146], J. Lorenz[112], N. Lorenzo Martinez[5], M. Losada[22], P.J. Lösel[112], A. Lösle[50], X. Lou[44], X. Lou[15a], A. Lounis[128], J. Love[6], P.A. Love[87], J.J. Lozano Bahilo[171], H. Lu[61a], M. Lu[58a], Y.J. Lu[62], H.J. Lubatti[145], C. Luci[70a,70b], A. Lucotte[56], C. Luedtke[50], F. Luehring[63], I. Luise[132], L. Luminari[70a], B. Lund-Jensen[151], M.S. Lutz[100], P.M. Luzi[132], D. Lynn[29], R. Lysak[137], E. Lytken[94], F. Lyu[15a], V. Lyubushkin[77], T. Lyubushkina[77], H. Ma[29], L.L. Ma[58b], Y. Ma[58b], G. Maccarrone[49], A. Macchiolo[113], C.M. Macdonald[146], J. Machado Miguens[133,136b], D. Madaffari[171], R. Madar[37], W.F. Mader[46], A. Madsen[44], N. Madysa[46], J. Maeda[80], K. Maekawa[160], S. Maeland[17], T. Maeno[29], M. Maerker[46], A.S. Maevskiy[111], V. Magerl[50], D.J. Mahon[38], C. Maidantchik[78b], T. Maier[112], A. Maio[136a,136b,136d], O. Majersky[28a], S. Majewski[127], Y. Makida[79], N. Makovec[128], B. Malaescu[132], Pa. Malecki[82], V.P. Maleev[134], F. Malek[56], U. Mallik[75], D. Malon[6], C. Malone[31], S. Maltezos[10], S. Malyukov[35], J. Mamuzic[171], G. Mancini[49], I. Mandić[89], J. Maneira[136a], L. Manhaes de Andrade Filho[78a], J. Manjarres Ramos[46], K.H. Mankinen[94], A. Mann[112], A. Manousos[74], B. Mansoulie[142], J.D. Mansour[15a], S. Manzoni[66a,66b], A. Marantis[159], G. Marceca[30], L. March[52], L. Marchese[131], G. Marchiori[132], M. Marcisovsky[137], C. Marcon[94],

JHEP04(2019)092

C.A. Marin Tobon[35], M. Marjanovic[37], F. Marroquim[78b], Z. Marshall[18], M.U.F Martensson[169], S. Marti-Garcia[171], C.B. Martin[122], T.A. Martin[175], V.J. Martin[48], B. Martin dit Latour[17], M. Martinez[14,y], V.I. Martinez Outschoorn[100], S. Martin-Haugh[141], V.S. Martoiu[27b], A.C. Martyniuk[92], A. Marzin[35], L. Masetti[97], T. Mashimo[160], R. Mashinistov[108], J. Masik[98], A.L. Maslennikov[120b,120a], L.H. Mason[102], L. Massa[71a,71b], P. Massarotti[67a,67b], P. Mastrandrea[152], A. Mastroberardino[40b,40a], T. Masubuchi[160], P. Mättig[179], J. Maurer[27b], B. Maček[89], S.J. Maxfield[88], D.A. Maximov[120b,120a], R. Mazini[155], I. Maznas[159], S.M. Mazza[143], G. Mc Goldrick[164], S.P. Mc Kee[103], A. McCarn[41], T.G. McCarthy[113], L.I. McClymont[92], W.P. McCormack[18], E.F. McDonald[102], J.A. Mcfayden[35], G. Mchedlidze[51], M.A. McKay[41], K.D. McLean[173], S.J. McMahon[141], P.C. McNamara[102], C.J. McNicol[175], R.A. McPherson[173,ac], J.E. Mdhluli[32c], Z.A. Meadows[100], S. Meehan[145], T.M. Megy[50], S. Mehlhase[112], A. Mehta[88], T. Meideck[56], B. Meirose[42], D. Melini[171,h], B.R. Mellado Garcia[32c], J.D. Mellenthin[51], M. Melo[28a], F. Meloni[44], A. Melzer[24], S.B. Menary[98], E.D. Mendes Gouveia[136a], L. Meng[88], X.T. Meng[103], S. Menke[113], E. Meoni[40b,40a], S. Mergelmeyer[19], S.A.M. Merkt[135], C. Merlassino[20], P. Mermod[52], L. Merola[67a,67b], C. Meroni[66a], F.S. Merritt[36], A. Messina[70a,70b], J. Metcalfe[6], A.S. Mete[168], C. Meyer[133], J. Meyer[157], J-P. Meyer[142], H. Meyer Zu Theenhausen[59a], F. Miano[153], R.P. Middleton[141], L. Mijović[48], G. Mikenberg[177], M. Mikestikova[137], M. Mikuž[89], M. Milesi[102], A. Milic[164], D.A. Millar[90], D.W. Miller[36], A. Milov[177], D.A. Milstead[43a,43b], R.A. Mina[150,q], A.A. Minaenko[140], M. Miñano Moya[171], I.A. Minashvili[156b], A.I. Mincer[121], B. Mindur[81a], M. Mineev[77], Y. Minegishi[160], Y. Ming[178], L.M. Mir[14], A. Mirto[65a,65b], K.P. Mistry[133], T. Mitani[176], J. Mitrevski[112], V.A. Mitsou[171], M. Mittal[58c], A. Miucci[20], P.S. Miyagawa[146], A. Mizukami[79], J.U. Mjörnmark[94], T. Mkrtchyan[181], M. Mlynarikova[139], T. Moa[43a,43b], K. Mochizuki[107], P. Mogg[50], S. Mohapatra[38], S. Molander[43a,43b], R. Moles-Valls[24], M.C. Mondragon[104], K. Mönig[44], J. Monk[39], E. Monnier[99], A. Montalbano[149], J. Montejo Berlingen[35], F. Monticelli[86], S. Monzani[66a], N. Morange[128], D. Moreno[22], M. Moreno Llácer[35], P. Morettini[53b], M. Morgenstern[118], S. Morgenstern[46], D. Mori[149], M. Morii[57], M. Morinaga[176], V. Morisbak[130], A.K. Morley[35], G. Mornacchi[35], A.P. Morris[92], J.D. Morris[90], L. Morvaj[152], P. Moschovakos[10], M. Mosidze[156b], H.J. Moss[146], J. Moss[150,n], K. Motohashi[162], R. Mount[150], E. Mountricha[35], E.J.W. Moyse[100], S. Muanza[99], F. Mueller[113], J. Mueller[135], R.S.P. Mueller[112], D. Muenstermann[87], G.A. Mullier[94], F.J. Munoz Sanchez[98], P. Murin[28b], W.J. Murray[175,141], A. Murrone[66a,66b], M. Muškinja[89], C. Mwewa[32a], A.G. Myagkov[140,am], J. Myers[127], M. Myska[138], B.P. Nachman[18], O. Nackenhorst[45], K. Nagai[131], K. Nagano[79], Y. Nagasaka[60], M. Nagel[50], E. Nagy[99], A.M. Nairz[35], Y. Nakahama[115], K. Nakamura[79], T. Nakamura[160], I. Nakano[123], H. Nanjo[129], F. Napolitano[59a], R.F. Naranjo Garcia[44], R. Narayan[11], D.I. Narrias Villar[59a], I. Naryshkin[134], T. Naumann[44], G. Navarro[22], R. Nayyar[7], H.A. Neal[103,*], P.Y. Nechaeva[108], T.J. Neep[142], A. Negri[68a,68b], M. Negrini[23b], S. Nektarijevic[117], C. Nellist[51], M.E. Nelson[131], S. Nemecek[137], P. Nemethy[121], M. Nessi[35,f], M.S. Neubauer[170], M. Neumann[179], P.R. Newman[21], T.Y. Ng[61c], Y.S. Ng[19], Y.W.Y. Ng[168], H.D.N. Nguyen[99], T. Nguyen Manh[107], E. Nibigira[37], R.B. Nickerson[131], R. Nicolaidou[142], D.S. Nielsen[39], J. Nielsen[143], N. Nikiforou[11], V. Nikolaenko[140,am], I. Nikolic-Audit[132], K. Nikolopoulos[21], P. Nilsson[29], Y. Ninomiya[79], A. Nisati[70a], N. Nishu[58c], R. Nisius[113], I. Nitsche[45], T. Nitta[176], T. Nobe[160], Y. Noguchi[83], M. Nomachi[129], I. Nomidis[132], M.A. Nomura[29], T. Nooney[90], M. Nordberg[35], N. Norjoharuddeen[131], T. Novak[89], O. Novgorodova[46], R. Novotny[138], L. Nozka[126], K. Ntekas[168], E. Nurse[92], F. Nuti[102], F.G. Oakham[33,at], H. Oberlack[113], J. Ocariz[132], A. Ochi[80], I. Ochoa[38], J.P. Ochoa-Ricoux[144a], K. O'Connor[26], S. Oda[85], S. Odaka[79], S. Oerdek[51], A. Oh[98], S.H. Oh[47], C.C. Ohm[151], H. Oide[53b,53a], M.L. Ojeda[164], H. Okawa[166], Y. Okazaki[83], Y. Okumura[160], T. Okuyama[79], A. Olariu[27b], L.F. Oleiro Seabra[136a], S.A. Olivares Pino[144a], D. Oliveira Damazio[29], J.L. Oliver[1],

JHEP04(2019)092

M.J.R. Olsson[36], A. Olszewski[82], J. Olszowska[82], D.C. O'Neil[149], A. Onofre[136a,136e], K. Onogi[115], P.U.E. Onyisi[11], H. Oppen[130], M.J. Oreglia[36], G.E. Orellana[86], Y. Oren[158], D. Orestano[72a,72b], E.C. Orgill[98], N. Orlando[61b], A.A. O'Rourke[44], R.S. Orr[164], B. Osculati[53b,53a,*], V. O'Shea[55], R. Ospanov[58a], G. Otero y Garzon[30], H. Otono[85], M. Ouchrif[34d], F. Ould-Saada[130], A. Ouraou[142], Q. Ouyang[15a], M. Owen[55], R.E. Owen[21], V.E. Ozcan[12c], N. Ozturk[8], J. Pacalt[126], H.A. Pacey[31], K. Pachal[149], A. Pacheco Pages[14], L. Pacheco Rodriguez[142], C. Padilla Aranda[14], S. Pagan Griso[18], M. Paganini[180], G. Palacino[63], S. Palazzo[48], S. Palestini[35], M. Palka[81b], D. Pallin[37], I. Panagoulias[10], C.E. Pandini[35], J.G. Panduro Vazquez[91], P. Pani[35], G. Panizzo[64a,64c], L. Paolozzi[52], T.D. Papadopoulou[10], K. Papageorgiou[9,j], A. Paramonov[6], D. Paredes Hernandez[61b], S.R. Paredes Saenz[131], B. Parida[163], T.H. Park[33], A.J. Parker[87], K.A. Parker[44], M.A. Parker[31], F. Parodi[53b,53a], J.A. Parsons[38], U. Parzefall[50], V.R. Pascuzzi[164], J.M.P. Pasner[143], E. Pasqualucci[70a], S. Passaggio[53b], F. Pastore[91], P. Pasuwan[43a,43b], S. Pataraia[97], J.R. Pater[98], A. Pathak[178,k], T. Pauly[35], B. Pearson[113], M. Pedersen[130], L. Pedraza Diaz[117], R. Pedro[136a,136b], S.V. Peleganchuk[120b,120a], O. Penc[137], C. Peng[15d], H. Peng[58a], B.S. Peralva[78a], M.M. Perego[128], A.P. Pereira Peixoto[136a], D.V. Perepelitsa[29], F. Peri[19], L. Perini[66a,66b], H. Pernegger[35], S. Perrella[67a,67b], V.D. Peshekhonov[77,*], K. Peters[44], R.F.Y. Peters[98], B.A. Petersen[35], T.C. Petersen[39], E. Petit[56], A. Petridis[1], C. Petridou[159], P. Petroff[128], M. Petrov[131], F. Petrucci[72a,72b], M. Pettee[180], N.E. Pettersson[100], A. Peyaud[142], R. Pezoa[144b], T. Pham[102], F.H. Phillips[104], P.W. Phillips[141], M.W. Phipps[170], G. Piacquadio[152], E. Pianori[18], A. Picazio[100], M.A. Pickering[131], R.H. Pickles[98], R. Piegaia[30], J.E. Pilcher[36], A.D. Pilkington[98], M. Pinamonti[71a,71b], J.L. Pinfold[3], M. Pitt[177], L. Pizzimento[71a,71b], M.-A. Pleier[29], V. Pleskot[139], E. Plotnikova[77], D. Pluth[76], P. Podberezko[120b,120a], R. Poettgen[94], R. Poggi[52], L. Poggioli[128], I. Pogrebnyak[104], D. Pohl[24], I. Pokharel[51], G. Polesello[68a], A. Poley[18], A. Policicchio[70a,70b], R. Polifka[35], A. Polini[23b], C.S. Pollard[44], V. Polychronakos[29], D. Ponomarenko[110], L. Pontecorvo[35], G.A. Popeneciu[27d], D.M. Portillo Quintero[132], S. Pospisil[138], K. Potamianos[44], I.N. Potrap[77], C.J. Potter[31], H. Potti[11], T. Poulsen[94], J. Poveda[35], T.D. Powell[146], M.E. Pozo Astigarraga[35], P. Pralavorio[99], S. Prell[76], D. Price[98], M. Primavera[65a], S. Prince[101], N. Proklova[110], K. Prokofiev[61c], F. Prokoshin[144b], S. Protopopescu[29], J. Proudfoot[6], M. Przybycien[81a], A. Puri[170], P. Puzo[128], J. Qian[103], Y. Qin[98], A. Quadt[51], M. Queitsch-Maitland[44], A. Qureshi[1], P. Rados[102], F. Ragusa[66a,66b], G. Rahal[95], J.A. Raine[52], S. Rajagopalan[29], A. Ramirez Morales[90], T. Rashid[128], S. Raspopov[5], M.G. Ratti[66a,66b], D.M. Rauch[44], F. Rauscher[112], S. Rave[97], B. Ravina[146], I. Ravinovich[177], J.H. Rawling[98], M. Raymond[35], A.L. Read[130], N.P. Readioff[56], M. Reale[65a,65b], D.M. Rebuzzi[68a,68b], A. Redelbach[174], G. Redlinger[29], R. Reece[143], R.G. Reed[32c], K. Reeves[42], L. Rehnisch[19], J. Reichert[133], D. Reikher[158], A. Reiss[97], C. Rembser[35], H. Ren[15d], M. Rescigno[70a], S. Resconi[66a], E.D. Resseguie[133], S. Rettie[172], E. Reynolds[21], O.L. Rezanova[120b,120a], P. Reznicek[139], E. Ricci[73a,73b], R. Richter[113], S. Richter[44], E. Richter-Was[81b], O. Ricken[24], M. Ridel[132], P. Rieck[113], C.J. Riegel[179], O. Rifki[44], M. Rijssenbeek[152], A. Rimoldi[68a,68b], M. Rimoldi[20], L. Rinaldi[23b], G. Ripellino[151], B. Ristić[87], E. Ritsch[35], I. Riu[14], J.C. Rivera Vergara[144a], F. Rizatdinova[125], E. Rizvi[90], C. Rizzi[14], R.T. Roberts[98], S.H. Robertson[101,ac], D. Robinson[31], J.E.M. Robinson[44], A. Robson[55], E. Rocco[97], C. Roda[69a,69b], Y. Rodina[99], S. Rodriguez Bosca[171], A. Rodriguez Perez[14], D. Rodriguez Rodriguez[171], A.M. Rodríguez Vera[165b], S. Roe[35], C.S. Rogan[57], O. Røhne[130], R. Röhrig[113], C.P.A. Roland[63], J. Roloff[57], A. Romaniouk[110], M. Romano[23b,23a], N. Rompotis[88], M. Ronzani[121], L. Roos[132], S. Rosati[70a], K. Rosbach[50], N-A. Rosien[51], B.J. Rosser[133], E. Rossi[44], E. Rossi[72a,72b], E. Rossi[67a,67b], L.P. Rossi[53b], L. Rossini[66a,66b], J.H.N. Rosten[31], R. Rosten[14], M. Rotaru[27b], J. Rothberg[145], D. Rousseau[128], D. Roy[32c], A. Rozanov[99], Y. Rozen[157], X. Ruan[32c], F. Rubbo[150], F. Rühr[50], A. Ruiz-Martinez[171], Z. Rurikova[50], N.A. Rusakovich[77], H.L. Russell[101],

JHEP04(2019)092

J.P. Rutherfoord[7], E.M. Rüttinger[44,l], Y.F. Ryabov[134], M. Rybar[170], G. Rybkin[128], S. Ryu[6], A. Ryzhov[140], G.F. Rzehorz[51], P. Sabatini[51], G. Sabato[118], S. Sacerdoti[128], H.F-W. Sadrozinski[143], R. Sadykov[77], F. Safai Tehrani[70a], P. Saha[119], M. Sahinsoy[59a], A. Sahu[179], M. Saimpert[44], M. Saito[160], T. Saito[160], H. Sakamoto[160], A. Sakharov[121,al], D. Salamani[52], G. Salamanna[72a,72b], J.E. Salazar Loyola[144b], P.H. Sales De Bruin[169], D. Salihagic[113], A. Salnikov[150], J. Salt[171], D. Salvatore[40b,40a], F. Salvatore[153], A. Salvucci[61a,61b,61c], A. Salzburger[35], J. Samarati[35], D. Sammel[50], D. Sampsonidis[159], D. Sampsonidou[159], J. Sánchez[171], A. Sanchez Pineda[64a,64c], H. Sandaker[130], C.O. Sander[44], M. Sandhoff[179], C. Sandoval[22], D.P.C. Sankey[141], M. Sannino[53b,53a], Y. Sano[115], A. Sansoni[49], C. Santoni[37], H. Santos[136a], I. Santoyo Castillo[153], A. Santra[171], A. Sapronov[77], J.G. Saraiva[136a,136d], O. Sasaki[79], K. Sato[166], E. Sauvan[5], P. Savard[164,at], N. Savic[113], R. Sawada[160], C. Sawyer[141], L. Sawyer[93,aj], C. Sbarra[23b], A. Sbrizzi[23b,23a], T. Scanlon[92], J. Schaarschmidt[145], P. Schacht[113], B.M. Schachtner[112], D. Schaefer[36], L. Schaefer[133], J. Schaeffer[97], S. Schaepe[35], U. Schäfer[97], A.C. Schaffer[128], D. Schaile[112], R.D. Schamberger[152], N. Scharmberg[98], V.A. Schegelsky[134], D. Scheirich[139], F. Schenck[19], M. Schernau[168], C. Schiavi[53b,53a], S. Schier[143], L.K. Schildgen[24], Z.M. Schillaci[26], E.J. Schioppa[35], M. Schioppa[40b,40a], K.E. Schleicher[50], S. Schlenker[35], K.R. Schmidt-Sommerfeld[113], K. Schmieden[35], C. Schmitt[97], S. Schmitt[44], S. Schmitz[97], J.C. Schmoeckel[44], U. Schnoor[50], L. Schoeffel[142], A. Schoening[59b], E. Schopf[131], M. Schott[97], J.F.P. Schouwenberg[117], J. Schovancova[35], S. Schramm[52], A. Schulte[97], H-C. Schultz-Coulon[59a], M. Schumacher[50], B.A. Schumm[143], Ph. Schune[142], A. Schwartzman[150], T.A. Schwarz[103], Ph. Schwemling[142], R. Schwienhorst[104], A. Sciandra[24], G. Sciolla[26], M. Scornajenghi[40b,40a], F. Scuri[69a], F. Scutti[102], L.M. Scyboz[113], C.D. Sebastiani[70a,70b], P. Seema[19], S.C. Seidel[116], A. Seiden[143], T. Seiss[36], J.M. Seixas[78b], G. Sekhniaidze[67a], K. Sekhon[103], S.J. Sekula[41], N. Semprini-Cesari[23b,23a], S. Sen[47], S. Senkin[37], C. Serfon[130], L. Serin[128], L. Serkin[64a,64b], M. Sessa[58a], H. Severini[124], F. Sforza[167], A. Sfyrla[52], E. Shabalina[51], J.D. Shahinian[143], N.W. Shaikh[43a,43b], D. Shaked Renous[177], L.Y. Shan[15a], R. Shang[170], J.T. Shank[25], M. Shapiro[18], A.S. Sharma[1], A. Sharma[131], P.B. Shatalov[109], K. Shaw[153], S.M. Shaw[98], A. Shcherbakova[134], Y. Shen[124], N. Sherafati[33], A.D. Sherman[25], P. Sherwood[92], L. Shi[155,ap], S. Shimizu[79], C.O. Shimmin[180], Y. Shimogama[176], M. Shimojima[114], I.P.J. Shipsey[131], S. Shirabe[85], M. Shiyakova[77], J. Shlomi[177], A. Shmeleva[108], D. Shoaleh Saadi[107], M.J. Shochet[36], S. Shojaii[102], D.R. Shope[124], S. Shrestha[122], E. Shulga[110], P. Sicho[137], A.M. Sickles[170], P.E. Sidebo[151], E. Sideras Haddad[32c], O. Sidiropoulou[35], A. Sidoti[23b,23a], F. Siegert[46], Dj. Sijacki[16], J. Silva[136a], M. Silva Jr.[178], M.V. Silva Oliveira[78a], S.B. Silverstein[43a], S. Simion[128], E. Simioni[97], M. Simon[97], R. Simoniello[97], P. Sinervo[164], N.B. Sinev[127], M. Sioli[23b,23a], I. Siral[103], S.Yu. Sivoklokov[111], J. Sjölin[43a,43b], P. Skubic[124], M. Slater[21], T. Slavicek[138], M. Slawinska[82], K. Sliwa[167], R. Slovak[139], V. Smakhtin[177], B.H. Smart[5], J. Smiesko[28a], N. Smirnov[110], S.Yu. Smirnov[110], Y. Smirnov[110], L.N. Smirnova[111], O. Smirnova[94], J.W. Smith[51], M. Smizanska[87], K. Smolek[138], A. Smykiewicz[82], A.A. Snesarev[108], I.M. Snyder[127], S. Snyder[29], R. Sobie[173,ac], A.M. Soffa[168], A. Soffer[158], A. Søgaard[48], D.A. Soh[155], G. Sokhrannyi[89], C.A. Solans Sanchez[35], M. Solar[138], E.Yu. Soldatov[110], U. Soldevila[171], A.A. Solodkov[140], A. Soloshenko[77], O.V. Solovyanov[140], V. Solovyev[134], P. Sommer[146], H. Son[167], W. Song[141], W.Y. Song[165b], A. Sopczak[138], F. Sopkova[28b], C.L. Sotiropoulou[69a,69b], S. Sottocornola[68a,68b], R. Soualah[64a,64c,i], A.M. Soukharev[120b,120a], D. South[44], B.C. Sowden[91], S. Spagnolo[65a,65b], M. Spalla[113], M. Spangenberg[175], F. Spanò[91], D. Sperlich[19], T.M. Spieker[59a], R. Spighi[23b], G. Spigo[35], L.A. Spiller[102], D.P. Spiteri[55], M. Spousta[139], A. Stabile[66a,66b], R. Stamen[59a], S. Stamm[19], E. Stanecka[82], R.W. Stanek[6], C. Stanescu[72a], B. Stanislaus[131], M.M. Stanitzki[44], B. Stapf[118], S. Stapnes[130], E.A. Starchenko[140], G.H. Stark[36], J. Stark[56], S.H Stark[39], P. Staroba[137], P. Starovoitov[59a], S. Stärz[35], R. Staszewski[82], M. Stegler[44], P. Steinberg[29],

JHEP04(2019)092

B. Stelzer[149], H.J. Stelzer[35], O. Stelzer-Chilton[165a], H. Stenzel[54], T.J. Stevenson[90], G.A. Stewart[55], M.C. Stockton[35], G. Stoicea[27b], P. Stolte[51], S. Stonjek[113], A. Straessner[46], J. Strandberg[151], S. Strandberg[43a,43b], M. Strauss[124], P. Strizenec[28b], R. Ströhmer[174], D.M. Strom[127], R. Stroynowski[41], A. Strubig[48], S.A. Stucci[29], B. Stugu[17], J. Stupak[124], N.A. Styles[44], D. Su[150], J. Su[135], S. Suchek[59a], Y. Sugaya[129], M. Suk[138], V.V. Sulin[108], M.J. Sullivan[88], D.M.S. Sultan[52], S. Sultansoy[4c], T. Sumida[83], S. Sun[103], X. Sun[3], K. Suruliz[153], C.J.E. Suster[154], M.R. Sutton[153], S. Suzuki[79], M. Svatos[137], M. Swiatlowski[36], S.P. Swift[2], A. Sydorenko[97], I. Sykora[28a], T. Sykora[139], D. Ta[97], K. Tackmann[44,z], J. Taenzer[158], A. Taffard[168], R. Tafirout[165a], E. Tahirovic[90], N. Taiblum[158], H. Takai[29], R. Takashima[84], E.H. Takasugi[113], K. Takeda[80], T. Takeshita[147], Y. Takubo[79], M. Talby[99], A.A. Talyshev[120b,120a], J. Tanaka[160], M. Tanaka[162], R. Tanaka[128], B.B. Tannenwald[122], S. Tapia Araya[144b], S. Tapprogge[97], A. Tarek Abouelfadl Mohamed[132], S. Tarem[157], G. Tarna[27b,e], G.F. Tartarelli[66a], P. Tas[139], M. Tasevsky[137], T. Tashiro[83], E. Tassi[40b,40a], A. Tavares Delgado[136a,136b], Y. Tayalati[34e], A.C. Taylor[116], A.J. Taylor[48], G.N. Taylor[102], P.T.E. Taylor[102], W. Taylor[165b], A.S. Tee[87], P. Teixeira-Dias[91], H. Ten Kate[35], J.J. Teoh[118], S. Terada[79], K. Terashi[160], J. Terron[96], S. Terzo[14], M. Testa[49], R.J. Teuscher[164,ac], S.J. Thais[180], T. Theveneaux-Pelzer[44], F. Thiele[39], D.W. Thomas[91], J.P. Thomas[21], A.S. Thompson[55], P.D. Thompson[21], L.A. Thomsen[180], E. Thomson[133], Y. Tian[38], R.E. Ticse Torres[51], V.O. Tikhomirov[108,an], Yu.A. Tikhonov[120b,120a], S. Timoshenko[110], P. Tipton[180], S. Tisserant[99], K. Todome[162], S. Todorova-Nova[5], S. Todt[46], J. Tojo[85], S. Tokár[28a], K. Tokushuku[79], E. Tolley[122], K.G. Tomiwa[32c], M. Tomoto[115], L. Tompkins[150,q], K. Toms[116], B. Tong[57], P. Tornambe[50], E. Torrence[127], H. Torres[46], E. Torró Pastor[145], C. Tosciri[131], J. Toth[99,ab], F. Touchard[99], D.R. Tovey[146], C.J. Treado[121], T. Trefzger[174], F. Tresoldi[153], A. Tricoli[29], I.M. Trigger[165a], S. Trincaz-Duvoid[132], M.F. Tripiana[14], W. Trischuk[164], B. Trocmé[56], A. Trofymov[128], C. Troncon[66a], M. Trovatelli[173], F. Trovato[153], L. Truong[32b], M. Trzebinski[82], A. Trzupek[82], F. Tsai[44], J.C-L. Tseng[131], P.V. Tsiareshka[105,ah], A. Tsirigotis[159], N. Tsirintanis[9], V. Tsiskaridze[152], E.G. Tskhadadze[156a], I.I. Tsukerman[109], V. Tsulaia[18], S. Tsuno[79], D. Tsybychev[152,163], Y. Tu[61b], A. Tudorache[27b], V. Tudorache[27b], T.T. Tulbure[27a], A.N. Tuna[57], S. Turchikhin[77], D. Turgeman[177], I. Turk Cakir[4b,t], R. Turra[66a], P.M. Tuts[38], E. Tzovara[97], G. Ucchielli[45], I. Ueda[79], M. Ughetto[43a,43b], F. Ukegawa[166], G. Unal[35], A. Undrus[29], G. Unel[168], F.C. Ungaro[102], Y. Unno[79], K. Uno[160], J. Urban[28b], P. Urquijo[102], P. Urrejola[97], G. Usai[8], J. Usui[79], L. Vacavant[99], V. Vacek[138], B. Vachon[101], K.O.H. Vadla[130], A. Vaidya[92], C. Valderanis[112], E. Valdes Santurio[43a,43b], M. Valente[52], S. Valentinetti[23b,23a], A. Valero[171], L. Valéry[44], R.A. Vallance[21], A. Vallier[5], J.A. Valls Ferrer[171], T.R. Van Daalen[14], H. Van der Graaf[118], P. Van Gemmeren[6], I. Van Vulpen[118], M. Vanadia[71a,71b], W. Vandelli[35], A. Vaniachine[163], P. Vankov[118], R. Vari[70a], E.W. Varnes[7], C. Varni[53b,53a], T. Varol[41], D. Varouchas[128], K.E. Varvell[154], G.A. Vasquez[144b], J.G. Vasquez[180], F. Vazeille[37], D. Vazquez Furelos[14], T. Vazquez Schroeder[35], J. Veatch[51], V. Vecchio[72a,72b], L.M. Veloce[164], F. Veloso[136a,136c], S. Veneziano[70a], A. Ventura[65a,65b], N. Venturi[35], V. Vercesi[68a], M. Verducci[72a,72b], C.M. Vergel Infante[76], C. Vergis[24], W. Verkerke[118], A.T. Vermeulen[118], J.C. Vermeulen[118], M.C. Vetterli[149,at], N. Viaux Maira[144b], M. Vicente Barreto Pinto[52], I. Vichou[170,*], T. Vickey[146], O.E. Vickey Boeriu[146], G.H.A. Viehhauser[131], S. Viel[18], L. Vigani[131], M. Villa[23b,23a], M. Villaplana Perez[66a,66b], E. Vilucchi[49], M.G. Vincter[33], V.B. Vinogradov[77], A. Vishwakarma[44], C. Vittori[23b,23a], I. Vivarelli[153], S. Vlachos[10], M. Vogel[179], P. Vokac[138], G. Volpi[14], S.E. von Buddenbrock[32c], E. Von Toerne[24], V. Vorobel[139], K. Vorobev[110], M. Vos[171], J.H. Vossebeld[88], N. Vranjes[16], M. Vranjes Milosavljevic[16], V. Vrba[138], M. Vreeswijk[118], T. Šfiligoj[89], R. Vuillermet[35], I. Vukotic[36], T. Ženiš[28a], L. Živković[16], P. Wagner[24], W. Wagner[179], J. Wagner-Kuhr[112], H. Wahlberg[86], S. Wahrmund[46], K. Wakamiya[80],

JHEP04(2019)092

V.M. Walbrecht[113], J. Walder[87], R. Walker[112], S.D. Walker[91], W. Walkowiak[148], V. Wallangen[43a,43b], A.M. Wang[57], C. Wang[58b], F. Wang[178], H. Wang[18], H. Wang[3], J. Wang[154], J. Wang[59b], P. Wang[41], Q. Wang[124], R.-J. Wang[132], R. Wang[58a], R. Wang[6], S.M. Wang[155], W.T. Wang[58a], W. Wang[15c,ad], W.X. Wang[58a,ad], Y. Wang[58a,ak], Z. Wang[58c], C. Wanotayaroj[44], A. Warburton[101], C.P. Ward[31], D.R. Wardrope[92], A. Washbrook[48], P.M. Watkins[21], A.T. Watson[21], M.F. Watson[21], G. Watts[145], S. Watts[98], B.M. Waugh[92], A.F. Webb[11], S. Webb[97], C. Weber[180], M.S. Weber[20], S.A. Weber[33], S.M. Weber[59a], A.R. Weidberg[131], J. Weingarten[45], M. Weirich[97], C. Weiser[50], P.S. Wells[35], T. Wenaus[29], T. Wengler[35], S. Wenig[35], N. Wermes[24], M.D. Werner[76], P. Werner[35], M. Wessels[59a], T.D. Weston[20], K. Whalen[127], N.L. Whallon[145], A.M. Wharton[87], A.S. White[103], A. White[8], M.J. White[1], R. White[144b], D. Whiteson[168], B.W. Whitmore[87], F.J. Wickens[141], W. Wiedenmann[178], M. Wielers[141], C. Wiglesworth[39], L.A.M. Wiik-Fuchs[50], F. Wilk[98], H.G. Wilkens[35], L.J. Wilkins[91], H.H. Williams[133], S. Williams[31], C. Willis[104], S. Willocq[100], J.A. Wilson[21], I. Wingerter-Seez[5], E. Winkels[153], F. Winklmeier[127], O.J. Winston[153], B.T. Winter[50], M. Wittgen[150], M. Wobisch[93], A. Wolf[97], T.M.H. Wolf[118], R. Wolff[99], M.W. Wolter[82], H. Wolters[136a,136c], V.W.S. Wong[172], N.L. Woods[143], S.D. Worm[21], B.K. Wosiek[82], K.W. Woźniak[82], K. Wraight[55], M. Wu[36], S.L. Wu[178], X. Wu[52], Y. Wu[58a], T.R. Wyatt[98], B.M. Wynne[48], S. Xella[39], Z. Xi[103], L. Xia[175], D. Xu[15a], H. Xu[58a,e], L. Xu[29], T. Xu[142], W. Xu[103], Z. Xu[150], B. Yabsley[154], S. Yacoob[32a], K. Yajima[129], D.P. Yallup[92], D. Yamaguchi[162], Y. Yamaguchi[162], A. Yamamoto[79], T. Yamanaka[160], F. Yamane[80], M. Yamatani[160], T. Yamazaki[160], Y. Yamazaki[80], Z. Yan[25], H.J. Yang[58c,58d], H.T. Yang[18], S. Yang[75], Y. Yang[160], Z. Yang[17], W-M. Yao[18], Y.C. Yap[44], Y. Yasu[79], E. Yatsenko[58c,58d], J. Ye[41], S. Ye[29], I. Yeletskikh[77], E. Yigitbasi[25], E. Yildirim[97], K. Yorita[176], K. Yoshihara[133], C.J.S. Young[35], C. Young[150], J. Yu[8], J. Yu[76], X. Yue[59a], S.P.Y. Yuen[24], B. Zabinski[82], G. Zacharis[10], E. Zaffaroni[52], R. Zaidan[14], A.M. Zaitsev[140,am], T. Zakareishvili[156b], N. Zakharchuk[33], J. Zalieckas[17], S. Zambito[57], D. Zanzi[35], D.R. Zaripovas[55], S.V. Zeißner[45], C. Zeitnitz[179], G. Zemaityte[131], J.C. Zeng[170], Q. Zeng[150], O. Zenin[140], D. Zerwas[128], M. Zgubič[131], D.F. Zhang[58b], D. Zhang[103], F. Zhang[178], G. Zhang[58a], G. Zhang[15b], H. Zhang[15c], J. Zhang[6], L. Zhang[15c], L. Zhang[58a], M. Zhang[170], P. Zhang[15c], R. Zhang[58a], R. Zhang[24], X. Zhang[58b], Y. Zhang[15d], Z. Zhang[128], P. Zhao[47], Y. Zhao[58b,128,ai], Z. Zhao[58a], A. Zhemchugov[77], Z. Zheng[103], D. Zhong[170], B. Zhou[103], C. Zhou[178], L. Zhou[41], M.S. Zhou[15d], M. Zhou[152], N. Zhou[58c], Y. Zhou[7], C.G. Zhu[58b], H.L. Zhu[58a], H. Zhu[15a], J. Zhu[103], Y. Zhu[58a], X. Zhuang[15a], K. Zhukov[108], V. Zhulanov[120b,120a], A. Zibell[174], D. Zieminska[63], N.I. Zimine[77], S. Zimmermann[50], Z. Zinonos[113], M. Ziolkowski[148], G. Zobernig[178], A. Zoccoli[23b,23a], K. Zoch[51], T.G. Zorbas[146], R. Zou[36], M. Zur Nedden[19] and L. Zwalinski[35]

[1] *Department of Physics, University of Adelaide, Adelaide; Australia*
[2] *Physics Department, SUNY Albany, Albany NY; United States of America*
[3] *Department of Physics, University of Alberta, Edmonton AB; Canada*
[4] [(a)] *Department of Physics, Ankara University, Ankara;* [(b)] *Istanbul Aydin University, Istanbul;* [(c)] *Division of Physics, TOBB University of Economics and Technology, Ankara; Turkey*
[5] *LAPP, Université Grenoble Alpes, Université Savoie Mont Blanc, CNRS/IN2P3, Annecy; France*
[6] *High Energy Physics Division, Argonne National Laboratory, Argonne IL; United States of America*
[7] *Department of Physics, University of Arizona, Tucson AZ; United States of America*
[8] *Department of Physics, University of Texas at Arlington, Arlington TX; United States of America*
[9] *Physics Department, National and Kapodistrian University of Athens, Athens; Greece*
[10] *Physics Department, National Technical University of Athens, Zografou; Greece*
[11] *Department of Physics, University of Texas at Austin, Austin TX; United States of America*
[12] [(a)] *Bahcesehir University, Faculty of Engineering and Natural Sciences, Istanbul;* [(b)] *Istanbul Bilgi University, Faculty of Engineering and Natural Sciences, Istanbul;* [(c)] *Department of Physics,*

JHEP04(2019)092

Bogazici University, Istanbul;[d] *Department of Physics Engineering, Gaziantep University, Gaziantep; Turkey*

[13] *Institute of Physics, Azerbaijan Academy of Sciences, Baku; Azerbaijan*

[14] *Institut de Física d'Altes Energies (IFAE), Barcelona Institute of Science and Technology, Barcelona; Spain*

[15] [a] *Institute of High Energy Physics, Chinese Academy of Sciences, Beijing;*[b] *Physics Department, Tsinghua University, Beijing;*[c] *Department of Physics, Nanjing University, Nanjing;*[d] *University of Chinese Academy of Science (UCAS), Beijing; China*

[16] *Institute of Physics, University of Belgrade, Belgrade; Serbia*

[17] *Department for Physics and Technology, University of Bergen, Bergen; Norway*

[18] *Physics Division, Lawrence Berkeley National Laboratory and University of California, Berkeley CA; United States of America*

[19] *Institut für Physik, Humboldt Universität zu Berlin, Berlin; Germany*

[20] *Albert Einstein Center for Fundamental Physics and Laboratory for High Energy Physics, University of Bern, Bern; Switzerland*

[21] *School of Physics and Astronomy, University of Birmingham, Birmingham; United Kingdom*

[22] *Centro de Investigaciónes, Universidad Antonio Nariño, Bogota; Colombia*

[23] [a] *Dipartimento di Fisica e Astronomia, Università di Bologna, Bologna;*[b] *INFN Sezione di Bologna; Italy*

[24] *Physikalisches Institut, Universität Bonn, Bonn; Germany*

[25] *Department of Physics, Boston University, Boston MA; United States of America*

[26] *Department of Physics, Brandeis University, Waltham MA; United States of America*

[27] [a] *Transilvania University of Brasov, Brasov;*[b] *Horia Hulubei National Institute of Physics and Nuclear Engineering, Bucharest;*[c] *Department of Physics, Alexandru Ioan Cuza University of Iasi, Iasi;*[d] *National Institute for Research and Development of Isotopic and Molecular Technologies, Physics Department, Cluj-Napoca;*[e] *University Politehnica Bucharest, Bucharest;*[f] *West University in Timisoara, Timisoara; Romania*

[28] [a] *Faculty of Mathematics, Physics and Informatics, Comenius University, Bratislava;*[b] *Department of Subnuclear Physics, Institute of Experimental Physics of the Slovak Academy of Sciences, Kosice; Slovak Republic*

[29] *Physics Department, Brookhaven National Laboratory, Upton NY; United States of America*

[30] *Departamento de Física, Universidad de Buenos Aires, Buenos Aires; Argentina*

[31] *Cavendish Laboratory, University of Cambridge, Cambridge; United Kingdom*

[32] [a] *Department of Physics, University of Cape Town, Cape Town;*[b] *Department of Mechanical Engineering Science, University of Johannesburg, Johannesburg;*[c] *School of Physics, University of the Witwatersrand, Johannesburg; South Africa*

[33] *Department of Physics, Carleton University, Ottawa ON; Canada*

[34] [a] *Faculté des Sciences Ain Chock, Réseau Universitaire de Physique des Hautes Energies — Université Hassan II, Casablanca;*[b] *Centre National de l'Energie des Sciences Techniques Nucleaires (CNESTEN), Rabat;*[c] *Faculté des Sciences Semlalia, Université Cadi Ayyad, LPHEA-Marrakech;*[d] *Faculté des Sciences, Université Mohamed Premier and LPTPM, Oujda;*[e] *Faculté des sciences, Université Mohammed V, Rabat; Morocco*

[35] *CERN, Geneva; Switzerland*

[36] *Enrico Fermi Institute, University of Chicago, Chicago IL; United States of America*

[37] *LPC, Université Clermont Auvergne, CNRS/IN2P3, Clermont-Ferrand; France*

[38] *Nevis Laboratory, Columbia University, Irvington NY; United States of America*

[39] *Niels Bohr Institute, University of Copenhagen, Copenhagen; Denmark*

[40] [a] *Dipartimento di Fisica, Università della Calabria, Rende;*[b] *INFN Gruppo Collegato di Cosenza, Laboratori Nazionali di Frascati; Italy*

[41] *Physics Department, Southern Methodist University, Dallas TX; United States of America*

[42] *Physics Department, University of Texas at Dallas, Richardson TX; United States of America*

[43] [a] *Department of Physics, Stockholm University;*[b] *Oskar Klein Centre, Stockholm; Sweden*

JHEP04(2019)092

[44] Deutsches Elektronen-Synchrotron DESY, Hamburg and Zeuthen; Germany
[45] Lehrstuhl für Experimentelle Physik IV, Technische Universität Dortmund, Dortmund; Germany
[46] Institut für Kern- und Teilchenphysik, Technische Universität Dresden, Dresden; Germany
[47] Department of Physics, Duke University, Durham NC; United States of America
[48] SUPA — School of Physics and Astronomy, University of Edinburgh, Edinburgh; United Kingdom
[49] INFN e Laboratori Nazionali di Frascati, Frascati; Italy
[50] Physikalisches Institut, Albert-Ludwigs-Universität Freiburg, Freiburg; Germany
[51] II. Physikalisches Institut, Georg-August-Universität Göttingen, Göttingen; Germany
[52] Département de Physique Nucléaire et Corpusculaire, Université de Genève, Genève; Switzerland
[53] [(a)] Dipartimento di Fisica, Università di Genova, Genova;[(b)] INFN Sezione di Genova; Italy
[54] II. Physikalisches Institut, Justus-Liebig-Universität Giessen, Giessen; Germany
[55] SUPA — School of Physics and Astronomy, University of Glasgow, Glasgow; United Kingdom
[56] LPSC, Université Grenoble Alpes, CNRS/IN2P3, Grenoble INP, Grenoble; France
[57] Laboratory for Particle Physics and Cosmology, Harvard University, Cambridge MA; United States of America
[58] [(a)] Department of Modern Physics and State Key Laboratory of Particle Detection and Electronics, University of Science and Technology of China, Hefei;[(b)] Institute of Frontier and Interdisciplinary Science and Key Laboratory of Particle Physics and Particle Irradiation (MOE), Shandong University, Qingdao;[(c)] School of Physics and Astronomy, Shanghai Jiao Tong University, KLPPAC-MoE, SKLPPC, Shanghai;[(d)] Tsung-Dao Lee Institute, Shanghai; China
[59] [(a)] Kirchhoff-Institut für Physik, Ruprecht-Karls-Universität Heidelberg, Heidelberg;[(b)] Physikalisches Institut, Ruprecht-Karls-Universität Heidelberg, Heidelberg; Germany
[60] Faculty of Applied Information Science, Hiroshima Institute of Technology, Hiroshima; Japan
[61] [(a)] Department of Physics, Chinese University of Hong Kong, Shatin, N.T., Hong Kong;[(b)] Department of Physics, University of Hong Kong, Hong Kong;[(c)] Department of Physics and Institute for Advanced Study, Hong Kong University of Science and Technology, Clear Water Bay, Kowloon, Hong Kong; China
[62] Department of Physics, National Tsing Hua University, Hsinchu; Taiwan
[63] Department of Physics, Indiana University, Bloomington IN; United States of America
[64] [(a)] INFN Gruppo Collegato di Udine, Sezione di Trieste, Udine;[(b)] ICTP, Trieste;[(c)] Dipartimento di Chimica, Fisica e Ambiente, Università di Udine, Udine; Italy
[65] [(a)] INFN Sezione di Lecce;[(b)] Dipartimento di Matematica e Fisica, Università del Salento, Lecce; Italy
[66] [(a)] INFN Sezione di Milano;[(b)] Dipartimento di Fisica, Università di Milano, Milano; Italy
[67] [(a)] INFN Sezione di Napoli;[(b)] Dipartimento di Fisica, Università di Napoli, Napoli; Italy
[68] [(a)] INFN Sezione di Pavia;[(b)] Dipartimento di Fisica, Università di Pavia, Pavia; Italy
[69] [(a)] INFN Sezione di Pisa;[(b)] Dipartimento di Fisica E. Fermi, Università di Pisa, Pisa; Italy
[70] [(a)] INFN Sezione di Roma;[(b)] Dipartimento di Fisica, Sapienza Università di Roma, Roma; Italy
[71] [(a)] INFN Sezione di Roma Tor Vergata;[(b)] Dipartimento di Fisica, Università di Roma Tor Vergata, Roma; Italy
[72] [(a)] INFN Sezione di Roma Tre;[(b)] Dipartimento di Matematica e Fisica, Università Roma Tre, Roma; Italy
[73] [(a)] INFN-TIFPA;[(b)] Università degli Studi di Trento, Trento; Italy
[74] Institut für Astro- und Teilchenphysik, Leopold-Franzens-Universität, Innsbruck; Austria
[75] University of Iowa, Iowa City IA; United States of America
[76] Department of Physics and Astronomy, Iowa State University, Ames IA; United States of America
[77] Joint Institute for Nuclear Research, Dubna; Russia
[78] [(a)] Departamento de Engenharia Elétrica, Universidade Federal de Juiz de Fora (UFJF), Juiz de Fora;[(b)] Universidade Federal do Rio De Janeiro COPPE/EE/IF, Rio de Janeiro;[(c)] Universidade Federal de São João del Rei (UFSJ), São João del Rei;[(d)] Instituto de Física, Universidade de São Paulo, São Paulo; Brazil
[79] KEK, High Energy Accelerator Research Organization, Tsukuba; Japan

JHEP04(2019)092

[80] Graduate School of Science, Kobe University, Kobe; Japan
[81] [(a)] AGH University of Science and Technology, Faculty of Physics and Applied Computer Science, Krakow;[(b)] Marian Smoluchowski Institute of Physics, Jagiellonian University, Krakow; Poland
[82] Institute of Nuclear Physics Polish Academy of Sciences, Krakow; Poland
[83] Faculty of Science, Kyoto University, Kyoto; Japan
[84] Kyoto University of Education, Kyoto; Japan
[85] Research Center for Advanced Particle Physics and Department of Physics, Kyushu University, Fukuoka; Japan
[86] Instituto de Física La Plata, Universidad Nacional de La Plata and CONICET, La Plata; Argentina
[87] Physics Department, Lancaster University, Lancaster; United Kingdom
[88] Oliver Lodge Laboratory, University of Liverpool, Liverpool; United Kingdom
[89] Department of Experimental Particle Physics, Jožef Stefan Institute and Department of Physics, University of Ljubljana, Ljubljana; Slovenia
[90] School of Physics and Astronomy, Queen Mary University of London, London; United Kingdom
[91] Department of Physics, Royal Holloway University of London, Egham; United Kingdom
[92] Department of Physics and Astronomy, University College London, London; United Kingdom
[93] Louisiana Tech University, Ruston LA; United States of America
[94] Fysiska institutionen, Lunds universitet, Lund; Sweden
[95] Centre de Calcul de l'Institut National de Physique Nucléaire et de Physique des Particules (IN2P3), Villeurbanne; France
[96] Departamento de Física Teorica C-15 and CIAFF, Universidad Autónoma de Madrid, Madrid; Spain
[97] Institut für Physik, Universität Mainz, Mainz; Germany
[98] School of Physics and Astronomy, University of Manchester, Manchester; United Kingdom
[99] CPPM, Aix-Marseille Université, CNRS/IN2P3, Marseille; France
[100] Department of Physics, University of Massachusetts, Amherst MA; United States of America
[101] Department of Physics, McGill University, Montreal QC; Canada
[102] School of Physics, University of Melbourne, Victoria; Australia
[103] Department of Physics, University of Michigan, Ann Arbor MI; United States of America
[104] Department of Physics and Astronomy, Michigan State University, East Lansing MI; United States of America
[105] B.I. Stepanov Institute of Physics, National Academy of Sciences of Belarus, Minsk; Belarus
[106] Research Institute for Nuclear Problems of Byelorussian State University, Minsk; Belarus
[107] Group of Particle Physics, University of Montreal, Montreal QC; Canada
[108] P.N. Lebedev Physical Institute of the Russian Academy of Sciences, Moscow; Russia
[109] Institute for Theoretical and Experimental Physics (ITEP), Moscow; Russia
[110] National Research Nuclear University MEPhI, Moscow; Russia
[111] D.V. Skobeltsyn Institute of Nuclear Physics, M.V. Lomonosov Moscow State University, Moscow; Russia
[112] Fakultät für Physik, Ludwig-Maximilians-Universität München, München; Germany
[113] Max-Planck-Institut für Physik (Werner-Heisenberg-Institut), München; Germany
[114] Nagasaki Institute of Applied Science, Nagasaki; Japan
[115] Graduate School of Science and Kobayashi-Maskawa Institute, Nagoya University, Nagoya; Japan
[116] Department of Physics and Astronomy, University of New Mexico, Albuquerque NM; United States of America
[117] Institute for Mathematics, Astrophysics and Particle Physics, Radboud University Nijmegen/Nikhef, Nijmegen; Netherlands
[118] Nikhef National Institute for Subatomic Physics and University of Amsterdam, Amsterdam; Netherlands
[119] Department of Physics, Northern Illinois University, DeKalb IL; United States of America
[120] [(a)] Budker Institute of Nuclear Physics, SB RAS, Novosibirsk;[(b)] Novosibirsk State University Novosibirsk; Russia

JHEP04(2019)092

[121] Department of Physics, New York University, New York NY; United States of America
[122] Ohio State University, Columbus OH; United States of America
[123] Faculty of Science, Okayama University, Okayama; Japan
[124] Homer L. Dodge Department of Physics and Astronomy, University of Oklahoma, Norman OK; United States of America
[125] Department of Physics, Oklahoma State University, Stillwater OK; United States of America
[126] Palacký University, RCPTM, Joint Laboratory of Optics, Olomouc; Czech Republic
[127] Center for High Energy Physics, University of Oregon, Eugene OR; United States of America
[128] LAL, Université Paris-Sud, CNRS/IN2P3, Université Paris-Saclay, Orsay; France
[129] Graduate School of Science, Osaka University, Osaka; Japan
[130] Department of Physics, University of Oslo, Oslo; Norway
[131] Department of Physics, Oxford University, Oxford; United Kingdom
[132] LPNHE, Sorbonne Université, Paris Diderot Sorbonne Paris Cité, CNRS/IN2P3, Paris; France
[133] Department of Physics, University of Pennsylvania, Philadelphia PA; United States of America
[134] Konstantinov Nuclear Physics Institute of National Research Centre "Kurchatov Institute", PNPI, St. Petersburg; Russia
[135] Department of Physics and Astronomy, University of Pittsburgh, Pittsburgh PA; United States of America
[136] [(a)] Laboratório de Instrumentação e Física Experimental de Partículas — LIP;[(b)] Departamento de Física, Faculdade de Ciências, Universidade de Lisboa, Lisboa;[(c)] Departamento de Física, Universidade de Coimbra, Coimbra;[(d)] Centro de Física Nuclear da Universidade de Lisboa, Lisboa;[(e)] Departamento de Física, Universidade do Minho, Braga;[(f)] Departamento de Física Teorica y del Cosmos, Universidad de Granada, Granada (Spain);[(g)] Dep Física and CEFITEC of Faculdade de Ciências e Tecnologia, Universidade Nova de Lisboa, Caparica; Portugal
[137] Institute of Physics, Academy of Sciences of the Czech Republic, Prague; Czech Republic
[138] Czech Technical University in Prague, Prague; Czech Republic
[139] Charles University, Faculty of Mathematics and Physics, Prague; Czech Republic
[140] State Research Center Institute for High Energy Physics, NRC KI, Protvino; Russia
[141] Particle Physics Department, Rutherford Appleton Laboratory, Didcot; United Kingdom
[142] IRFU, CEA, Université Paris-Saclay, Gif-sur-Yvette; France
[143] Santa Cruz Institute for Particle Physics, University of California Santa Cruz, Santa Cruz CA; United States of America
[144] [(a)] Departamento de Física, Pontificia Universidad Católica de Chile, Santiago;[(b)] Departamento de Física, Universidad Técnica Federico Santa María, Valparaíso; Chile
[145] Department of Physics, University of Washington, Seattle WA; United States of America
[146] Department of Physics and Astronomy, University of Sheffield, Sheffield; United Kingdom
[147] Department of Physics, Shinshu University, Nagano; Japan
[148] Department Physik, Universität Siegen, Siegen; Germany
[149] Department of Physics, Simon Fraser University, Burnaby BC; Canada
[150] SLAC National Accelerator Laboratory, Stanford CA; United States of America
[151] Physics Department, Royal Institute of Technology, Stockholm; Sweden
[152] Departments of Physics and Astronomy, Stony Brook University, Stony Brook NY; United States of America
[153] Department of Physics and Astronomy, University of Sussex, Brighton; United Kingdom
[154] School of Physics, University of Sydney, Sydney; Australia
[155] Institute of Physics, Academia Sinica, Taipei; Taiwan
[156] [(a)] E. Andronikashvili Institute of Physics, Iv. Javakhishvili Tbilisi State University, Tbilisi;[(b)] High Energy Physics Institute, Tbilisi State University, Tbilisi; Georgia
[157] Department of Physics, Technion, Israel Institute of Technology, Haifa; Israel
[158] Raymond and Beverly Sackler School of Physics and Astronomy, Tel Aviv University, Tel Aviv; Israel
[159] Department of Physics, Aristotle University of Thessaloniki, Thessaloniki; Greece

JHEP04(2019)092

[160] International Center for Elementary Particle Physics and Department of Physics, University of Tokyo, Tokyo; Japan
[161] Graduate School of Science and Technology, Tokyo Metropolitan University, Tokyo; Japan
[162] Department of Physics, Tokyo Institute of Technology, Tokyo; Japan
[163] Tomsk State University, Tomsk; Russia
[164] Department of Physics, University of Toronto, Toronto ON; Canada
[165] [(a)] TRIUMF, Vancouver BC; [(b)] Department of Physics and Astronomy, York University, Toronto ON; Canada
[166] Division of Physics and Tomonaga Center for the History of the Universe, Faculty of Pure and Applied Sciences, University of Tsukuba, Tsukuba; Japan
[167] Department of Physics and Astronomy, Tufts University, Medford MA; United States of America
[168] Department of Physics and Astronomy, University of California Irvine, Irvine CA; United States of America
[169] Department of Physics and Astronomy, University of Uppsala, Uppsala; Sweden
[170] Department of Physics, University of Illinois, Urbana IL; United States of America
[171] Instituto de Física Corpuscular (IFIC), Centro Mixto Universidad de Valencia — CSIC, Valencia; Spain
[172] Department of Physics, University of British Columbia, Vancouver BC; Canada
[173] Department of Physics and Astronomy, University of Victoria, Victoria BC; Canada
[174] Fakultät für Physik und Astronomie, Julius-Maximilians-Universität Würzburg, Würzburg; Germany
[175] Department of Physics, University of Warwick, Coventry; United Kingdom
[176] Waseda University, Tokyo; Japan
[177] Department of Particle Physics, Weizmann Institute of Science, Rehovot; Israel
[178] Department of Physics, University of Wisconsin, Madison WI; United States of America
[179] Fakultät für Mathematik und Naturwissenschaften, Fachgruppe Physik, Bergische Universität Wuppertal, Wuppertal; Germany
[180] Department of Physics, Yale University, New Haven CT; United States of America
[181] Yerevan Physics Institute, Yerevan; Armenia

[a] Also at Borough of Manhattan Community College, City University of New York, NY; United States of America
[b] Also at California State University, East Bay; United States of America
[c] Also at Centre for High Performance Computing, CSIR Campus, Rosebank, Cape Town; South Africa
[d] Also at CERN, Geneva; Switzerland
[e] Also at CPPM, Aix-Marseille Université, CNRS/IN2P3, Marseille; France
[f] Also at Département de Physique Nucléaire et Corpusculaire, Université de Genève, Genève; Switzerland
[g] Also at Departament de Fisica de la Universitat Autonoma de Barcelona, Barcelona; Spain
[h] Also at Departamento de Física Teorica y del Cosmos, Universidad de Granada, Granada (Spain); Spain
[i] Also at Department of Applied Physics and Astronomy, University of Sharjah, Sharjah; United Arab Emirates
[j] Also at Department of Financial and Management Engineering, University of the Aegean, Chios; Greece
[k] Also at Department of Physics and Astronomy, University of Louisville, Louisville, KY; United States of America
[l] Also at Department of Physics and Astronomy, University of Sheffield, Sheffield; United Kingdom
[m] Also at Department of Physics, California State University, Fresno CA; United States of America
[n] Also at Department of Physics, California State University, Sacramento CA; United States of America

JHEP04(2019)092

[o] Also at Department of Physics, King's College London, London; United Kingdom
[p] Also at Department of Physics, St. Petersburg State Polytechnical University, St. Petersburg; Russia
[q] Also at Department of Physics, Stanford University; United States of America
[r] Also at Department of Physics, University of Fribourg, Fribourg; Switzerland
[s] Also at Department of Physics, University of Michigan, Ann Arbor MI; United States of America
[t] Also at Giresun University, Faculty of Engineering, Giresun; Turkey
[u] Also at Graduate School of Science, Osaka University, Osaka; Japan
[v] Also at Hellenic Open University, Patras; Greece
[w] Also at Horia Hulubei National Institute of Physics and Nuclear Engineering, Bucharest; Romania
[x] Also at II. Physikalisches Institut, Georg-August-Universität Göttingen, Göttingen; Germany
[y] Also at Institucio Catalana de Recerca i Estudis Avancats, ICREA, Barcelona; Spain
[z] Also at Institut für Experimentalphysik, Universität Hamburg, Hamburg; Germany
[aa] Also at Institute for Mathematics, Astrophysics and Particle Physics, Radboud University Nijmegen/Nikhef, Nijmegen; Netherlands
[ab] Also at Institute for Particle and Nuclear Physics, Wigner Research Centre for Physics, Budapest; Hungary
[ac] Also at Institute of Particle Physics (IPP); Canada
[ad] Also at Institute of Physics, Academia Sinica, Taipei; Taiwan
[ae] Also at Institute of Physics, Azerbaijan Academy of Sciences, Baku; Azerbaijan
[af] Also at Institute of Theoretical Physics, Ilia State University, Tbilisi; Georgia
[ag] Also at Istanbul University, Dept. of Physics, Istanbul; Turkey
[ah] Also at Joint Institute for Nuclear Research, Dubna; Russia
[ai] Also at LAL, Université Paris-Sud, CNRS/IN2P3, Université Paris-Saclay, Orsay; France
[aj] Also at Louisiana Tech University, Ruston LA; United States of America
[ak] Also at LPNHE, Sorbonne Université, Paris Diderot Sorbonne Paris Cité, CNRS/IN2P3, Paris; France
[al] Also at Manhattan College, New York NY; United States of America
[am] Also at Moscow Institute of Physics and Technology State University, Dolgoprudny; Russia
[an] Also at National Research Nuclear University MEPhI, Moscow; Russia
[ao] Also at Physikalisches Institut, Albert-Ludwigs-Universität Freiburg, Freiburg; Germany
[ap] Also at School of Physics, Sun Yat-sen University, Guangzhou; China
[aq] Also at The City College of New York, New York NY; United States of America
[ar] Also at The Collaborative Innovation Center of Quantum Matter (CICQM), Beijing; China
[as] Also at Tomsk State University, Tomsk, and Moscow Institute of Physics and Technology State University, Dolgoprudny; Russia
[at] Also at TRIUMF, Vancouver BC; Canada
[au] Also at Universita di Napoli Parthenope, Napoli; Italy
[*] Deceased

JHEP04(2019)092